

Tribological Properties of
Diamond Nanoparticle and
Graphene Oxide Dispersions in
Water Lubrication

2015, September

Aidil Azli bin Alias

Graduate School of
Natural Science and Technology
(Doctor's Course)
OKAYAMA UNIVERSITY

Tribological Properties of Diamond
Nanoparticle and Graphene Oxide
Dispersions in Water Lubrication

ナノダイヤモンド粒子および酸化グラ
フェン分散水のトライボロジー特性

Aidil Azli bin Alias

アイディル アズリ ビン アリアス

Graduate School of

Natural Science and Technology

(Doctor's Course)

OKAYAMA UNIVERSITY

Contents

Introduction	1
Literature Review.....	6
1.1 Lubricant	6
1.1.1 Oil Based Lubricant	9
1.1.2 Water Lubrication	10
1.2 Additives	11
1.3 Nano Materials	13
1.3.1 Diamond Nanoparticles.....	14
1.3.2 Graphene Oxides	16
Research Methodology.....	21
2.1 Methodology	21
2.2 Friction Coefficient	23
2.2.1 Tribometer.....	24
2.2.2 Data Acquisition and Analysis.....	26
2.3 Wear Observation.....	29
2.3.1 Optical Microscopy	30
2.3.2 Surface Profiler	31
2.4 Other Material Characterization Techniques	32
2.4.1 Scanning Electron Microscope.....	32
2.4.2 X-ray Photoelectron Spectroscopy.....	34
2.4.3 Raman Spectroscopy	34

Diamond Nano Particles as an Additive in Water Lubrication	36
Abstract	36
3.1 Introduction	37
3.2 Experiments.....	37
3.3 Results and discussion.....	39
3.3.1 Materials dependence	39
3.3.2 Speed Dependence	43
3.3.3 DNP's Concentration Dependence.....	44
3.4 Summary	54
Single Layered Graphene Oxide as an Additive in Water Lubrication.....	58
Abstract	58
4.1 Introduction	58
4.2 Experiments.....	61
4.3 Results and Discussion.....	62
4.3.1 Material Dependence.....	62
4.3.2 Concentration Dependence of Graphene Oxide.....	70
4.3.3 Load dependence with different speed.....	73
4.3.4 Speed dependence of varies wear length.....	78
4.4 Summary	80
Tribological Effect by the Modification of Graphene Oxide in Water Lubrication	82
Abstract	82
5.1 Introduction	82
5.2 Experimental	84
5.2.1 Size Modification	85
5.2.2 pH level Regulation.....	86

5.4 Results and discussion.....	90
5.4.1 Size and pH level.....	90
5.4.2 Materials Dependent	96
5.4.3 Centrifugation effect	105
5.5 Summary	106
Summary	108
Acknowledgements.....	111

Introduction

Concerns regarding undesirable factors such as high cost, environmental compatibility, safety issues and disposal problems with mineral-based lubricants have led to the necessity for progressive studies on lubrication [1]. Therefore, the notion of promoting the utilization of water-based lubricant in mechanical systems and machining has been discussed [2–4]. Although this concept represents an important breakthrough, water poses a number of drawbacks, such as high oxidation effect on metal and low viscosity, which cause corrosion and poor reaction in hydrodynamic lubricant [4]. In order to transform the disadvantages of water-based lubrication to enhance friction reduction, the ability of dispersions containing additives will be the main object of investigation in this study. The additives engaged are diamond nanoparticles (DNP) and graphene oxide (GO), both of which were highly dispersed in water.

Inorganic material DNPs are known as a nontoxic substance. These inorganic nanoparticles are recognized for facilitating stable dispersion formation in liquid by surface modification [5]. The stable dispersion formed by hydrogen content at the surface of particles is thus uniformly distributed in water-based lubrication. Therefore, not only will the viscosity of water-based lubricant significantly improve, but the potential of DNP will also be simultaneously fully attained in the lubricating system. Furthermore, other studies have already demonstrated that DNPs provide good results in terms of tribological properties, such as their effect on friction reduction and oil lubricant anti-wear, composite fibre fillers and coatings [6–11]. What is more important is the lesser concern with DNP resources due to the production capacity on an industrial scale by chemical vapour deposition or by detonating highly explosive material [12,13].

Meanwhile, graphene oxide (GO) in the form of a thin carbon layer and with two-dimensional structure was selected as an additive to be studied due to its novelty. Originating from graphene, GO is a single, tightly packed layer of carbon atoms that are bonded together in a hexagonal honeycomb lattice. Graphene is widely used for its

unique properties including lubricating potential [18,19]. In addition, graphene has been extensively studied since its discovery in 2004 and is known to exhibit excellent thermal conductivity, good mechanical properties and extraordinary electronic transport properties [14–17]. On a macro-scale, tribological studies indicate that mixing graphene with polymers provides excellent wear resistance to the resultant composite material [20]. In another study, graphene platelets were used as an oil additive for improved lubricity and wear resistance [21]. One of the best properties of graphene is that it acts as an excellent corrosion protection layer on refined metals [22]. The most important is an advantage gained by the dispersion ability of graphene after being derived into GO. The dispersion ability is achievable due to the carbon oxygen functionalities in GO.

This thesis is divided into 5 chapters. The first chapter presents a literature review on the mechanism of lubricant functionality. The chapter includes an explanation of the lubricant's working capability in reducing the friction coefficient that governs the contact area, protecting it from severe contact material wear. The discussion also focuses on the general study of the lubricant regime involved in various conditions. Then the significance of oil and water lubricant is discussed. Here, the structures of both liquid lubricant types that support the lubricating ability are briefly explained. This is followed by presenting materials that are generally used as additives to improve lubricity and add value to the lubricants. Lastly, the nanomaterials used as additives in water lubrication are introduced, namely DNP and GO. The review includes the applications of DNP and GO dispersion in various other types of lubricant.

The second chapter describes the methodology used to accomplish this study. The research methodology concerns the method employed to obtain and analyse the tribological data. The experimental equipment engaged in this study is introduced along with its functionalities. Tribological data are analysed by two methods in order to justify the mechanism involved in friction reduction and wear control. The first method entails obtaining the friction coefficient and the second method is observation of the wear occurring due to friction.

In chapter 3, the effectiveness of DNP dispersed in water as a lubricant additive is studied along with its friction reduction mechanism. The results obtained for several parameters show the significant potential of DNP dispersion through the combination of an SUS304 plate and WC ball. It is likely that DNPs were embedded mainly in the

stainless steel plates, thus protecting the plates and wearing the balls in the steady-state period.

In chapter 4, the effectiveness of GO dispersion and its friction reduction mechanism are studied. Similar to the previous chapter, an initial study is done on several types of materials. The results also show that all friction coefficients were reduced to as low as 0.05 (WC ball), 0.1 (SUJ2 ball) and 0.2 (SUS304 ball) on the SUS304 flat plate. It was found that GO adsorption occurs on the lubricated surfaces of both the ball and flat plate, suggesting that the GO sheets may behave as protective coatings.

Chapter 5 describes an extended study of single-layer GO. The extended study is done in consequence to the good friction and wear results obtained in Chapter 4, which show the greater potential of GO to be used as an additive in water lubrication compared to DNP dispersion. In addition, a dynamic factor offered by GO structure requires further investigation for better understanding. Therefore, the tribological properties of different sizes of GO basal flakes and the effect of pH level modification on each dispersion sample are studied in this chapter, where the clear formation of tribofilm is observed. In addition, pH level regulation also results in the presence of ions in the dispersion. The ions can be reduced by centrifugation. Reducing the ions consequently reduces the friction coefficient according to the results presented in the last section of this chapter.

In conclusion, DNP and GO dispersions are able to improve the tribological effect between two sliding surfaces of several material types. The dependence of the dispersions applied in this study on several parameters is also identified. The study additionally reveals the differences between two carbon nanomaterials in terms of friction reduction and the wear improvement mechanism. The GO reduction through the formation of tribofilm still requires further investigation. This can be done by studying tribofilm formed in terms of thickness and durability. Further research on other parameters is also important to obtain better insight into tribofilm formation from GO dispersion.

References

- [1] Bartz WJ. Lubricants and the environment. *Tribol Int* 1998;31:35–47.
- [2] Sukumaran J, Rodriguez V, Baets P De, Perez Y, Ando M, Dhieb H, et al. A review on water lubrication of polymers. *Sustain. Constr.*, 2012, p. 3–8.
- [3] Masuda M, Nanao H, Mori S, Osawa E. Water lubrication properties of hydrophilic nanodiamond and Au nano particle. *日本トライボロジー会議予稿集 (東京)*, 2010, p. 263–4.
- [4] Zhang C, Zhang S, Yu L, Zhang Z, Wu Z, Zhang P. Preparation and tribological properties of water-soluble copper/silica nanocomposite as a water-based lubricant additive. *Appl Surf Sci* 2012;259:824–30.
- [5] Bakunin VN, Suslov AY, Kuzmina GN, Parenago OP. Synthesis and application of inorganic nanoparticles as lubricant components – a review. *J Nanoparticle Res* 2004;6:273–84.
- [6] Elomaa O, Hakala TJ, Myllymäki V, Oksanen J, Ronkainen H, Singh VK, et al. Diamond nanoparticles in ethylene glycol lubrication on steel – steel high load contact. *Diam Relat Mater* 2013;34:89–94.
- [7] Field SK, Jarratt M, Teer DG. Tribological properties of graphite-like and diamond-like carbon coatings. *Tribol Int* 2004;37:949–56.
- [8] Hoffman a., Gouzman I, Michaelson S. Formation mechanism of nano-diamond films from energetic species: From experiment to theory. *Thin Solid Films* 2006;515:14–26.
- [9] Yu-lin Q, Xiao-feng S, Bin-shi X, Shi-ning M. High temperature tribological behaviors of nano-diamond as oil additive. *J Cent South Univ Technol* 2005;12:181–5.
- [10] Lee J-Y, Lim D-S. Tribological behavior of PTFE film with nanodiamond. *Surf Coatings Technol* 2004;188-189:534–8.
- [11] Lee K, Hwang Y, Cheong S, Choi Y, Kwon L, Lee J, et al. Understanding the Role of Nanoparticles in Nano-oil Lubrication. *Tribol Lett* 2009;35:127–31.
- [12] Galli G. Computer-Based Modeling of Novel Carbon Systems and Their Properties. In: Colombo L, Fasolino A, editors. *Carbon Mater. Chem. Phys.* 3, vol. 3, Dordrecht: Springer Netherlands; 2010, p. 37–57.

- [13] Holt KB. Diamond at the nanoscale: applications of diamond nanoparticles from cellular biomarkers to quantum computing. *Philos Trans A Math Phys Eng Sci* 2007;365:2845–61.
- [14] Lei H, Guan W, Luo J. Tribological behavior of fullerene–styrene sulfonic acid copolymer as water-based lubricant additive. *Wear* 2002;252:345–50.
- [15] Du X, Skachko I, Barker A, Andrei EY. Approaching ballistic transport in suspended graphene. *Nat Nanotechnol* 2008;3:491–5.
- [16] Lee C, Wei X, Kysar JW, Hone J. Strength of Monolayer Graphene Measurement of the Elastic Properties and Intrinsic. *Science (80-)* 2008;321:385–8.
- [17] Gunlycke D, Areshkin DA, Li J, Mintmire JW, White CT. Graphene nanostrip digital memory device. *Nano Lett* 2007;7:3608–11.
- [18] Novoselov KSKS, Geim AKAK, Morozov SVS V, Jiang D, Zhang Y, Dubonos SV V, et al. Electric field effect in atomically thin carbon films. *Science (80-)* 2004;306:666–9.
- [19] Berman D, Erdemir A, Sumant A V. Few layer graphene to reduce wear and friction on sliding steel surfaces. *Carbon N Y* 2012;54:454–9.
- [20] Lin J, Wang L, Chen G. Modification of Graphene Platelets and their Tribological Properties as a Lubricant Additive. *Tribol Lett* 2010;41:209–15.
- [21] Kandanur SS, Rafiee MA, Yavari F, Schrameyer M, Yu ZZ, Blanchet TA, et al. Suppression of wear in graphene polymer composites. *Carbon N Y* 2012;50:3178–83.
- [22] Prasai D, Tuberquia JC, Harl RR, Jennings GK, Bolotin KI. Graphene: Corrosion-inhibiting coating. *ACS Nano* 2012;6:1102–8.

Chapter 1

Literature Review

1.1 Lubricant

Lubricant is an important element in any system that involves relative motion between two surfaces. The rapid progress in mechanical systems engaged in industries requires extensive studies and developments to produce sustainable and environmentally friendly lubricant. This requirement is due to the large-scale industries' significant effects on environmental sustainability [1,2]. Environmental sustainability is highly related to efficiency as well as waste management of the lubricant used. Therefore, studying lubricant is vital, because lubricant is directly related to this matter. This study presents alternatives to current lubricant and also additive development.

The function of lubricant is evident in its ability to withstand the pressure generated between surfaces and holding the load in very close proximity. Load between two contacting surfaces occurs when the surfaces are experiencing resistance due to surface asperities. The force required to overcome such resistance is generally determined using the friction coefficient. Lower friction coefficient values obtained in the system indicate the smoothness of the surfaces' sliding motion. Therefore, applying lubrication in a system is crucial, especially to reduce wear of the materials employed in the system.

The lubricant involved in a lubrication system can be in different forms, such as solid, gas and liquid [3,4]. However, the most common type used in various applications is the fluid lubricant type. Fluid lubricant can most easily carry the applied load and is easy to manage. In fluid lubricant, the applied load is upheld by the pressure within the fluid. The pressure is generated by frictional viscous resistance to the lubricating fluid's motion between the surfaces. Apart of being a force transmitter, the fluid type of lubrication is also able to transport foreign particles and control the temperature of the material surfaces owing to the presence of long chains of molecules in fluid lubricant.

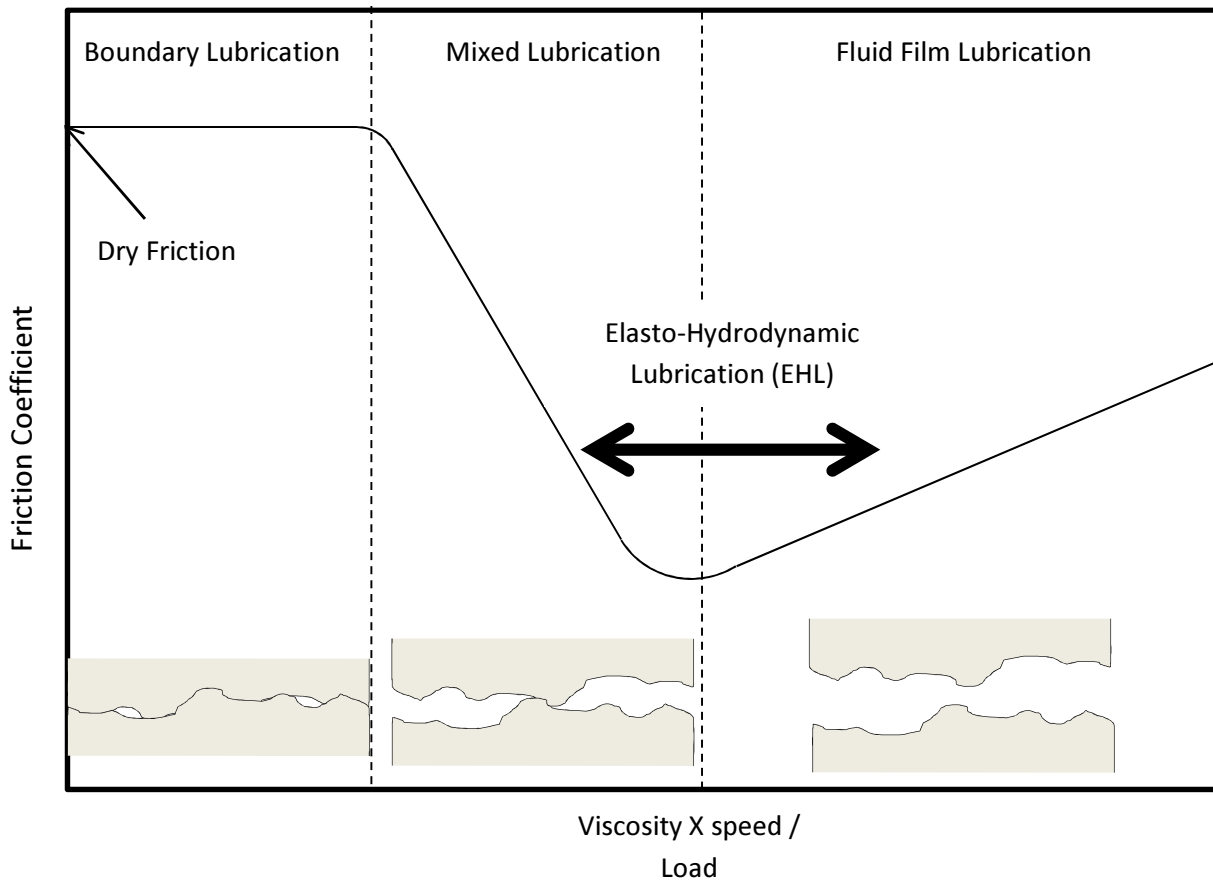


Fig. 1.1 Stribeck curve and lubrication modes

However, when these chains break down, the fluid’s lubricating ability degrades, consequently exposing the material components to damage and leading to mechanical system failure. In other words, the optimal operational range of a fluid lubricant is highly dependent on these molecule chains.

In lubrication systems, the lubricant’s condition on the contacting surfaces can be differentiated by the distinction in fluid dynamic viscosity, applied load and the velocity of the motion. All of these attributes help distinguish the lubrication mode applied in the system. The mode of lubrication is also called the regime of lubrication, which can be expressed by the Stribeck curve (Fig. 1.1). The figure illustrates how the characteristics of the lubrication regimes, such as fluid film lubrication, elasto-hydrodynamic lubrication (EHL), mixed lubrication and boundary lubrication are determined.

The first regime is called fluid film lubrication, where the applied load is supported by the fluid film pressure from the lubricant's viscous forces. This condition allows for a gap between the parts in motion, completely isolating the asperities contact for both surfaces. A stable mode of fluid film lubrication can be provided by hydrostatic and hydrodynamic lubrication. Hydrostatic lubrication is the condition when external pressure is supplied to the lubricant in order to maintain a lubricant film. Therefore, the dependence on relative motion can be avoided and hydrostatic lubrication may be enabled to accommodate heavy loads at low speeds. However, hydrostatic lubrication is complex and requires high system cost while hydrodynamic lubrication is dependent on component design besides the lubricant's ability to maintain separation between the asperities. In addition, hydrodynamic lubrication will only occur at sufficiently high velocity that generates pressure for the complete separation of the surfaces and at the same time to support the applied load.

The second regime, elastohydrodynamic lubrication, is the condition in which the load is sufficiently high for the surfaces to elastically deform during hydrodynamic lubrication in the contact region. The strain creates a load-bearing area that provides a gap for the fluid to flow through the asperities. Therefore, similar to hydrodynamic lubrication, the motion of the contacting surfaces will generate a flow that induces pressure. The pressure will bear the load applied over the contact areas. The fluid viscosity may significantly increase at high pressure. In contrast, when separation between the contact surfaces decreases, the asperities come into contact, hence leading to mixed-lubrication hydrodynamic and boundary lubrication regimes.

Lastly, boundary lubrication mode is when the parallel surfaces get closer and the friction surface asperities come in contact at the micro level. In this mode, the stick-slip asperities break off owing to the heat generated by the localized pressure. In addition, for boundary lubrication, the lubricant's hydrodynamic effects do not significantly influence the tribological characteristics of the system since the load is carried by the surface asperities rather than the lubricant. Here, the interactions in the contact between friction surfaces, and between friction surfaces and the lubricant dominate the tribological characteristics.

1.1.1 Oil-Based Lubricant

In general, nearly all lubricants used in industrial applications are based on oil. The oil bases can be divided into mineral and synthetic oil. Mineral oil is derived from the refining process of crude oil, which separates fuel and non-fuel products and therefore defines the quality and grade of the lubricant [5]. Refined mineral oil comes in distinctive grades and quality, rendering it an option for industrial applications. The quality of mineral oil is determined by the chemical composition and physical properties of the hydrocarbon-based substances. The properties are viscosity, viscosity index, low temperature properties, high temperature properties, density, demulsification, foam characteristics, pressure/viscosity characteristics, thermal conductivity, electrical properties and surface tension. These properties determine whether the oil is from the aromatic, naphthenic or paraffin base groups [4].

The common, mineral-based paraffinic oil has a long, straight-chained structure of alkane hydrocarbons. The hydrocarbon chains exist in both straight and branched molecular chains. Paraffin-based products possess excellent oxidation stability and are relatively non-reactive. The high wax content and high viscosity make them mainly useful as lubricant in engine oils, industrial lubricants and processing oils. On the other hand, there are also artificial, man-made fluids called synthetic oils, which have a straight chain structure identical to paraffin. Synthetic oils have constant molecular size and weight unlike mineral oil, and these properties offer the advantage of non-fluctuation and ease of prediction. However, the high cost, toxicity, environmental incompatibility and hazardous disposal require other lubricant alternatives.

By contrast, naphthenic oils have a saturated ring structure and are most common in moderate-temperature applications due to the high proportion of cycloalkane structure with very few or no alkanes. Finally, aromatic oils, also known as polycyclic aromatic hydrocarbons (PAHs), have a benzene ring-type chemical structure. The chemical behaviour of benzene, such as higher reactivity and higher solvency than naphthenic and paraffinic products. For this reason, aromatic oils are useful as petrochemical building blocks. They can be used to produce synthetic fluids and other petrochemical compounds such as seal compounds and adhesives.

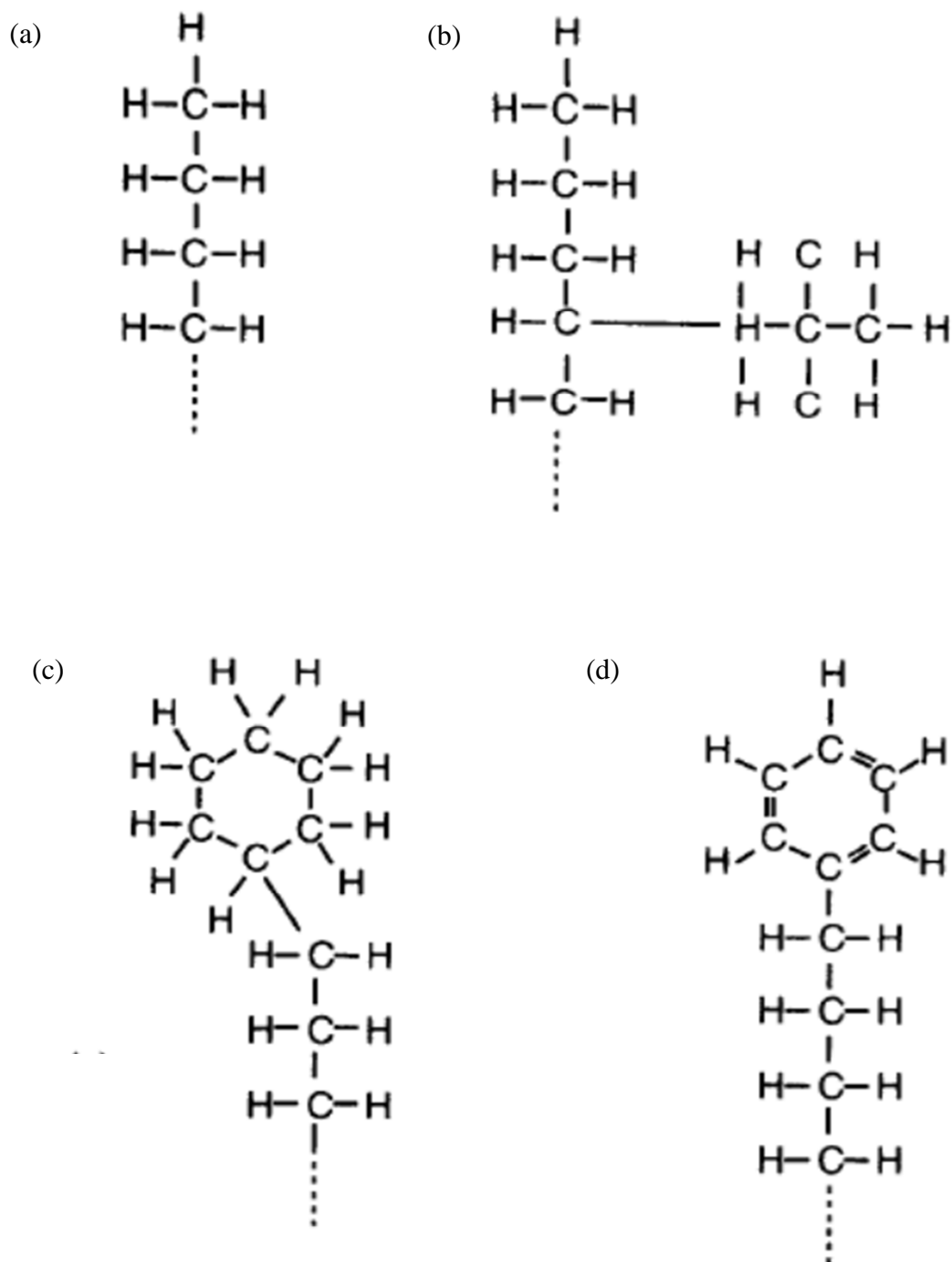


Fig. 1.2 Chemical structure of lubricating oils (a) Paraffin, (b) Branched Paraffin, (c) Naphthalene, (d) Aromatic [4]

1.1.2 Water Lubrication

Oil-based lubricants pose a concern with undesirable factors such as high cost, environmental compatibility, safety issues and disposal problems, which has led to the necessity for progressive investigations into alternative lubricants [1]. Therefore, some discussions have addressed the idea of increasing the utilization of water-based lubricants in mechanical systems and machining [6–8]. This is due to the advantage of water availability that would make low-cost lubricant. In addition, water also possesses high cooling capacity, enabling the transfer of heat from contact surfaces and also easy disposal. Although the idea of water is an important breakthrough, water has some drawbacks, such as high oxidation effect on metal and low viscosity that lead to corrosion and poor reaction in hydrodynamic lubricant [8]. Therefore, water in its original condition is not suitable for lubrication of metal or steel-based materials, which are often used in mechanical systems.

Fig. 1.3 shows the chemical structure of water. Water is a polar molecule, where the sharing of electrons between Oxygen and Hydrogen is not equal. As a result, hydrogen bonding can easily occur with other polar or charged particles. In order to mitigate the disadvantages of water-based lubrication and attain better friction reduction, the ability of additive that can bond to water molecules is the main topic of investigation in this study. The capability of dispersions is then measured by tribological observations of the friction coefficient, friction reduction mechanism and wear. In addition, higher efficiency, longer life, better reliability and less maintenance are also important objectives of water-based lubrication as a lubricant alternative.

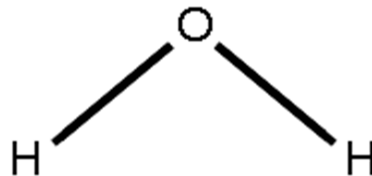


Fig. 1.3 Chemical structure of water

1.2 Additives

Lubricants are generally exposed to extreme environments during machining processes, machine operation or when used in general mechanical systems. Exposure to high operating temperatures, extreme pressure and contamination mostly lead to chemical breakdown, and hence the reduced ability of lubricant to sustain viscosity and lubricity. Therefore, the presence of additives is expected to provide proper lubrication, increase lubricant longevity and at the same protect contact surfaces from wear. The additive properties required for both oil and water-based lubricants are different due to the various lubricant chemical structures and bonding. Nevertheless, the purpose, objectives and mechanism of lubricant additives are similar.

Several attributes of additives offer a distinctive purpose for lubricant. If the lubricant is highly dependent on the long chemical chains in lubricating the contact surfaces, it is important to control the lubricant's chemical breakdown. Chemical breakdown can usually be controlled with detergent additives. Detergents work to clean oil impurities that cause deposits on the contact surfaces and neutralize acids in oil [9]. Furthermore, metal-to-metal contact surfaces are exposed to corrosion if the original protective layer on the contact surfaces gets worn due to surfaces asperities. Therefore, anti-wear additives that are able to react with the contact surfaces can be engaged. Anti-wear additives form a thin protective layer to prevent contact between metal asperities [2,10,11]. Other than that, rust inhibitors are also able to protect surfaces against rust by forming a thin water repellent film on the contact surfaces [12,13].

In addition, one of the most important attributes of additives is viscosity modification or sustainability. Lubricant viscosity is vital, especially for water-based lubricant, which possesses very low viscosity. Viscosity has the capacity to enhance lubricant performance by affording resistance to shear and flow. The viscosity attribute maintains the lubricant between contact surfaces, separating the asperities of both contact surfaces. The difference in viscosity can be determined by the viscosity index. The higher the viscosity index, the less the viscosity is affected by temperature. It is known that most applications in mechanical systems are highly dependent on viscosity in order to function at their optimum levels. Therefore, considering the function and ability of an additive and also its effect on other types of additives is important for

lubricants [14]. This matter calls for attention because some lubricants require more than one additive to achieve the application objectives. Furthermore, certain combinations of additives might degrade the expected performance of individual additives.

1.3 Nanomaterials

Nanomaterials are defined by size rather than on the basis of chemistry like other bulk materials. However, nanomaterial is still one of the most rudimentary types of material in metals, ceramics, polymers and composites. The size of a single unit size of material to distinguish it as a nanomaterial is between 1 and 100 nm, in at least one direction. This extremely small particle size provides special physicochemical properties that are significantly different from common bulk materials. Therefore, nanomaterials are expected to be able to chemically react with water lubricant to effectively handle contact surface asperities. Besides, the manipulation of nanomaterials also represents potential in industrial, biomedical and electronic applications.

Carbon is a common element that resembles nanomaterials and is also the most widely studied element in nanomaterials. Carbon exists in various polymorphic forms and does not actually fall within the groups of traditional metals, ceramics or polymers. The polymorphic form of carbon is due to a broad range of metastable phases. The common allotropes of carbon are sp^2 and sp^3 and these can occur in different crystallographic forms of graphite-like and diamond-like phases. Therefore, the characteristics of carbon structure will determine the potential uses of the material. The structure of selected carbon allotropes is observed in Fig. 1.4.

Among the nanocarbon materials, the decision was made to study diamond nanoparticles (DNP) with sp^3 carbon allotropes and Graphene Oxide (GO) dispersion with sp^2 carbon allotropes. An investigation of both types of allotropes reveals the functionality of different structures of carbon materials. In addition, both materials have been studied for a long time and have attracted a lot of attention recently in terms of their applications.

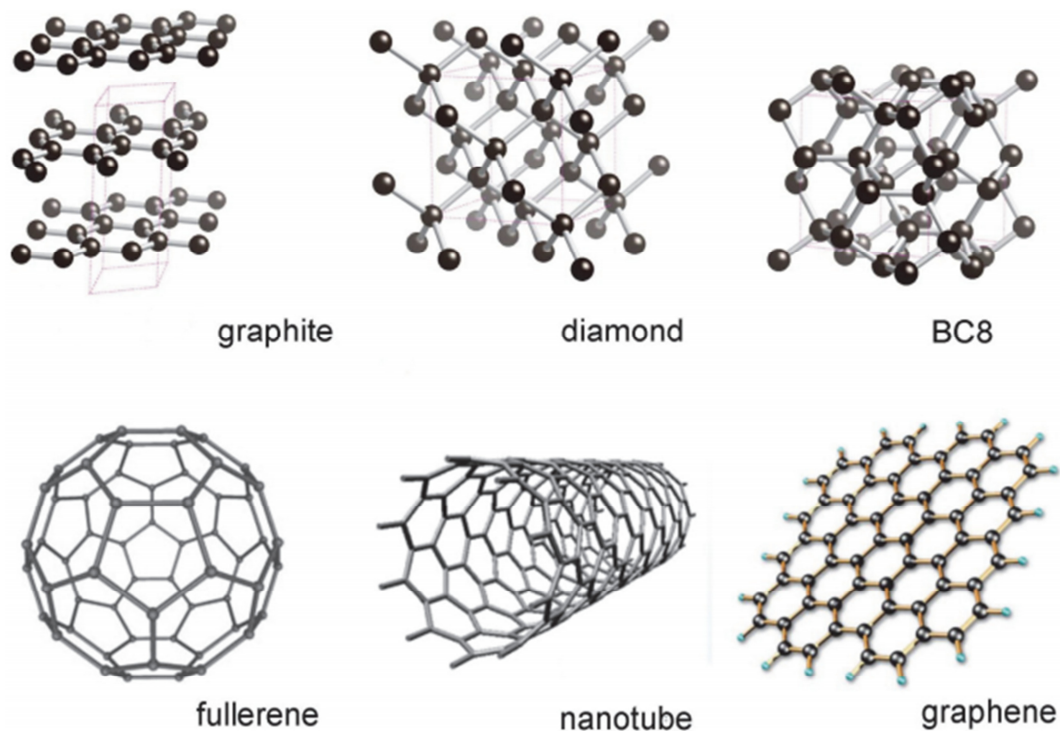


Fig.1.4 Structures of carbon allotropes [32]

1.3.1 Diamond Nanoparticles

The prominent inorganic diamond nanoparticles (DNP) were chosen as the water-based additive for this study. Known as nontoxic, inorganic nanoparticles are recognized for facilitating stable dispersion formation in liquid by surface modification [9]. Stable dispersion is formed by hydrogen content at the surface of particles that are uniformly distributed in water-based lubricant. Therefore not only does the viscosity of water-based lubricant significantly improve, but the potential of DNP is also fully utilized in lubricating systems at the same time. Other studies have also already indicated that DNPs have good tribological properties, such as their effect on friction reduction and anti-wear in oil lubricant, composite fibre fillers and coatings [15–20]. In addition, the source of DNPs is of very little concern due to their production capacity on an industrial scale using chemical vapour deposition or detonating highly explosive material [21,22].

As stated previously, the presence of DNPs increases lubrication viscosity, which consequently helps the water lubrication layer sustain on the sliding surfaces and promotes hydrodynamic lubrication. However, other than lubricant viscosity, lubricating ability is supposed to be dominated by boundary lubrication of particles during sliding of metal-based materials. The addition of DNPs in a lubricating system facilitates enhancement in two ways: the surface enhancement effect and direct effect [20]. Abrasive polishing is expected to have a surface enhancement effect in friction reduction by decreasing sliding surface asperities. At this stage, small size DNPs also embed in surface cavities, hence increasing the surface hardness [10,23]. Therefore, the wear resistance of the surface can be increased simultaneously. With the direct effect, it is believed that agglomerates and graphitized DNPs also play a role in increasing the lubricant's tribological ability [18]. DNP agglomerates afford a rolling effect for sliding materials, whereas graphitization offers thin film lubrication. However, excessively high concentrations of agglomeration may, in contrast, result in the deterioration of the lubricant's tribological properties [19].

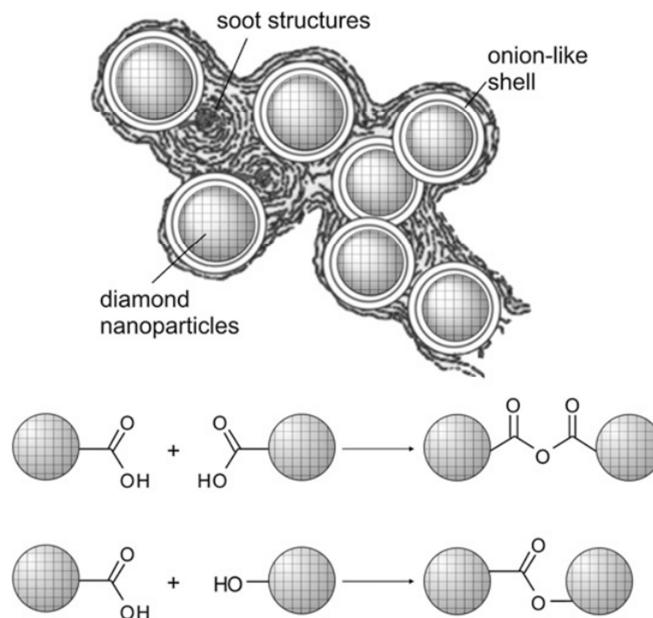


Fig.1.5 Possible DNP structure model [33]

1.3.2 Graphene Oxide

Graphene is a thin layer of carbon with two-dimensional structure. In basic terms, graphene is described as a single, one-atom thick layer of the commonly found mineral graphite. Graphite is essentially made up of hundreds of thousands of graphene layers, made it as a 3-dimensional carbon based material. Graphite oxidation can be done using strong oxidizing agents. The oxygenated functionalities are introduced in the graphite structure, which not only expand the layer separation but also makes the material hydrophilic at the basal edges. This property enables the exfoliation of graphite oxide in water using sonication techniques, ultimately producing single or a few layers of graphene known as graphene oxide (GO) [24]. The distinction in the structures of graphene and graphite is shown in Fig. 1.4.

GO is in the form of molecular sheets or flakes, with bulk graphite material dispersed in basic solution. Interest in GO has increased dramatically in the search for a cheaper, simpler, more efficient and better method of producing graphene. GO can be scaled up massively compared to conventional methods and is financially suitable for industrial or commercial applications. Furthermore, with strong layer composition, GO is expected to have high lubrication ability. The structure and properties of GO depend on the particular synthesis method and degree of oxidation. GO flakes are about 1.1 ± 0.2 nm thick [25,26]. The edges of each layer end with carboxyl and carbonyl groups [26] that considerably affect the GO functionalization, as GO flakes can be easily dispersed in water.

Actually, an abundance of studies have been conducted on graphene as lubricating coating from ultra-thin solid film since it was initially discovered [8,27–29]. However, graphene as an additive to lubricant did not capture interest at the very beginning due to the poor dispersability of graphene in lubricant. Only in recent years have the vast studies on the development of GO become a game changing factor. Numerous applications of GO in a range of research areas have been explored [30,31]. Furthermore, in contrast to graphene, GO possesses excellent dispersion ability in water. These reasons have encouraged the pursuit to study GO as an additive to water lubrication in the current study as well as to compare its ability to the well-known DNP.

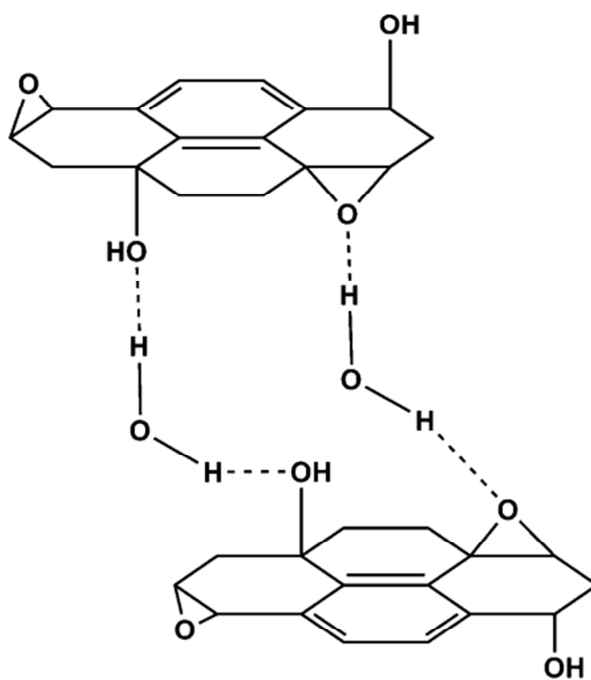


Fig. 1.5 Proposed hydrogen bonding between GO and water [30]

References

- [1] W.J. Bartz, Lubricants and the environment, *Tribol. Int.* 31 (1998) 35–47. doi:10.1016/S0301-679X(98)00006-1.
- [2] T.K. Woo, N.J. Mosey, M.H. Mu, Molecular Mechanisms for the Functionality of Lubricant Additives, *Sci. Magazine.* 307 (2005) 1612–1615.
- [3] T. Haque, a. Morina, a. Neville, R. Kapadia, S. Arrowsmith, Non-ferrous coating/lubricant interactions in tribological contacts: Assessment of tribofilms, *Tribol. Int.* 40 (2007) 1603–1612. doi:10.1016/j.triboint.2007.01.023.
- [4] N.S. Ahmed, A.M. Nassar, Lubrication and Lubricants, in: *Tribol. - Fundam. Adv.*, 2013: pp. 55–76.
- [5] J. Wright, *The Fundamentals of Mineral Base Oil Refining.pdf*, *Mach. Lubr.* (2012).
- [6] J. Sukumaran, V. Rodriguez, P. De Baets, Y. Perez, M. Ando, H. Dhieb, et al., A review on water lubrication of polymers, in: *Sustain. Constr.*, 2012: pp. 3–8.
- [7] M. Masuda, H. Nanao, S. Mori, E. Osawa, Water lubrication properties of hydrophilic nanodiamond and Au nano particle, in: *日本トライボロジー会議予稿集(東京)*, 2010: pp. 263–264.
- [8] C. Zhang, S. Zhang, L. Yu, Z. Zhang, Z. Wu, P. Zhang, Preparation and tribological properties of water-soluble copper/silica nanocomposite as a water-based lubricant additive, *Appl. Surf. Sci.* 259 (2012) 824–830. doi:10.1016/j.apsusc.2012.07.132.
- [9] V.N. Bakunin, A.Y. Suslov, G.N. Kuzmina, O.P. Parenago, Synthesis and application of inorganic nanoparticles as lubricant components – a review, *J. Nanoparticle Res.* 6 (2004) 273–284.
- [10] A.P. Puzyr, A.E. Burov, G.E. Selyutin, V. a. Voroshilov, V.S. Bondar, Modified Nanodiamonds as Antiwear Additives to Commercial Oils, *Tribol. Trans.* 55 (2012) 149–154. doi:10.1080/10402004.2011.637662.
- [11] A. Pettersson, K. Elisabet, I. Minami, Additives for Environmentally Adapted Lubricants – Tribo Film Formation, 3 (2008) 168–172. doi:10.2474/trol3.168.
- [12] J. Ziemer, W.R. Herguth, R.W. Bruce, D. Godfrey, R. Ryason, E.R. Booser, et al., *Basic of Wear*, *Soc. Tribol. Lubr. Eng.* (n.d.) 1–24.
- [13] R. Articles, *Basic Wear Modes in Lubricated Systems*, (2014) 1–6.

- [14] A. Tomala, ., A. Karpinska, W.S.M. Werner, A. Olver, H. Störi, Tribological properties of additives for water-based lubricants, *Wear*. 269 (2010) 804–810. doi:10.1016/j.wear.2010.08.008.
- [15] O. Elomaa, T.J. Hakala, V. Myllymäki, J. Oksanen, H. Ronkainen, V.K. Singh, et al., Diamond nanoparticles in ethylene glycol lubrication on steel – steel high load contact, *Diam. Relat. Mater.* 34 (2013) 89–94. doi:10.1016/j.diamond.2013.02.008.
- [16] S.K. Field, M. Jarratt, D.G. Teer, Tribological properties of graphite-like and diamond-like carbon coatings, *Tribol. Int.* 37 (2004) 949–956. doi:10.1016/j.triboint.2004.07.012.
- [17] a. Hoffman, I. Gouzman, S. Michaelson, Formation mechanism of nano-diamond films from energetic species: From experiment to theory, *Thin Solid Films*. 515 (2006) 14–26. doi:10.1016/j.tsf.2005.12.019.
- [18] Q. Yu-lin, S. Xiao-feng, X. Bin-shi, M. Shi-ning, High temperature tribological behaviors of nano-diamond as oil additive, *J. Cent. South Univ. Technol.* 12 (2005) 181–185.
- [19] J.-Y. Lee, D.-S. Lim, Tribological behavior of PTFE film with nanodiamond, *Surf. Coatings Technol.* 188-189 (2004) 534–538. doi:10.1016/j.surfcoat.2004.07.102.
- [20] K. Lee, Y. Hwang, S. Cheong, Y. Choi, L. Kwon, J. Lee, et al., Understanding the Role of Nanoparticles in Nano-oil Lubrication, *Tribol. Lett.* 35 (2009) 127–131. doi:10.1007/s11249-009-9441-7.
- [21] G. Galli, Computer-Based Modeling of Novel Carbon Systems and Their Properties, in: L. Colombo, A. Fasolino (Eds.), *Carbon Mater. Chem. Phys.* 3, Springer Netherlands, Dordrecht, 2010: pp. 37–57. doi:10.1007/978-1-4020-9718-8.
- [22] K.B. Holt, Diamond at the nanoscale: applications of diamond nanoparticles from cellular biomarkers to quantum computing., *Philos. Trans. A. Math. Phys. Eng. Sci.* 365 (2007) 2845–2861. doi:10.1098/rsta.2007.0005.
- [23] C.-C. Chou, S.-H. Lee, Tribological behavior of nanodiamond-dispersed lubricants on carbon steels and aluminum alloy, *Wear*. 269 (2010) 757–762. doi:10.1016/j.wear.2010.08.001.
- [24] Y. Zhu, S. Murali, W. Cai, X. Li, J.W. Suk, J.R. Potts, et al., Graphene and graphene oxide: synthesis, properties, and applications., *Adv. Mater.* 22 (2010) 3906–24. doi:10.1002/adma.201001068.

- [25] D. Pandey, R. Reifengerger, R. Piner, Scanning probe microscopy study of exfoliated oxidized graphene sheets, *Surf. Sci.* 602 (2008) 1607–1613. doi:10.1016/j.susc.2008.02.025.
- [26] H.C. Schniepp, J.L. Li, M.J. McAllister, H. Sai, M. Herrera-Alonson, D.H. Adamson, et al., Functionalized single graphene sheets derived from splitting graphite oxide, *J. Phys. Chem. B.* 110 (2006) 8535–8539. doi:10.1021/jp060936f.
- [27] J. Ou, J. Wang, S. Liu, B. Mu, J. Ren, H. Wang, et al., Tribology study of reduced graphene oxide sheets on silicon substrate synthesized via covalent assembly, *Langmuir.* 26 (2010) 15830–15836. doi:10.1021/la102862d.
- [28] S. Liu, J. Ou, Z. Li, S. Yang, J. Wang, Layer-by-layer assembly and tribological property of multilayer ultrathin films constructed by modified graphene sheets and polyethyleneimine, *Appl. Surf. Sci.* 258 (2012) 2231–2236. doi:10.1016/j.apsusc.2011.09.011.
- [29] J. Ou, Y. Wang, J. Wang, S. Liu, Z. Li, S. Yang, Self-assembly of octadecyltrichlorosilane on graphene oxide and the tribological performances of the resultant film, *J. Phys. Chem. C.* 115 (2011) 10080–10086. doi:10.1021/jp200597k.
- [30] D.R. Dreyer, S. Park, C.W. Bielawski, R.S. Ruoff, The chemistry of graphene oxide., *Chem. Soc. Rev.* 39 (2010) 228–40. doi:10.1039/b917103g.
- [31] A.M. Dimiev, L.B. Alemany, J.M. Tour, Graphene oxide. Origin of acidity, its instability in water, and a new dynamic structural model., *ACS Nano.* 7 (2013) 576–88. doi:10.1021/nn3047378.
- [32] A.R. Oganov, R.J. Hemley, R.M. Hazen, A. P.Jones, Structure, bonding, and mineralogy of carbon at extreme conditions, *Rev. Mineral. Geochemistry.* 75 (2013) 47–77.
- [33] A. Krueger, The structure and reactivity of nanoscale diamond, *J. Mater. Chem.* 18 (2008) 1485. doi:10.1039/b716673g.

Chapter 2

Research Methodology

This chapter describes the methodology of this research. The main focus of this thesis is mainly on the coefficient of friction obtained using different types of additives in water lubrication. The effect of the additives is investigated by observing the worn areas after testing. The friction coefficient results obtained are analysed in order to justify the effectiveness of water as a lubricant with added diamond nanoparticles (DNP) and Graphene Oxide (GO). The friction reduction mechanisms are studied through micrograph observations and material composition analysis of the worn contact surface areas. Therefore, this chapter presents a description of the equipment employed and some basic information.

2.1 Methodology

The methodology of this study is depicted in a chart in Fig. 2.1. The study was conducted by preparing the lubricants with distilled water as the main solution in the initial step. Then, the prepared DNP and GO dispersions were diluted in distilled water to different concentrations. The concentrations were set to 0.01, 0.1 and 1 wt.% additive in order to obtain optimum results with minimum amounts of additive. Both prepared DNP and GO dispersions used in the study are presented in chapters 3 and 4 respectively. For an extended study of GO dispersions in chapter 5, 0.1 wt.% GO dispersion was used. This concentration was selected based on the results obtained and presented in chapter 4, where the optimum friction reduction was achieved with that particular GO dispersion concentration. The 0.1 wt.% of GO was modified to 3 different sizes, namely GO1, GO2 and GO3. However, the size modification was not executed at our facility. Furthermore, the pH levels of these GO dispersions were regulated to investigate the effect of pH level on the tribological properties of the dispersions.

The ability of each prepared lubricant was then evaluated with a tribological sliding test. This test can promptly show whether the tendency of the friction coefficient

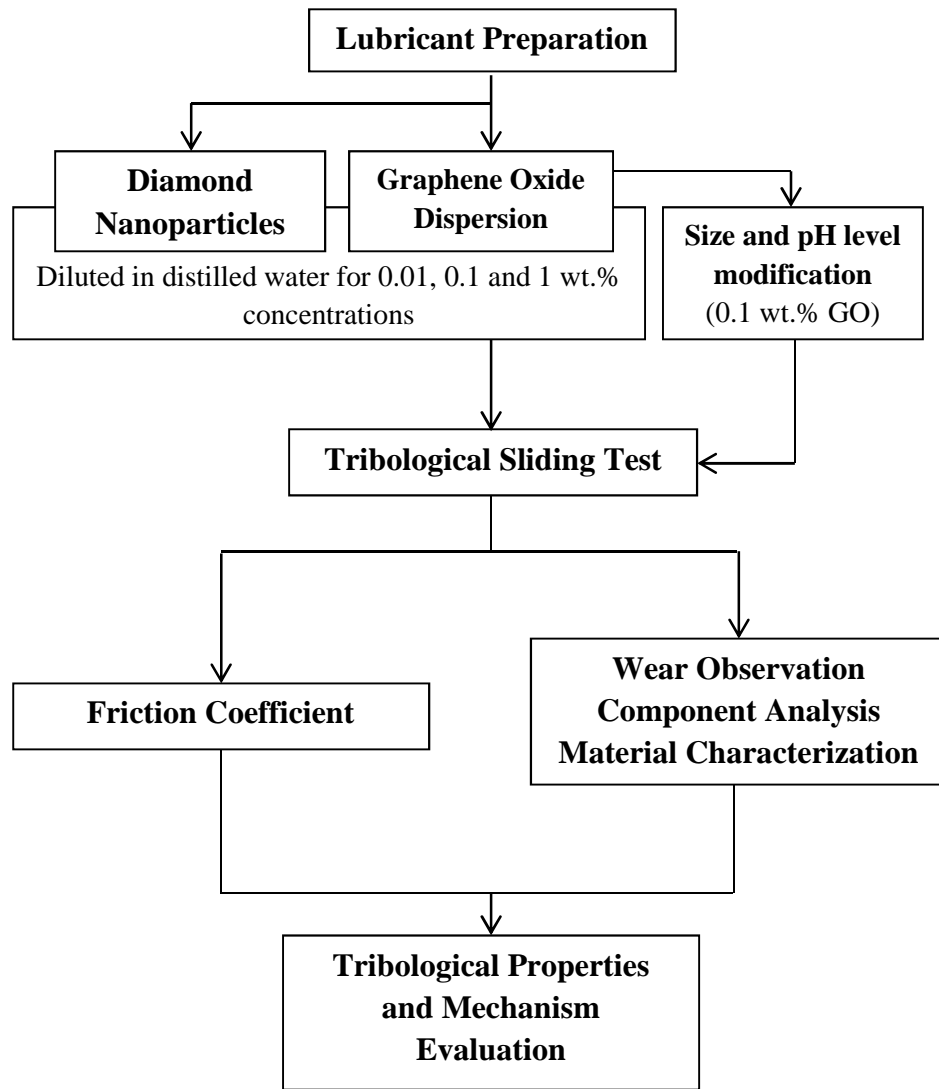


Fig. 2.1 Study methodology

is to increase, decrease or stabilize. The specimens used in this test were combinations of various types of materials. The materials were prepared with two parts: a ball used as the stationed pin and a flat plate substrate as sliding material. After testing, the wear occurring on both contact surfaces was evaluated by observing micrographs captured mostly by optical microscope. However, if the wear could not be evaluated with optical microscopy, further observation was carried out with a scanning electron microscope (SEM). SEM observation can also be extended to the analysis of the chemical composition in the wear areas using Energy-Dispersive X-ray Spectroscopy (EDS). The analysis can help determine the composition of any substances adhering to the worn region. It also differentiates wear debris from the tribofilm formed. In addition, the

surface profiler was also important in evaluating the wear width and depth profiles to show the wear level in each test. The surface profiler tests additionally served to verify the micrograph wear observations.

Finally, Raman spectroscopy and XPS analysis were carried out, particularly on the wear developed during DNP dispersion testing, due to difficulty detecting and evaluating the DNP substance from micrograph observations. Moreover, Raman spectroscopy and XPS characterized the materials' chemical bonding properties.

2.2 Friction Coefficient

The friction coefficient analysis is a general method of obtaining initial insight into the tribological properties of the lubrication employed in the system related to the contact between two sliding surfaces. The obtained friction coefficient can translate the ability of any configuration and modification in the lubrication parameters involved in the system to overcome the resisting force of the relative sliding motion. The friction coefficient displays the characteristics of friction reduction and the stability of the value obtained. Therefore, analysing the friction coefficient is vital for this study.

Descriptive analysis was used to describe the friction coefficient and number of cycles in the experiments. In this study, a general equation was used to determine the resistive force of friction when two solid objects are sliding against each other. The resistive force of friction equals the coefficient of friction times the normal force pushing the two objects together. This equation is written as:

$$\mathbf{F}_R = \mu \mathbf{F}_N \quad (1)$$

where:

- \mathbf{F}_R is the resistive force of friction
- μ is the coefficient of friction for the two surfaces (Greek letter "mu")
- \mathbf{F}_N is the normal or perpendicular force pushing the two objects together
- $\mu \mathbf{F}_N$ is μ times \mathbf{F}_N

F_r and N are measured in units of force, or newtons. When an object is under the force applied to move it along the contact surface, the object will experience resistive force of friction. This resistive force of friction is parallel to the contact surfaces and acts in the opposite direction of the force applied. The resistive force is obtained from the strain gages attached. On the other hand, normal force is the force pushing the two objects together, perpendicular to their surfaces. In this particular experiment, the normal force was determined by the load of the dead weight.

2.2.1 Tribometer

Fig. 2.2 shows the actual tribometer used in this study and Fig. 2.3 illustrates a side diagram of the tribometer. This tribometer is a laboratory setup which can be operated specifically for the reciprocating pin-on-plate sliding test in lubrication condition. The reciprocating motion of the tribometer is supplied by a speed-controllable motor. The motor used was a BLFM230-A brushless DC motor from Oriental Motor, and it provides a wide speed range with flat torque. The motor speed can be easily controlled with a digital operator up to 4000 rpm. The maximum speed ability of this motor is very high compared to the speed used in this study, which is in the range of 150 to 600 rpm. The motor's rotational motion was converted into linear motion by the crank arm attached to the motor and the bearing stationed on the sliding track. The sliding distance displacement was set up by offsetting the centre of the motor and the crank arm stopper position. The sliding displacement for this tribometer can be set to 1 mm, 2 mm, 6 mm and 8 mm. However, the default displacement in this particular study was set to 2 mm due to the substrate size, acrylic box and preliminary test done.

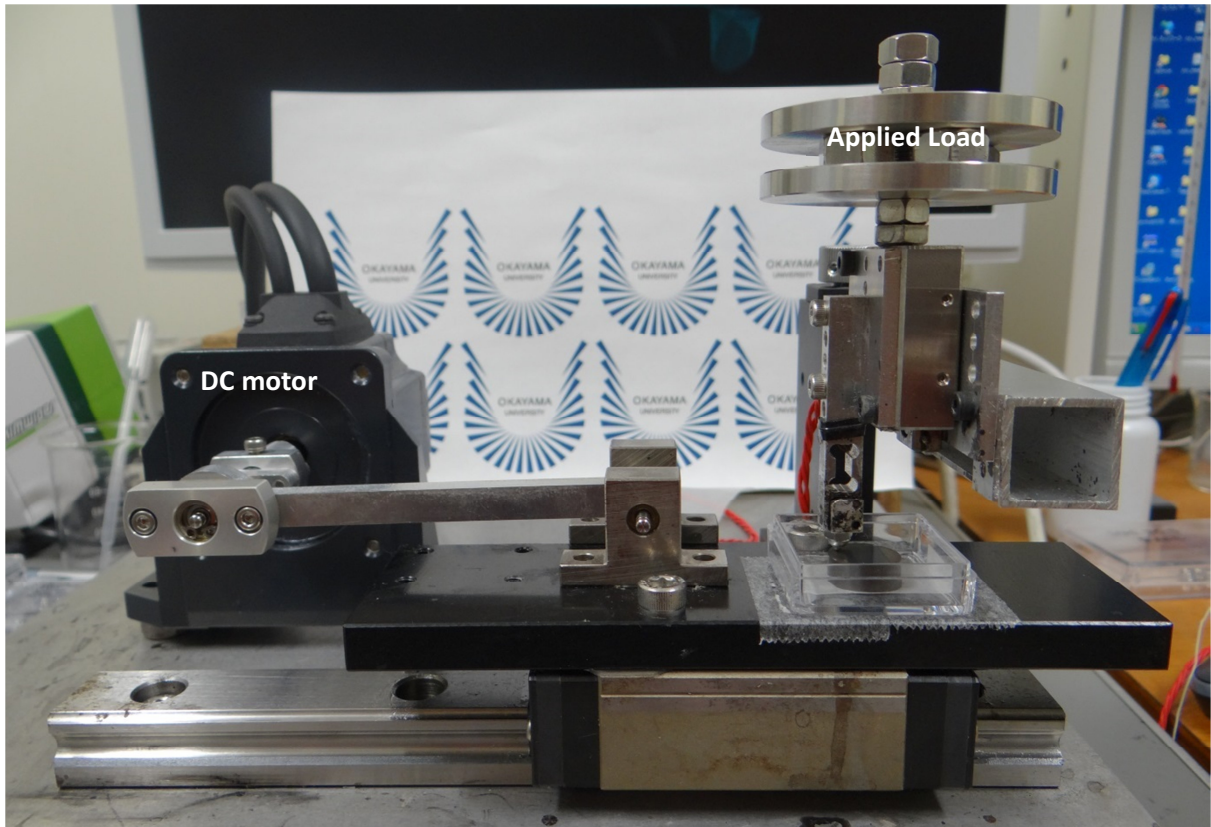


Fig. 2.2 Reciprocating sliding test tribometer

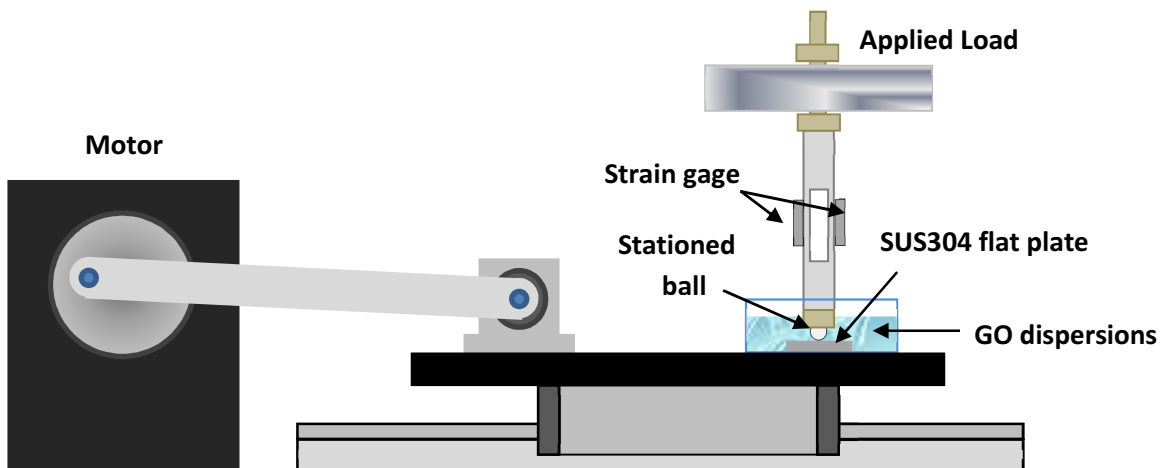


Fig.2.3 Side profile of the tribometer

The 10 mm² size substrate sample was positioned in the acrylic box located on the sliding track. The acrylic box served as a reservoir for the testing lubricant made from the DNP and GO dispersions. The amount of lubricant used in each experiment

was about 2 ml, which is ample to cover the substrate during the sliding test. The lubricant is enough to entirely cover the substrate surface and contact surfaces without any solution spill-out. In addition, during the longest test carried out on DNP dispersion, no significant evaporation of the lubricant was observed. The longest test was performed for approximately 6 hours and 240,000 running cycles. This condition was achievable due to the tape that covered the acrylic box. A bearing ball with 2 mm diameter was used as a stationary counter-material pin. The ball was attached to the vertical cantilever that was designed to hold adjustable dead weight on top. The bearing ball materials can be replaced depending on the study objective. The materials employed will be further explained in each respective chapter.

The dead weight load used for this study ranged from 1.8 N to 10.59 N. However, most of the tests were done using a moderate load of 3 N. The location of the contact area of the pin on the flat plate substrate can be manually adjusted using the XY stage. The XY stage holds the cantilever where the ball is stationed. The cantilever was also designed with a hollow area, sufficient to provide a sensitive space for the strain gages to collect the bending stress. As illustrated, two strain gages were bonded symmetrically on both the right and left sides of the cantilever hollow area. This type of bending stress measurement is similar to an adjacent side, active, half-bridge system for more accurate data.

2.2.2 Data Acquisition and Analysis

The strains produced by the force required to overcome the resistance during back and forth sliding were collected by two strain gages adhered on the vertically stationed cantilever. As described in the previous section, the strain gages provided bending stress measurement data through an adjacent side, active, half-bridge system. The strain gages were connected to a sensor interface, PCD-300A by KYOWA Electronic Instruments Co., Ltd. PCD-300A consisting of a bridge circuit to enable direct connection to the strain gages. The strain amplifier used throughout the sensor interface was the AC type, to ensure high resistance to external noise and improve reliability. The collected strain data was then directed to dynamic data acquisition



Fig. 2.4 DSC-100A interface

software, DSC-100A, also by KYOWA Electronic Instruments Co., Ltd. DSC-100A to provide various graphs and value windows for monitoring purposes.

The interface of the DSC-100A data acquisition software is displayed in Fig. 2.4. This software provided real-time monitoring of the friction coefficient during the tribological sliding test. Therefore, the ability of each lubricant to reduce the friction coefficient was easily monitored. The data were collected for 100 to 200 cycles depending on the number of cycles to be investigated. For the current thesis research, 20,000, 60,000 and 240,000 cycles were carried out for the different objectives and experiments in the respective chapters. The 20,000-cycle test was done especially for GO dispersion where the friction coefficient was low and stable **from** the initial test. Meanwhile 60,000 and 240,000 cycles were for DNP dispersion and some GO dispersions, where the effects on material wear were studied.

The sampling frequency was 1000 kHz and 1000 data were recorded for one second. These data were saved as raw data in *csv* format and then further analysed using self-developed friction analysis software in order to obtain the friction coefficient values. This friction analysis software is compatible with the *csv* format data collected by DSC-

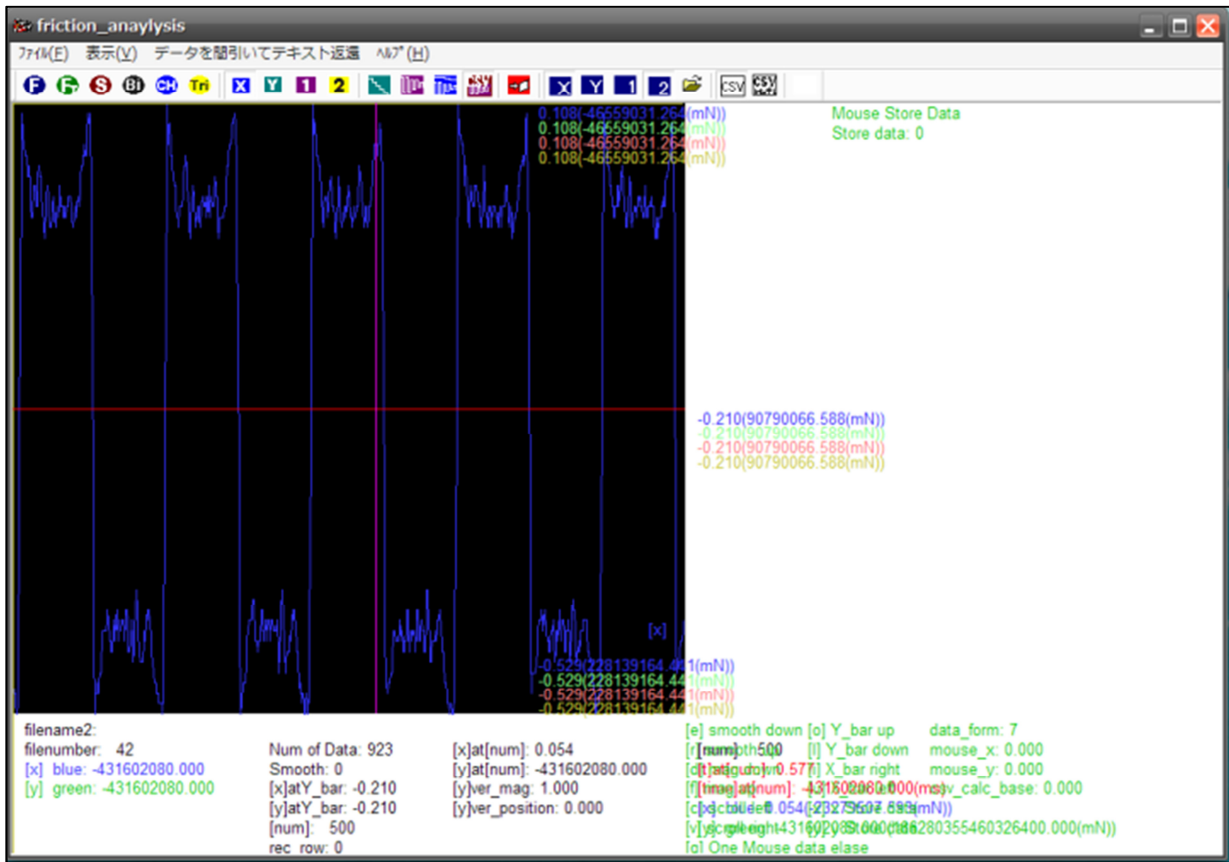


Fig. 2.5 Friction analysis interface

100A for displaying the reciprocating force. The friction forces were displayed on the interface of this software (Fig. 2.5).

The data were analysed by selecting the highest and lowest data points. The highest value represents the attribute of force required to move to one side in the sliding direction, while the lowest value is the attribute of force required from the other side of the sliding direction to return to the starting position in the reciprocating movement. The collected data known as F_1 for high peak and F_2 for the lowest peak were finally analysed in Microsoft Excel software to interpret the system friction coefficient with the following equation:

$$\text{Friction coefficient, } \mu = (F_1 - F_2) / 2F_N \dots \dots \dots (2)$$

2.3 Wear Observation

Analysing the data from the friction coefficient only helped identify the ability of each lubricant in reducing the friction force between two sliding surfaces. In other words, it was only possible to differentiate the lubricant's performance in lubricating the contact surfaces. Therefore, friction coefficient data only is insufficient to justify the mechanism of friction reduction in the system. Thus, observations of the material surfaces before the test as well as the wear track condition following the test are very important in this study. The wear track condition describes the structures of any substances formed with the developed wear. Apart from the size and formation of wear scarring, observations of the tribofilm on the wear tracks also indicate the mechanism and type of wear that occurred during sliding in water lubrication with and without additive in the lubricant. Table 2.1 lists the instruments appropriate for different tribofilm characterizations. However, the main instruments used in this study are optical microscopy and surface profiler.

Table 2.1 Classification of material characterization

Instruments	Tribofilm Characteristics
Optical Microscopy	Microstructure
Surface Profiler	Surface morphology
Raman Spectroscopy	Chemical bonding property
Scanning Electron Microscopy (SEM)	Surface morphology Microstructure
X-ray Photoelectron spectroscopy (XPS)	Chemical composition Chemical bonding property
Energy dispersive X-ray spectroscopy (EDS)	Chemical composition

2.3.1 Optical Microscopy

Optical microscopy is the main equipment used in the current study as it facilitates easy observation of the wear on both the pin (ball) and flat plate surface. The magnified images of the specimen microstructure can describe the mechanism of friction reduction in the system. In this study, an upright type microscope was used, DSX500 Opto-digital Microscope by Olympus[®]. This type of microscope enables observations of the specimens from the upside, furthermore expanding the ability to observe the concave surface of the ball used in this study. An optical microscope has two major, fundamental functions: creating magnified images of specimens and illuminating the specimens. These major functions have, in turn, three basic functions: to magnify the specimen, obtain clear and sharp images, and change the magnification and focusing ability. The latter is to supply, collect and change the light intensity.

The DSX500 used to observe the worn areas in the current study is a high-resolution, upright, motorized microscope. This microscope has magnifying ability of up to 13 times zoom optics and digital zoom of up to 30 times. Therefore, a single optical lens is able to cover the typical magnification range of conventional optical microscopes. In addition, two lenses can be mounted at once for a greater magnification range. The best function of this microscope is that observation can be done directly on a computer screen complete with a touch screen panel and joystick and mouse control. The simplicity of the microscope operation ensures the reliability of the images captured along with the best results, even for newbies to the microscope system. The short and simple steps with several auxiliary options also help shorten the observation time and provide quick study results.

The surface image enhancement option available with this particular microscope is also helpful in this study. The software interface used by this microscope can be set at HDR for high definition visualization, WIDER for easy inspection of samples with high reflectance difference and also MIX observation method for easy detection of any defects and imperfections of the observed samples.

2.3.2 Surface Profiler

A surface profiler was used to evaluate the surface morphology of the samples, particularly the surface prior to testing and the wear profile following the tribological testing in water lubrication. It is common practice to employ a surface profiler in the study of tribological properties related to tribological effects on sliding surfaces [1–4] . In this particular study, a portable surface roughness tester by Mitutoyo, SURFTEST SJ-210 series, was deployed. This equipment is small, lightweight and extremely easy to use. The surface roughness can be directly observed on the LCD screen on the profiler. The collected data can be directly transferred to a computer and analysed with general graph-related programs. The data obtained from the surface profiler are displayed as a wear profile that is reflected in the optical microscopy observations of each wear area occurring on the contact surfaces. However, the surface profiler can only be used on flat surfaces and not curved surfaces like balls. Therefore, wear on the ball was only observed by microscope and estimations.



Fig. 2.6 SURFTEST SJ-210 surface profiler

2.4 Other Material Characterization Techniques

Besides the wear condition, observations of tribofilm are also important in order to determine the friction reduction mechanism. It is due to the diversity of tribofilm formed and also to compare the main areas investigated. An abundance of literature has addressed the material characterization and analysis of tribofilm surfaces [1,5,6]. However, in the present study, only few techniques were used due to equipment limitations at the facility. Nonetheless, the techniques employed were sufficient to verify the characteristics of tribofilm formed on the contact surfaces.

2.4.1 Scanning Electron Microscopy

Scanning Electron Microscopy (SEM) was used to observe and characterize the microstructural features and composition at the surface of the tested materials. In addition, the distribution condition of GO was also observed by SEM. Nanometre-scale observation of the images was possible by using spatial resolution in low-KV secondary electron imaging mode available in SEM. Furthermore, the topography and chemical composition were analysed with SEM owing to the additional function, Energy Dispersive X-ray Spectroscopy, also known as EDS or EDX or EXDS. This is a qualitative and quantitative X-ray micro-analytical technique capable of providing chemical composition information of the investigated materials' surfaces. EDS is also a non-destructive analytical technique for samples. As such, the same sample can be analysed several times. However, EDS in SEM has some limitations in detection ability, depending on the composition amount in the sample being analysed. Therefore, this analysis is only effective for major and minor element analysis but is not very sensitive for less than average elemental concentrations. Two types of analysis were conducted with EDS as shown in Fig. 2.7 and Fig. 2.8. Both images are real observations of the wear materials in the present study. Fig. 2.7 represents the carbon element mapping of the (b) WC ball and (c) stainless steel flat plate. Fig. 2.8 indicates the line mapping of

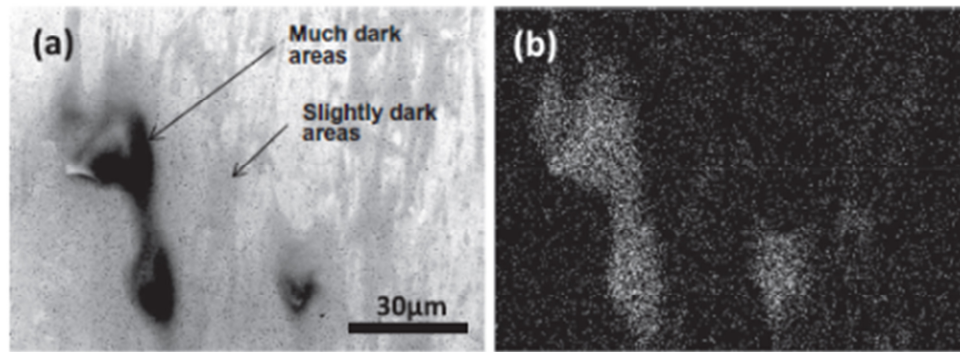


Fig. 2.7 Example SEM images of carbon elemental mapping of WC ball and stainless steel flat plate lubricated with GO dispersion after friction testing for 60,000 cycles. (a) SEM image and (b) carbon elemental mapping by EDS of WC ball surfaces [11]

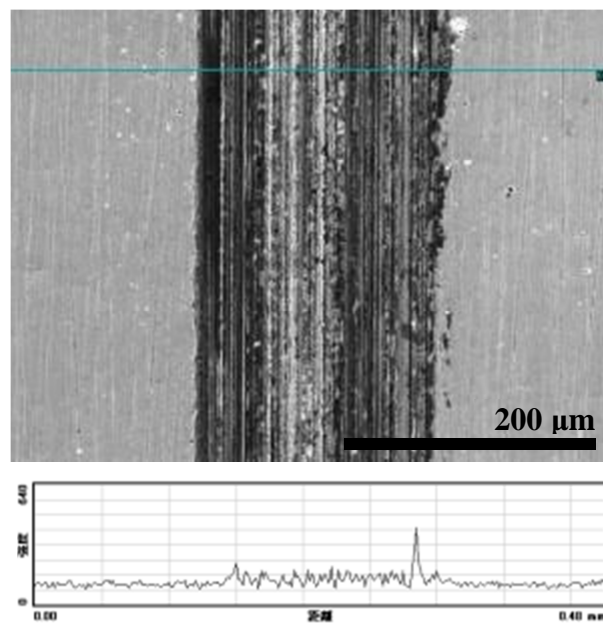


Fig. 2.8 Example of carbon elemental mapping by EDS on SUS304 flat plate substrate

the wear tracks. This type of mapping offers the advantage of differentiating the carbon element inside and outside the wear tracks. Therefore, it is easier to determine the formation of tribofilm from carbon element on the tested materials.

2.4.2 X-ray Photoelectron Spectroscopy

X-ray Photoelectron Spectroscopy (XPS) was used to study the worn area of the wear track after the tribological test. In XPS, X-rays are directed to the sample surface, causing the emission of core electrons from the atoms on the studied surface. Electron emission produces kinetic energy that represents the difference in electron binding energy. The binding energy can provide the atomic composition, as the electron orbitals in the atoms are known [5,7,8]. Therefore, the peak positions in the spectrum from the energy binding assist with identifying the chemical state of the sample under investigation. Unfortunately, in this study, XPS was only executed to observe the wear track of the reciprocating sliding of the test under DNP dispersion (chapter 3) due to accessibility to equipment. Nevertheless, other material component analyses, such as optical microscope observation, SEM and EDS analyses were adequate to determine the wear track condition in the studies on GO dispersion effect in chapters 4 and 5.

2.4.3 Raman Spectroscopy

Lastly, characterization of materials on the worn surface was conducted with Raman spectroscopy. In Raman spectroscopy, the vibrational modes of the material being observed are analysed. The differences in vibrational modes that reflect in the amount of shift of the laser line correspond to the different orientations of the material atoms as well as their bonding characteristics. The amount of laser shifting is therefore represented on a Raman spectrum. Since each different material possesses unique and specific vibration mode frequencies, the Raman spectrum clearly shows the material components in the observed area [9,10].

This observation was only carried out for the tests on DNP dispersion, similar to the XPS employed in this study. This is due to the limitation in determining the DNP embedded on the material surfaces' wear tracks according to the micrograph observations. In addition, several SEM observations also made it difficult to determine the DNP structure after the sliding test.

References

- [1] Liu Y, Wang X, Pan G, Luo J. A comparative study between graphene oxide and diamond nanoparticles as water-based lubricating additives. *Sci China Technol Sci* 2012;56:152–7.
- [2] Ding Q, Wang L, Wang Y, Wang SC, Hu L, Xue Q. Improved Tribological Behavior of DLC Films Under Water Lubrication by Surface Texturing. *Tribol Lett* 2010;41:439–49.
- [3] Liu Y, Liu P, Che L, Shu C, Lu X. Tunable tribological properties in water-based lubrication of water-soluble fullerene derivatives via varying terminal groups. *Chinese Sci Bull* 2012;57:4641–5.
- [4] Mori S, Kanno A, Nanao H, Minami I, Ösawa E. Tribological Performance of Nano-Diamond for Water Lubrication. 3rd Int. Symp. Detonation Nanodiamonds Technol. Prop. Appl., St. Petersburg, Russia: Ioffe Physico-Technical Institute; 2008, p. 21–8.
- [5] Pettersson A, Elisabet K, Minami I. Additives for Environmentally Adapted Lubricants – Tribo Film Formation 2008;3:168–72.
- [6] Joly-Pottuz L, Matsumoto N, Kinoshita H, Vacher B, Belin M, Montagnac G, et al. Diamond-derived carbon onions as lubricant additives. *Tribol Int* 2008;41:69–78.
- [7] Yu-lin Q, Xiao-feng S, Bin-shi X, Shi-ning M. High temperature tribological behaviors of nano-diamond as oil additive. *J Cent South Univ Technol* 2005;12:181–5.
- [8] Dreyer DR, Park S, Bielawski CW, Ruoff RS. The chemistry of graphene oxide. *Chem Soc Rev* 2010;39:228–40.
- [9] Praver S, Nugent K., Jamieson D., Orwa J., Bursill L., Peng J. The Raman spectrum of nanocrystalline diamond. *Chem Phys Lett* 2000;332:93–7.
- [10] Ferrari, Andrea Carlo RJ, Ferrari AC, Robertson J. Raman spectroscopy of amorphous, nanostructured, diamond-like carbon, and nanodiamond. *R Soc* 2004;2:2477–512.
- [11] Kinoshita H, Yuta N, Alias AA, Fujii M. Properties of monolayer graphene oxide sheets as water-based lubricant additives. *Carbon N Y* 2013;66:720–3.
- [12] Corporation MA. Portable Surface Roughness Tester SURFTEST SJ-210 Series. 2014.

Chapter 3

Diamond Nano Particles as an Additive in Water Lubrication

Abstract

In this chapter, we studied the effectiveness of diamond nanoparticles (DNPs) dispersed in water as a lubricant additive and their friction reduction mechanism. Firstly, the study has been carried out to investigate the tribological properties offered by DNP dispersion between sintered carbide (WC) ball on stainless steel (SUS304) and aluminium (A5052P) flat plate substrates. The obtained results shown significant potential of DNP dispersions by the combination of SUS304 plate and WC ball, lead the extensive study for this combination. In further study, DNP dispersions with densities of 0.01, 0.1 and 1 wt.% were prepared and used as lubricants under a load of 1.88 N, for 240,000 friction cycles. High-friction coefficients of more than 0.3 were observed in an initial period. Then friction coefficients declined and stabilised at values of approximately 0.1. The steady-state friction coefficients were independent of the DNP density and lower than that for distilled water. In the initial period, wear of both the plates and ball was obvious. In the steady-state period, additional wear on the plates was a little; however, ball wear scars were clearly observed. The size of the ball wear scars decreased with decreasing the DNP density. When the lubrication was carried out by the 0.01 wt.% DNP dispersion, the ball wear scar size was smaller than that under distilled water lubrication. It is likely that DNPs were embedded mainly in the stainless steel plates, and the embedded DNPs protected the plates and wore the balls in the steady-state period. Compared with the lubrication under distilled water, the friction coefficient and wear of the plate under the lubrication by the 0.01 wt.% DNP dispersion were lower, and the wear of the ball by this lubrication condition was not high.

3.1 Introduction

Recently carbon nanomaterials such as fullerene, carbon nanotubes, and graphene (oxide) have been studied as the additives of water lubrications for their good tribological properties [1–3]. These carbon nanomaterials above mentioned have graphite structures composed of sp^2 bonding. In carbon nanomaterials, only diamond nanoparticles (DNPs) have single crystal diamond structure composed of sp^3 bonding, with a size of less than 10 nm.

Diamond-structured materials such as diamond-like carbon (DLC) coatings are hard and their friction and wear are very low in water environment [4]. DNPs are also expected to have good tribological properties under water lubrications. In addition, DNPs can be obtained with the production capacity in industrial scales by chemical vapor deposition or by detonating high explosive material [5,6]. DNPs have showed good tribological properties as additives in oils [7,8]. A tribological property of DNPs as additives in water is only studied under the lubrication between SiC and silicon [12]. It is necessary to study tribological properties of DNP additives under water lubrications between materials used in mechanical systems.

In this study, tribological properties of DNP dispersions in water were investigated using steel plates and tungsten carbide (WC) balls which are widely used in metal working, and the influence of DNP density in the dispersion was discussed. The lubricated surfaces on plates and balls were analysed by optical microscopy, contact surface profilometry and Raman spectroscopy.

3.2 Experiments

Commercial DNPs (Carbodeon uDiamond® Molto, Carbodeon NanoMaterial) were used in this study. This product is a DNP powder with crystal sizes of 4–6 nm that has a DNP content of more than 97%. Lubricant dispersions were prepared by adding DNP powder to distilled water and mixing for 5 min by ultrasonication. DNP dispersions with densities of 0.01 wt.%, 0.1 wt.% and 1 wt.% were prepared. Fig.3.1 shows the as-prepared DNP dispersions. The test materials used in this study were

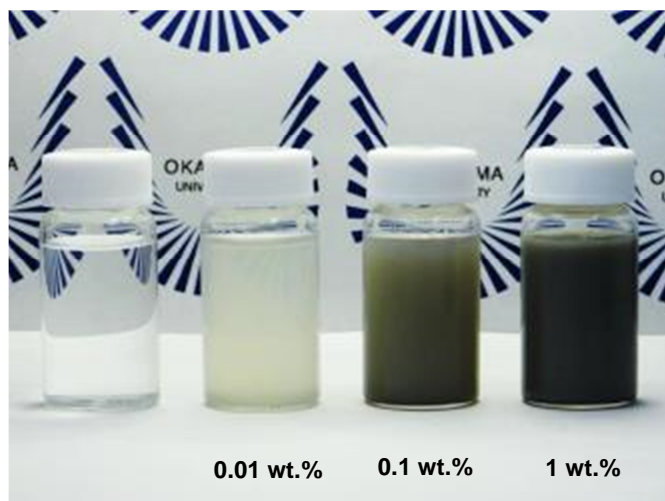


Fig.3.1 As-prepared DNP dispersions with concentrations of 0.01, 0.1 and 1 wt.% in comparison to distilled water.

lapped stainless steel (JIS-SUS304) plates and sintered tungsten carbide (WC) balls with a diameter of 2 mm. The surface roughness of the lapped plate surfaces was approximately 33 nm, and that of the ball surfaces was approximately 2 nm.

A tribometer with a reciprocating sliding configuration was used for the friction tests in this study. Friction tests were performed with a sliding distance of approximately 2 mm, a sliding frequency of 600 rpm, duration of 240,000 cycles, under an applied normal load of 1.88 N. The average sliding speed was 40 mm/s, which implies that the sliding condition of lubrication regime is the boundary lubrication. Both the SUS304 plates and WC balls were pre-cleaned in ethanol, and then water for 5 min each using an ultrasonicator. The cleaned samples were placed in an acrylic box positioned on the sliding track of the tribometer. A sufficient amount of lubricant to cover the sliding area was added (approximately 2 ml). The acrylic box was covered and no water condensation observed inside the box's wall during the 6-h friction experiment, which indicates no significant evaporation of the water. The lubricated surfaces of the plates and balls were investigated by optical microscopy, contact surface profilometry, and Raman spectroscopy. All of the plates and balls were carefully washed by ultrasonicing in ethanol before analyses. Widths of plate wear tracks were determined by 3 times measurement average on each two different points. Widths of ball wear scars did by 3 times measurement average on one point.

3.3 Results and discussion

The results and discussion are describe about several parameters and factors which were affect the ability of DNP dispersions in offering good tribological properties on the metal. It was separated into 3 sections. The first section is the materials dependence, the second section is sliding speed dependence and the last section is DNP concentration dependence. Each topic will show the dependence of tribological properties to the prepared DNP dispersions and how it relates to the friction reduction and wear protection mechanism.

3.3.1 Materials dependence

The material dependent by the application of water lubricant is important. It is because different materials will experience different mechanism of friction reduction. The results obtained in this section discusses about the effect by the addition of 1 wt.% of DNP to the friction coefficient of distilled water. The study was carried out for two types of mating materials. WC ball was decided as the stationed pin for both tests. The flat plates were SUS304 and A5052. Both of the materials were generally used in mechanical systems and also in the machining. In general, the distinctions of the parameters were the material hardness and surface roughness of each material.

The analyzed results in Fig.3.2 and Fig.3.3 shows the tribological properties by the addition of 1wt.% of DNP powder in distilled water for WC ball and SUS304 flat plate. It is clear that the friction coefficient was high for the test in distilled water without any addition of the DNP, which was approximately around 0.5 in steady state. On the other hand, DNP dispersion showed significantly low friction coefficient at the steady state which was about 0.15. However, the friction coefficient of 1 wt.% of DNP dispersion is higher than distilled water at the initial stage. The friction coefficient in this period was slightly higher than distilled water, which was approximately 0.6. The reduction of DNP was observed with a sharp reduction when the number of cycles was approximately 10,000 cycles. It was reduced as low as 0.1 before gradually increased to around 0.15 at the steady state. During the initial state, the abrasive effect of DNP taking place in between the surfaces and reducing asperities of the contact surfaces. This

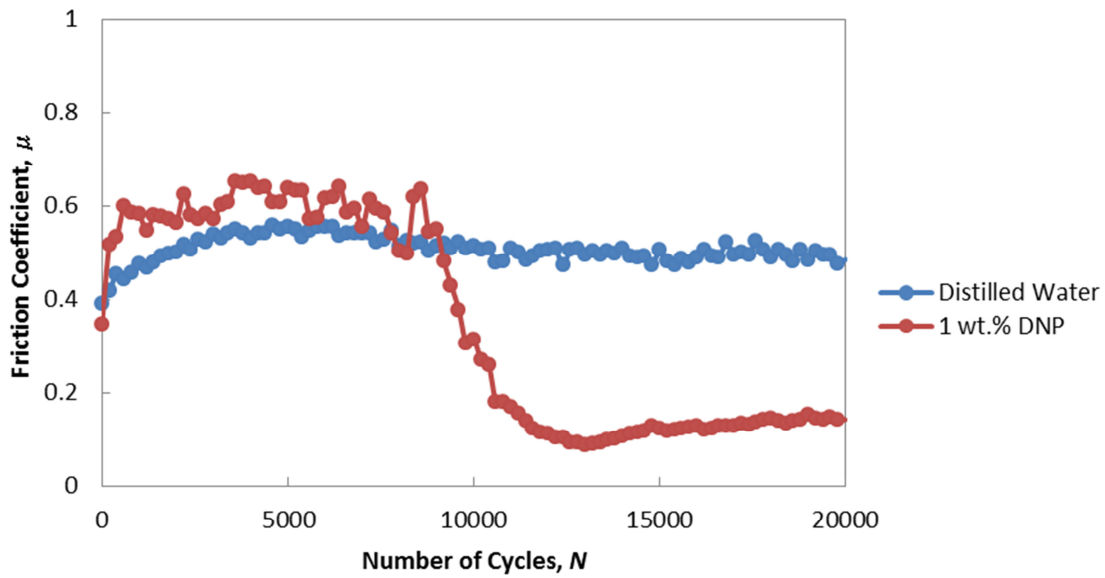


Fig.3.2 Friction coefficients of WC ball and SUS304 flat plate.

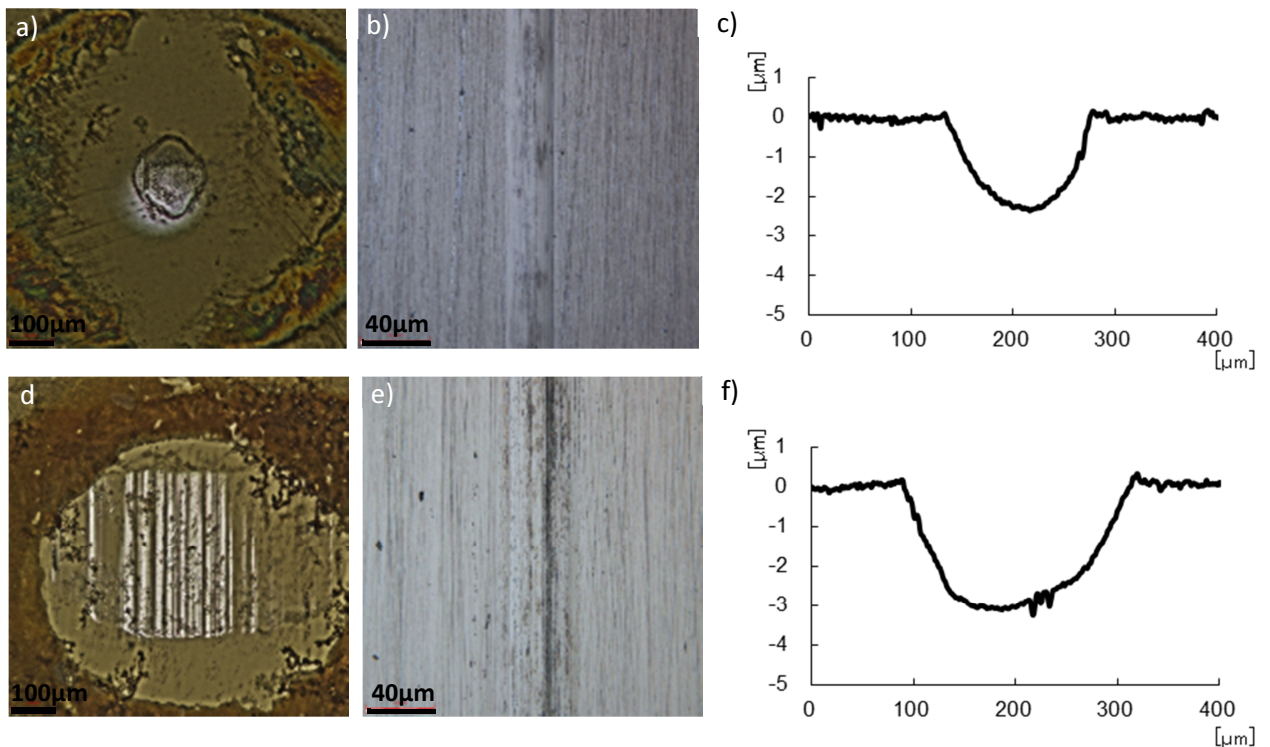


Fig.3.3 Wear condition on the balls and substrates with the wear profiles of the substrates. Images a),b) and c) are the test under 1 wt.% DNP and d),e) and f) are the test under distilled water.

situation makes the friction coefficient prone to be higher than distilled water as distilled water was only experienced the direct rubbing at boundary regime.

The distinction of the worn developed from the test on the materials are shown in Fig.3.3. It is obvious that DNP dispersion offered better lubricant ability to the contact materials. Instead of higher friction coefficient at the initial state, only small wear can be seen on the tip of the ball and also the wear track. The wear volume as shown in the wear track profile also proving the ability of DNP dispersions in reduces the wear.

The similar improvement for the test of WC ball onto the softer material, A5052P flat plate as shown in Fig.3.4 and Fig.3.5 also can be observed. However, the friction coefficient for both the distilled water and DNP dispersion showed similar tendencies of the reduction. The friction coefficient of distilled water was as high as 1.0 at the initial state and gradually reduced to approximately 0.5. DNP dispersion on the other hand showed same friction coefficient at the initial state as Fig.3.2. This friction coefficient was stable at 0.6 until 15,000 cycles. After that, it was gradually reduced to 0.2, which is lower than the one in distilled water. From the results, similar mechanism as WC ball against SUS304 can be predicted. However, the high friction coefficient was caused by the adhesion of the materials which was softer an easier to be adhered to the ball.

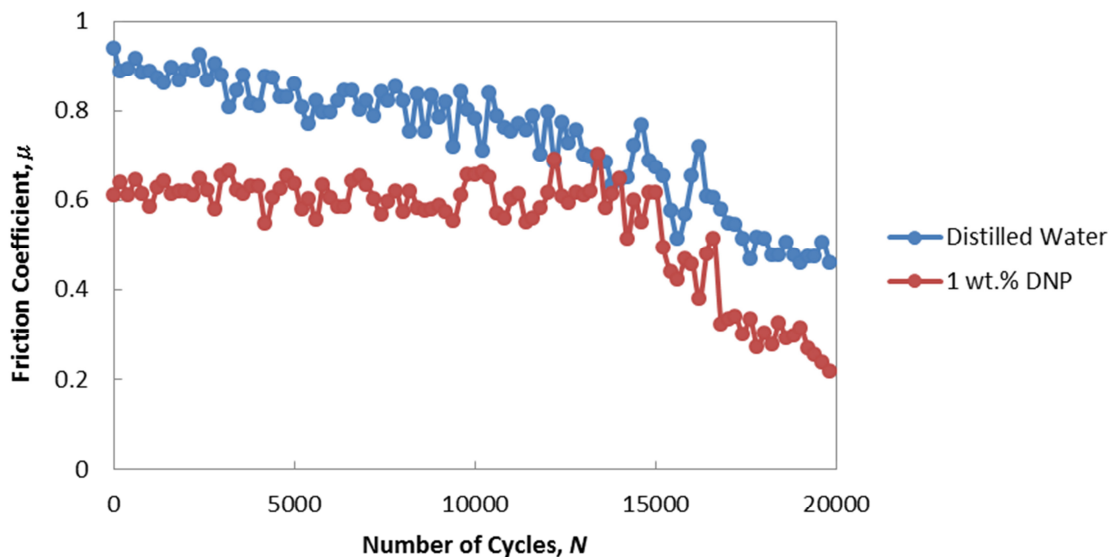


Fig.3.4 Friction coefficient of WC ball and A5052P substrate

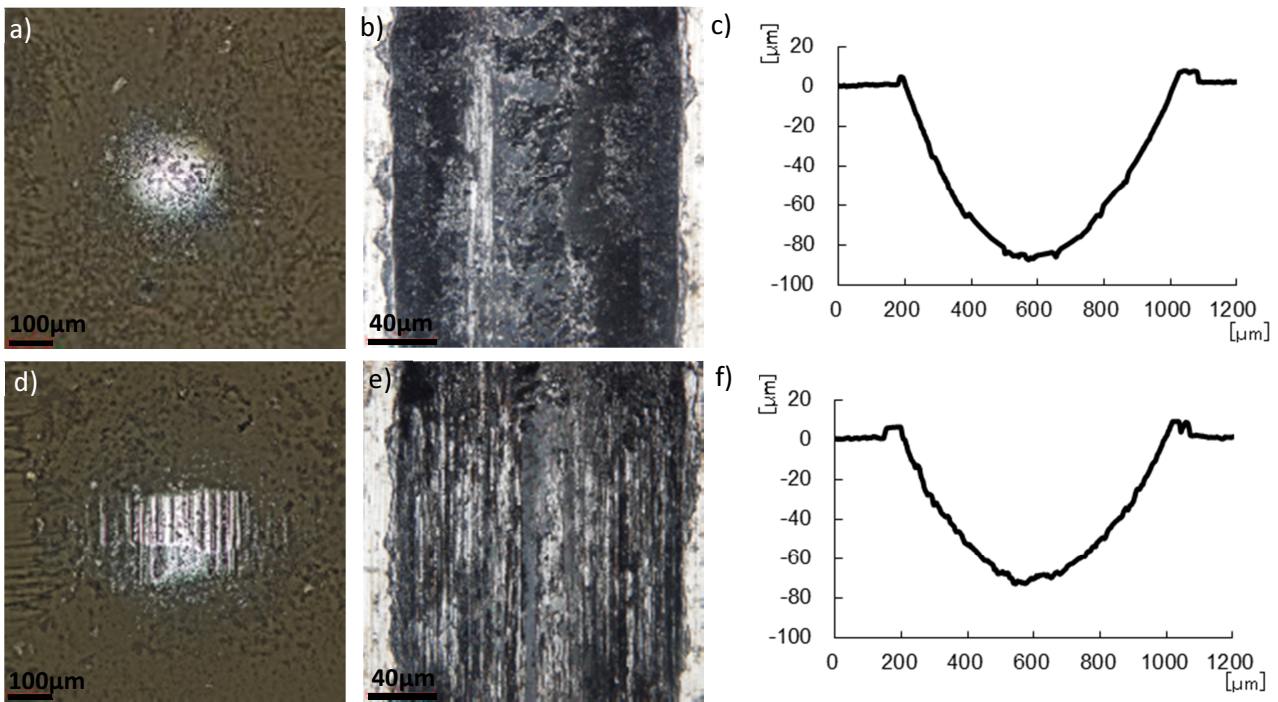


Fig.3.5 Wear condition on the balls and substrates with the wear profiles of the substrates. Images a),b) and c) are the test under 1 wt.% DNP and d),e) and f) are the test under distilled water.

The wear on the ball as shown in Fig.3.5 clearly show that DNP dispersion also able to govern the ball from the wear propagation. However, the distinction of the worn on the wear track was difficult to be differentiated by the observation of wear volume. Both distilled water and DNP dispersion show approximately similar wear volume and width on the wear tracks. Nevertheless, the deformation structures of the wear tracks were different. The wear track of the sliding test in distilled water shows extreme scarring effect where the scar line along the sliding direction was clear. Meanwhile, the similar scar was unable to be seen on the wear track of the test in DNP dispersions. In this condition, the DNP particles were embedded into the materials surfaces and hardened the particular area. Perhaps, the distinction of both wear tracks can be seen for longer sliding test.

In addition, the differences of steel and aluminium in friction reduction by DNP dispersions also due to the different mechanism. In the study of DNP in oil, although DNP able to improve tribological behaviour on both materials, the improvement in the steel was significantly by enhancement of contact surface's toughness. Meanwhile, the wear mechanism was nominated by viscosity in aluminium alloy [13].

3.3.2 Speed Dependence

The study on the addition of DNP powder to the distilled water was also carried out in order to understand the dependence of friction reduction to sliding speed. The sliding speeds were regulated at 150, 300, 450 and 600 rpm. The DNP dispersion was prepared for 1 wt.% and the testing materials are WC ball and SUS304 flat plate.

The result obtained in Fig.3.6 shows the distinction in the friction reduction by each sliding speed. As expected from the result obtained in previous section, all of the friction coefficients were high at the initial state. It is noticeable that the friction coefficients were stable at 0.4 to 0.5 during that period. The slowest sliding speed, 150 rpm was able to reduce the friction coefficient faster than other sliding speed at 5,000 cycles. It was followed by 300 rpm at 10,000 cycles and 450 rpm at 15,000 cycles. Lastly, the friction reduction was only seen at 35,000 for the speed of 600 rpm.

The results indicate that the slower of the speed for the sliding test, the easier diamond particles to be embedded into the contact surfaces. On the other hand, higher speed increased the motion of the particles; hence reduce the ability to be embedded into surface asperities.

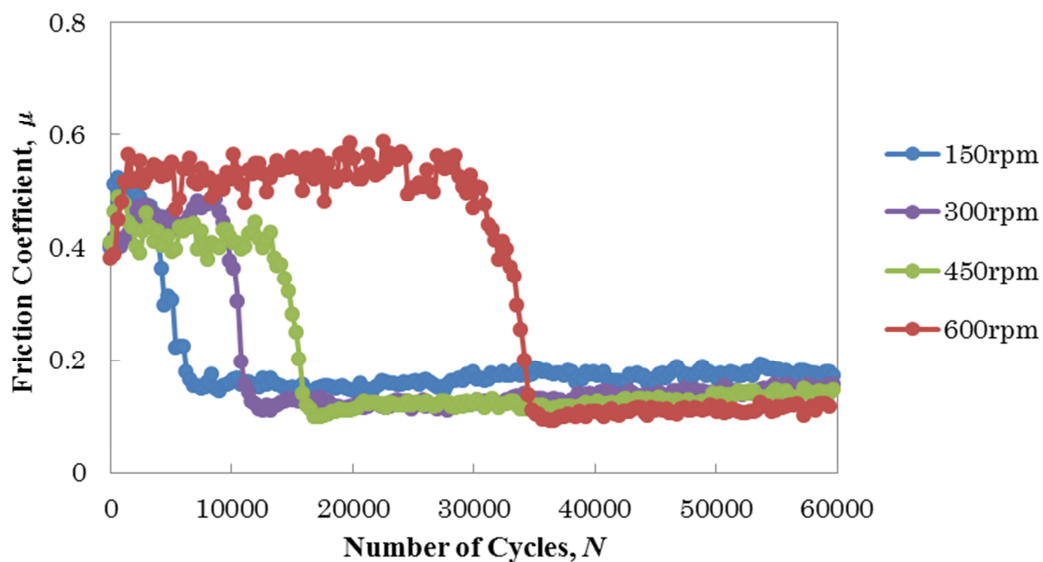


Fig.3.6 Friction coefficient of WC ball against SUS304 flat plate in 1 wt.% DNP dispersion for different sliding speed

3.3.3 DNP's Concentration Dependence

Fig. 3.7 shows the change in friction coefficients for the distilled water and the DNP dispersions (densities 0.01, 0.1 and 1 wt.%) for 240,000 cycles. The friction coefficient measured under lubrication with distilled water was relatively constant at 0.4. The friction coefficients measured under lubrication by the DNP dispersions were initially high, and decreased to steady-state values. The lowest friction coefficient in the initial period was measured for the 0.01 wt.% DNP dispersion, and was approximately the same value as that of distilled water. Meanwhile, the friction coefficients for both the 0.1 wt.% and 1 wt.% DNP dispersions were initially greater than 0.5. The 1 wt.% DNP dispersion showed a sharp decline in friction from 0.5 to 0.12 after around 25,000 cycles. The 0.1 wt.% DNP dispersion also decreased to 0.12 after around 35,000 cycles. The 0.01 wt.% DNP dispersion required the longest time to reach a steady-state value of 0.12 after around 75,000 cycles.

Noticeable differences at the initial period can be seen in Fig.3.8. Fig.3.8 is depicted the same graph as in Fig.3.7. However, the number of cycles was shortened up to 60,000 cycles. This is because the steady state of the entire results was able to be observed within the period of 60,000 cycles. It is clear that the amount of particles is

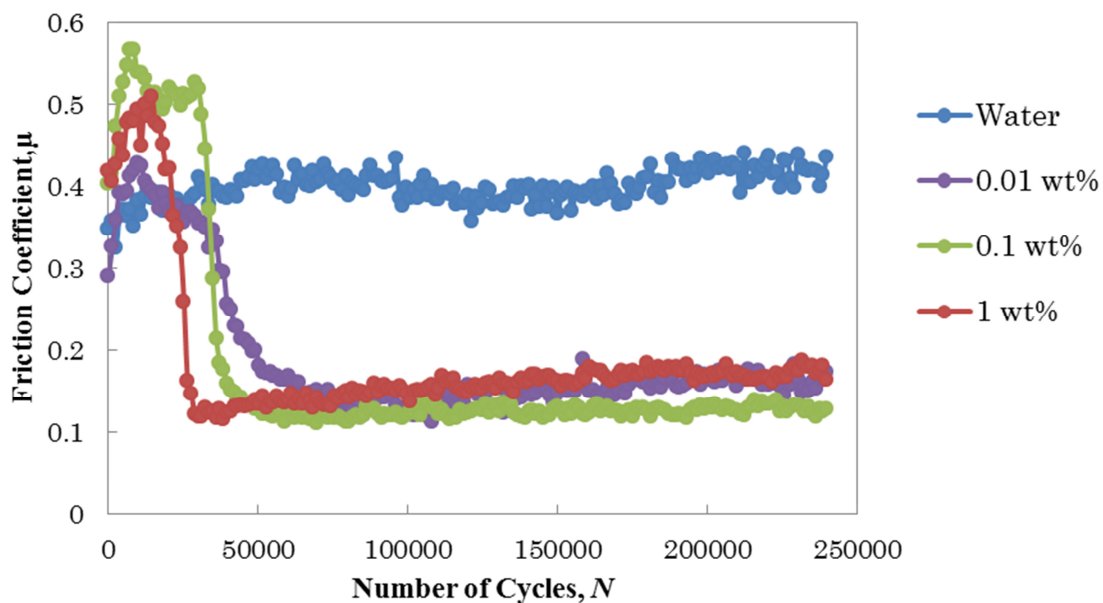


Fig.3.7 Friction coefficient of WC ball against SUS304 plate under distilled water and the DNP dispersions for different concentrations.

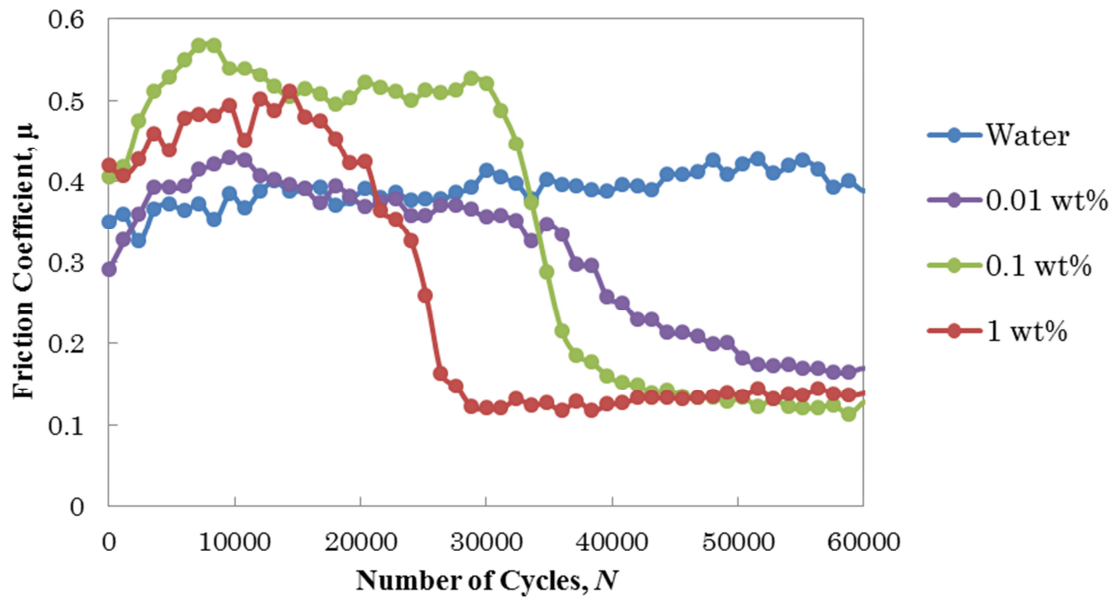


Fig.3.8 Friction coefficient of WC ball against SUS304 plate under distilled water and the DNP dispersions for different concentrations.

important in shortened the time of friction to be reduced. A sharp declination of friction coefficient to the steady state also indicates that once the contact surfaces have been hardened, the lubrication effect will be attained. 0.01 wt.% of DNP however, not able to provide quick lubrication effect as the particles' embedded progress was slower by the small amount of particles in DNP dispersions. Eventually, it will reach the similar tribological ability as the higher concentrations of particles at the steady state. Apparently, the surface modifications by the reduction of asperities and the hardened of surfaces by nano size diamond particles were significant in increasing tribological ability of water lubrication for steel.

Optical microscope images of wear on the plates and balls at 1,000, 10,000 and 100,000 cycles under lubrication by the 1 wt.% DNP dispersion are shown in Fig. 3.9. The observation on each number of cycles purposely done to investigate the mechanism of friction at high friction coefficient until it was reduced. From the Fig.3.9, Wear was obvious on both the plate and ball surfaces. The ball surfaces after 1,000 and 10,000 cycles (in the initial high-friction period) appeared one feature. These cycles were when the friction coefficient is high. Therefore, high friction coefficient might also due to the high surface pressure form the ball onto the plate. On the other hand, a central striation

parallel to the sliding direction was observed on the ball wear scar that experienced 100,000 cycles (in the steady-state low friction period). This central striation was originated from initial high-friction period. After enough DNP embedded onto the flat surface, the wear started to occurred on the ball. Therefore, the obvious wear on the plate was actually developed only at the high friction.

Furthermore, Fig. 3.10 shows optical microscope images of the wear tracks that formed on the plates after 240,000 cycles under different lubrication conditions. The observation until 240,000 with intent to observed the wear propagation on both plate and ball under different concentrations of DNP dispersions. As expected from the result of Fig.3.9, the wear tracks on all the plates appeared clear central striations parallel to the direction of sliding in Fig.3.10 for DNP dispersions. The width of the central striations was also approximately the same. On the other hand, the wear on the plate under the sliding test in distilled water left severe wear. The wear condition of central striation of the wear track by DNP dispersions was similar to the wear condition of full width of distilled water.

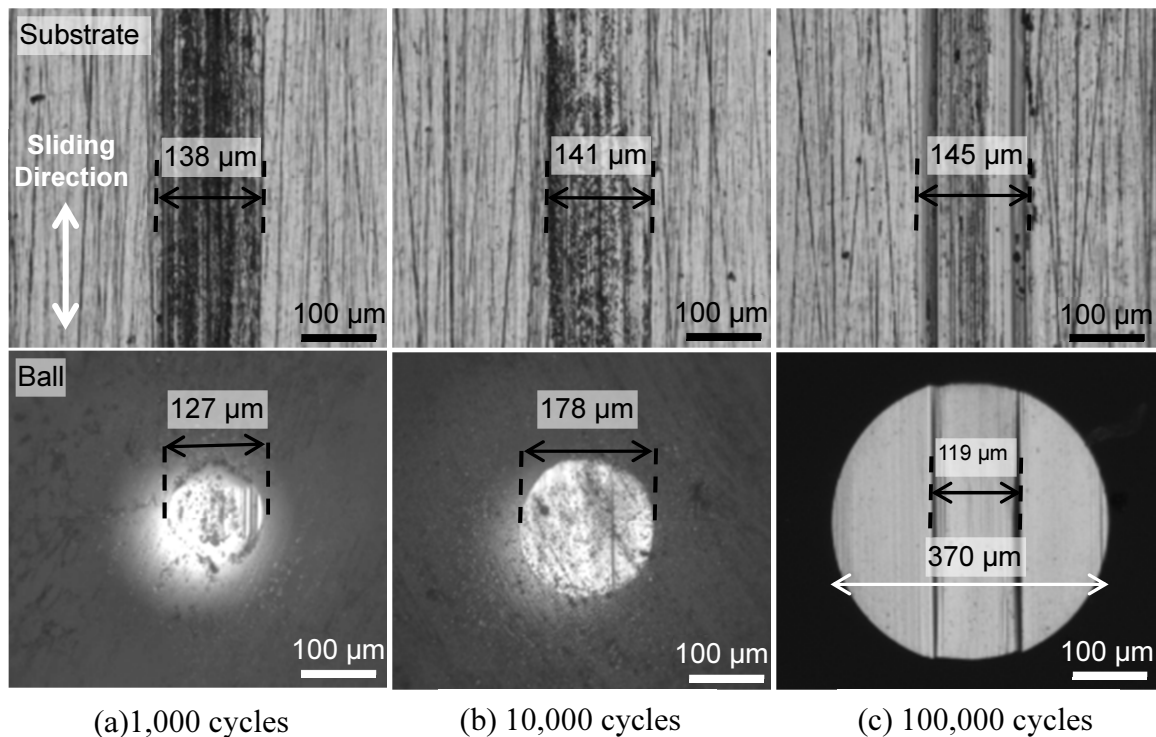


Fig.3.9 Optical microscope images of the wear tracks on plates and wear scars on balls under lubrication by the 1 wt.% DNP dispersion.

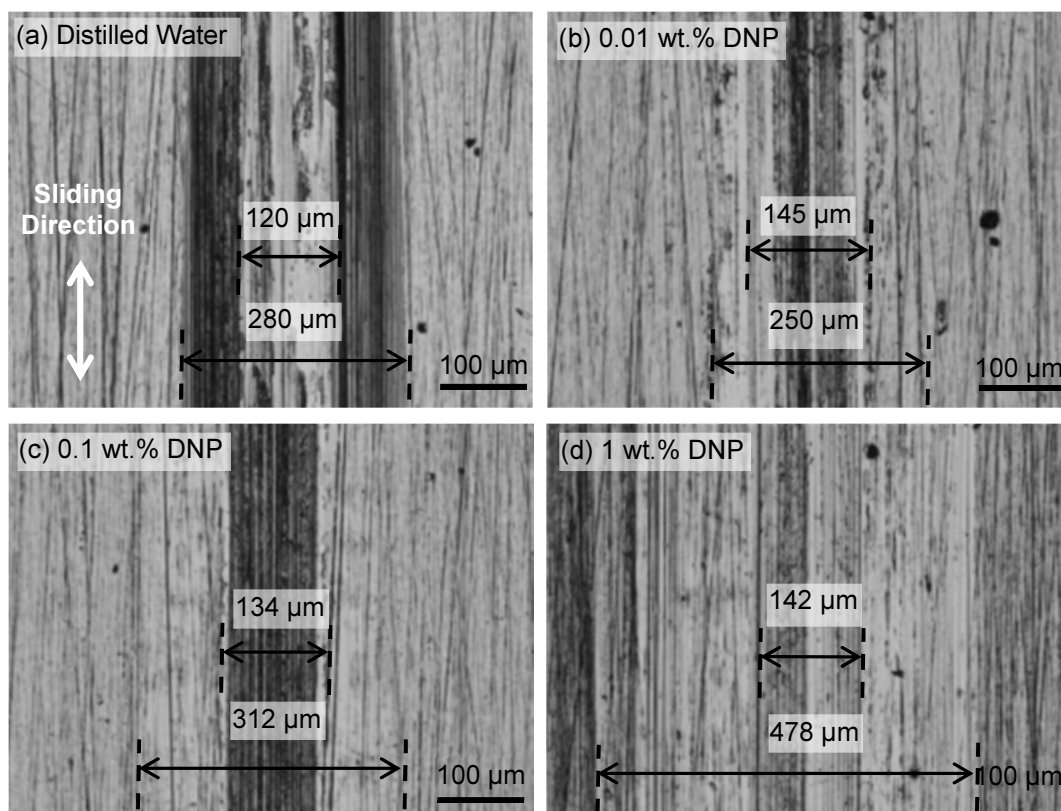


Fig. 3.10 Optical microscope images of the plate wear tracks under distilled water and the DNP dispersions with the different densities after 240,000 cycles of friction testing.

In addition, for the DNP dispersion lubricated plates, the wear outside of the central striations were not obvious. The wears outside of the central striation were noticeable in Fig.3.10 where the contrasts of the images were different. The surface profiles of the same wear tracks shown in Fig. 3.10 are presented in Fig. 3.11. The surface profiles appeared only single-groove indicates the depth of central striations were significant. Optical microscope images of the balls after 240,000 cycles were shown in Fig. 3.12. Central striations parallel to the direction of sliding were also observed on the all ball wear scars. In contrast to the plates, the wear was obvious outside of the central striations on the ball surfaces. Therefore, it is probably the surfaces of the plates were hardened by embedded DNP and tend to produce wear on the ball surfaces. This condition was occurred in steady-state period, where the friction coefficient was extremely low.

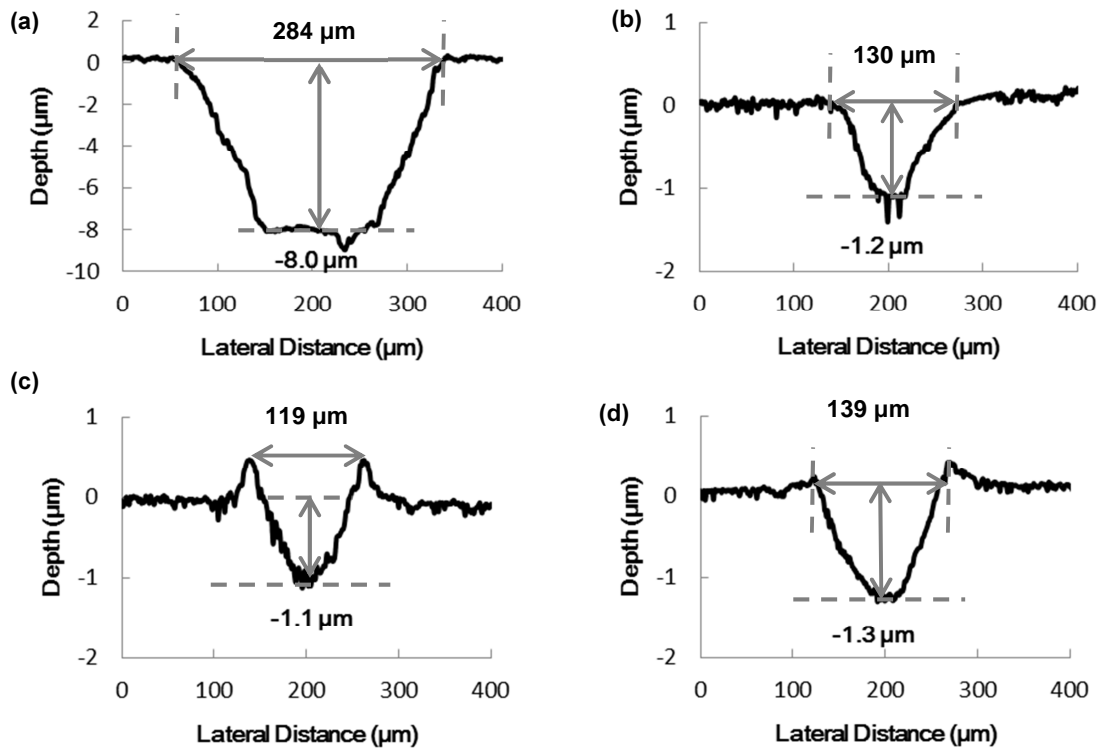


Fig.3.11 Surface profiles of the same plate wear tracks shown in Fig. 3.17
 (a) Distilled water. (b) 0.01 wt.%, (c) 0.1 wt.%, and (d) 1 wt.% DNP dispersions.

Table 3.1 summarizes widths of the plate wear tracks and ball wear scars for the 1 wt. % DNP dispersion lubrications, which were obtained from Figs. 3.9, 3.10(d), and 3.12(d). After 1,000 and 10,000 cycles (in the initial high friction period), full widths of the plate wear tracks and ball wear scars, which did not have the central striations, show similar values to each other. These full widths were also nearly close to the widths of the central striations on the wear tracks and scars after 100,000 and 240,000 cycles (in the steady-state period). These similar widths were shown by grey background in Table 3.1. Table 3.2 shows widths of the plate wear tracks and ball wear scars after 240,000

Table 3.1 Widths of the plate wear tracks and ball wear scars for the 1 wt. % DNP dispersion lubricated system until 100,000 cycles, which were obtained from Figs. 3, 4(d), and 6(d).

	Plate wear track (μm)		Ball wear scar width (μm)	
	Full width	Central striation width	Full width	Central striation width
1,000	138	—————	127	—————
10,000	141	—————	178	—————
100,000	145	—————	370	119
240,000	478	142	485	180

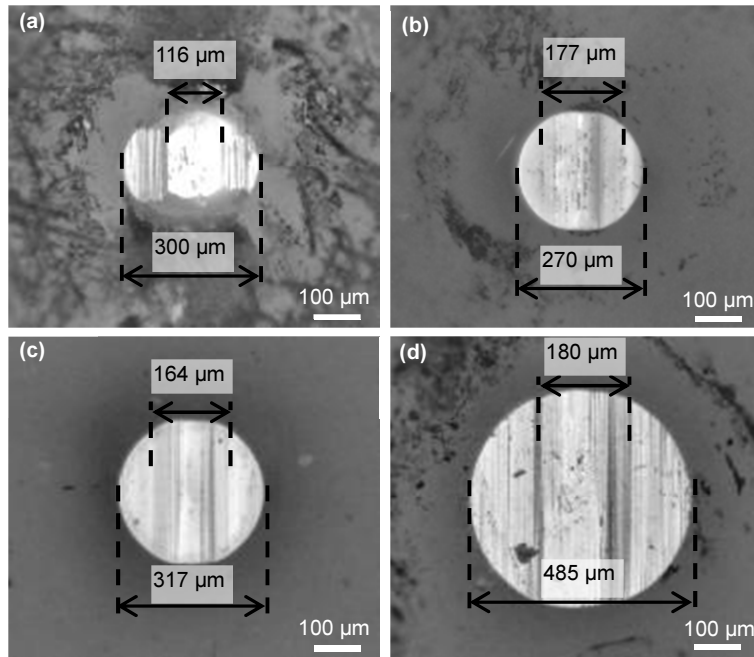


Fig. 3.12 Optical microscope images of the wear scars on WC balls after the tests in distilled water and the DNP dispersions with the different densities after 240,000 cycles.

(a) Distilled water. (b) 0.01 wt.%, (c) 0.1 wt.%, and (d) 1 wt.% DNP dispersions.

Table 3.2 Widths of the plate wear tracks and ball wear scars after 240,000 cycles with different lubrication conditions, which were obtained from Figs. 4, 5 and 6.

	Plate wear track (μm)				Ball wear scar (μm)	
	From photos in Fig.3.10		From profiles in Fig.3.11		From photos in Fig.3.12	
	Full width	Central striation width	Groove width	Groove depth	Full width	Central striation width
Distilled water	280	120	284	8	300	116
0.01wt.% DNP dispersion	250	145	130	1.2	270	177
0.1wt.% DNP dispersion	312	134	119	1.1	317	164
1wt.% DNP dispersion	478	142	139	1.3	485	180

cycles with different lubrication conditions, which were summarized from Figs. 3.10, 3.11 and 3.12. Under distilled water lubrication, the width of the grooves of the plate wear track corresponds to both the full widths of the plate wear track and the ball wear scar. Thus, under distilled water lubrication, wear was happened on areas of the full widths of both the plate wear track and ball wear scar.

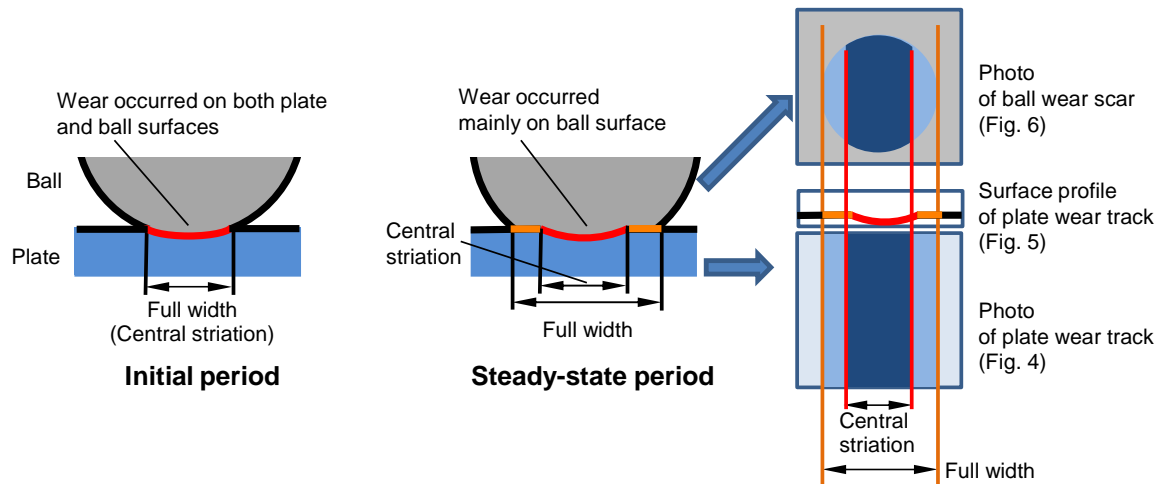


Fig. 3.13 Model of wear on plate and ball surfaces under DNP dispersion lubrications in the initial and steady-state periods.

Under the lubrications by the DNP dispersions, the central striation widths of the plate wear tracks and ball wear scars showed nearly similar values to each other with the different DNP density. The widths and depths of the grooves for the DNP dispersions were also nearly identical with the different DNP density. The widths of the grooves were nearly same to the widths of the central striations, not the full widths, of the plate wear tracks. These similar widths concerning about the central striations were shown by grey background in Table 3.2.

From these experimental results, we assumed a model of wear on the plate and ball surfaces in the initial and steady-state period shown in Fig. 3.13. The full widths of the plate wear tracks in the initial period were almost same to the widths of the central striations on the plate and ball surfaces in the steady-state period (Table 3.1). These results imply that the central striations would be formed only in the initial period and did not grow in the steady-state period (indicated red line of the contact area between the plate and ball in Fig. 3.13). From the surface profiles in Figs. 3.11 (b)-(d), wear outside of the grooves (the central striations) was hardly recognized, which agree in that the wear outside of the central striations shown in Figs. 3.10 (b)-(d) was not clear (indicated orange line of the contact area between the plate and ball in Fig. 7). The wear of the ball surfaces was obviously appeared (Figs. 3.12 (b)-(d)). As mentioned above,

the central striations grew mainly in the initial period. Considering these facts, in the steady-state period, wear on the plates was very little and wear was occurred mainly on the ball surfaces as shown in Fig 3.13. The assumption in the model shown in Fig. 3.13 that the central striations would be formed only in the initial period and wear would occur mainly on the ball surface in the steady-state period can explain the photos of the plate wear tracks and ball wear scars, and the surface profiles of the plate wear tracks.

Raman spectra measured on the worn plate and ball surfaces are shown in Fig. 3.14. The Raman spectrum of the plate wear tracks lubricated by distilled water showed no carbon composite peak spectra. In contrast, the Raman spectra measured on the plate wear tracks under the lubrications by the DNP dispersions showed peaks at 1332 cm^{-1} and around 1600 cm^{-1} , which correspond to first-order diamond Raman line and carbon components including sp^2 bonds, respectively [14]. These peaks could also be measured in the as-received DNPs. This suggests that the DNPs were deposited on the plate wear tracks during the friction tests using the DNP dispersions. A peak at 1070 cm^{-1} was measured for all conditions used, including distilled water. On the ball wear scars lubricated by both distilled water and DNP dispersions, the Raman spectra showed no peaks between 1200 and 2000 cm^{-1} . The peaks at 1070 cm^{-1} were observed that can be attributed to stretching and bending modes of carbonate in WC ball itself [15–17]. It is summarized from the Raman spectra that DNPs existed in the steel plate surfaces and did not on the WC ball surfaces after the DNP dispersion lubrication.

From Table 3.1, the full widths of the ball wear scars by the DNP dispersions increased with the friction cycles. This means that the wear of the ball continuously occurred even in the steady-state period. In addition, from Table 3.2, the full widths of the ball wear scars under lubrication by the DNP dispersions increased with the DNP density. These results indicate that DNPs would wear the ball surfaces. The wear on the hard ball surfaces (Vickers hardness of WC is greater than 1,000 HV) without DNPs was larger than that of the soft steel plate surfaces (Vickers hardness of SUS304 is 129 HV) with DNPs. It is reported that DNPs dispersed in oil was tightly embedded to contact steel surfaces and increase wear resistance of the steels [13,18]. Thus, also in this study, it is expected that DNPs were embedded on the plate surfaces due to the lubrication and that the embedded DNPs protected the steel surfaces. The low friction coefficients that were achieved in the steady-state period would arise from the

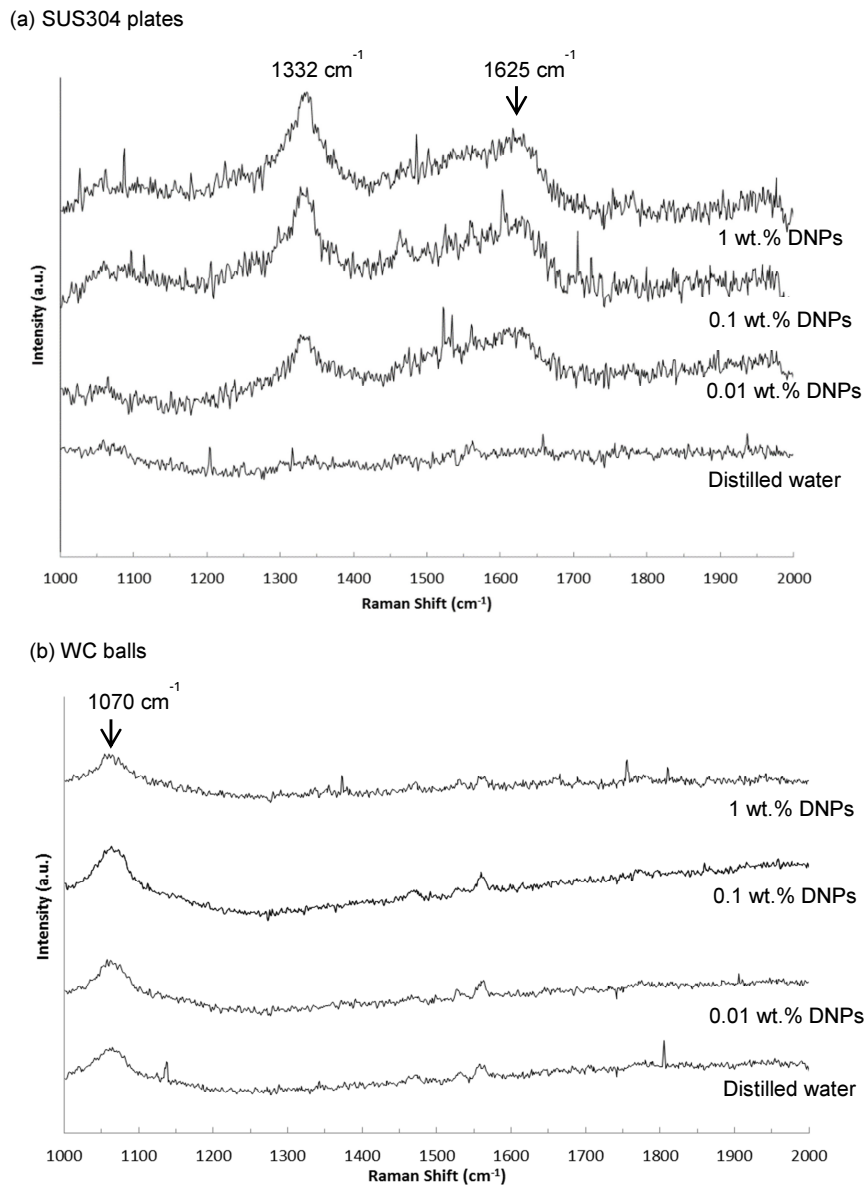


Fig. 3.14 Raman spectra of the plate wear tracks and ball wear scars after 240,000 cycles of friction testing.

interaction between these hard surfaces of the embedded DNPs and the WC balls.

In addition, Fig. 3.15 shows XPS survey spectra in and out of the middle area on the substrate wear track on the substrate surface for the 1 wt.% DNP dispersion. The spectra were obtained after the Ar^+ sputter cleaning for 30 sec to clean contaminations. The spectrum in the middle worn area had a carbon component (C_{1s}) peak, however, there are no carbon peaks outside of the middle area. Since the carbon peak was

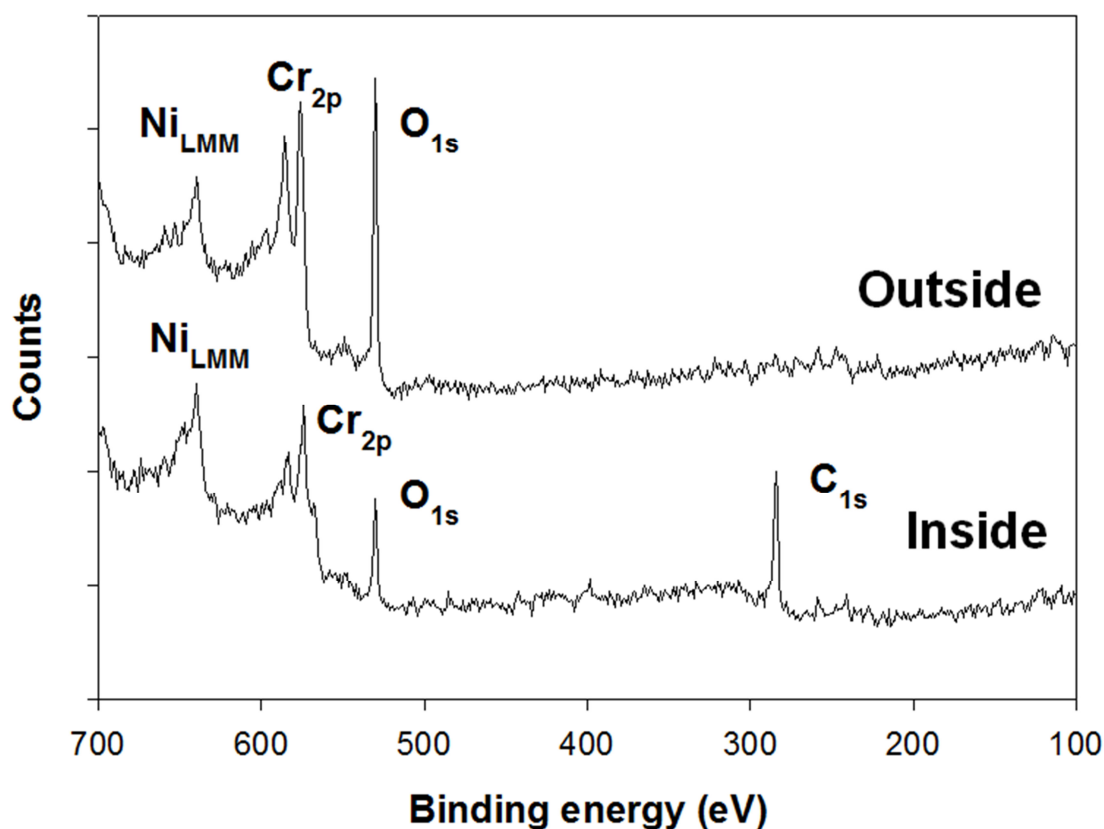


Fig. 3.15 XPS spectra of the areas inside and outside the middle area on the wear track for the 1 wt.% DNP dispersion after the friction test of 240,000 cycles, obtained after the sputter cleaning

observed after the sputtering, DNPs were adsorbed on the middle area of the worn substrate surface thickly and/or tightly. In contrast, outside of the middle area, there were no adsorbed DNPs, or an only little adsorbed DNPs.

DNPs would provide not only protective effect but also abrasive wear. As shown in Fig.3.7, with increasing the DNP density, the initial friction coefficients became higher and the number of initial cycles having the high friction decreased. In the initial period, the plate surface would not have enough amounts of the embedded DNPs to protect itself, and DNPs would wear the plate surface. It is expected that the higher density of DNP increased the rates of both abrasive wear and embedding. The higher rate of the abrasive wear increased the friction coefficients, and the higher rate of the embedding reduced the number of cycles to reach a steady-state friction.

The friction coefficients after reaching steady-state frictions and the depths of wear tracks on the plates under the lubrications by DNP dispersions were lower than

that using distilled water. Additionally, the width of the plate wear track and the diameter of the ball wear scar when lubricated by the 0.01 DNP wt.% dispersion were lower than distilled water. We concluded that the optimum DNP density reduced friction and wear around 0.01 wt.%.

3.4 Summary

In order to study the ability of DNP as an additive in water lubrication, several parameters has been considered. In this chapter, the dependents of DNP dispersed lubricant on different combination of materials, the sliding speeds and the concentrations of the particles were studied. The experimental results are summarized as follows;

- 1) DNP is well dispersed in water with a special treatment of supersonic method. The dispersion was free from agglomerated of the particles and DNP is physically changed the properties of water. It can be seen from the viscosity of the dispersion which is expected to be increased by the addition of diamond particles.
- 2) The investigation of different combination of materials was done on steel and aluminum plate. DNP dispersion was able to reduce the friction coefficient in comparison to distilled water for both materials. However, the different results on the wear showed different tribological effect on each plate. In the steel, diamond particles seem to reduce the asperities of the surface, polished and be embedded into the surface hence hardened the surface. On the other hand, DNP dispersions effect on the aluminum was limited to the viscosity of the dispersion. The friction coefficient was slightly reduced but not as low as the one for steel.
- 3) For the sliding speed dependence, the faster the sliding speeds, the longer it takes to achieve steady state. It is due to the instability of the nano particles dispersions during fast reciprocating motion of tribometer. This condition therefore reduces the rate speed of embedment effect of the particles into the contact surface. However,

once the friction coefficients achieved the steady state, the values were the same regardless of the setup of sliding speeds.

- 4) The tribological properties of the DNP dispersions in water with the different DNP densities were investigated using the steel plates and WC balls. Initially, the lubricated systems showed high friction, which declined and stabilized after the several numbers of cycles. In the initial period, DNPs would wear both the plate and ball surfaces, forming the central striations. At the same time, DNPs were also embedded on the stainless steel plate surface. The steady-state period would be reached when the amount of the embedded DNPs became sufficient to protect the plate surfaces.

- 5) High density of DNPs resulted higher friction coefficient and shorter cycles at the initial period. Meanwhile at the steady-state period, it can be consider that the embedded DNPs is directly contacted the hard WC ball surfaces, which resulted in the low friction and low plate wear, and high ball wear. Under the 0.01 wt.% DNP dispersion, the friction coefficient and wear of both the plate and the ball were better than those under the distilled water.

References

- [1] Kinoshita H, Yuta N, Alias AA, Fujii M. Properties of monolayer graphene oxide sheets as water-based lubricant additives. *Carbon N Y* 2013;66:720–3.
- [2] Liu Y, Liu P, Che L, Shu C, Lu X. Tunable tribological properties in water-based lubrication of water-soluble fullerene derivatives via varying terminal groups. *Chinese Sci Bull* 2012;57:4641–5.
- [3] Song H-J, Li N. Frictional behavior of oxide graphene nanosheets as water-base lubricant additive. *Appl Phys A* 2011;105:827–32.
- [4] Sutton DC, Limbert G, Stewart D, Wood RJK. The friction of diamond-like carbon coatings in a water environment. *Friction* 2013;1:210–21.
- [5] Galli G. Computer-Based Modeling of Novel Carbon Systems and Their Properties. In: Colombo L, Fasolino A, editors. *Carbon Mater. Chem. Phys.* 3, vol. 3, Dordrecht: Springer Netherlands; 2010, p. 37–57.
- [6] Holt KB. Diamond at the nanoscale: applications of diamond nanoparticles from cellular biomarkers to quantum computing. *Philos Trans A Math Phys Eng Sci* 2007;365:2845–61.
- [7] Chu HY, Hsu WC, Lin JF. Scuffing mechanism during oil-lubricated block-on-ring test with diamond nanoparticles as oil additive. *Wear* 2010;268:1423–33.
- [8] Shen M, Luo J, Wen S. The Tribological Properties of Oils Added with Diamond Nano-Particles. *Tribol Trans* 2001;44:494–8.
- [9] Yu-lin Q, Xiao-feng S, Bin-shi X, Shi-ning M. High temperature tribological behaviors of nano-diamond as oil additive. *J Cent South Univ Technol* 2005;12:181–5.
- [10] Chu HY, Hsu WC, Lin JF. The anti-scuffing performance of diamond nanoparticles as an oil additive. *Wear* 2010;268:960–7.
- [11] Wu YY, Tsui WC, Liu TC. Experimental analysis of tribological properties of lubricating oils with nanoparticle additives. *Wear* 2007;262:819–25.
- [12] Mori S, Kanno A, Nanao H, Minami I, Ösawa E. Tribological Performance of Nano-Diamond for Water Lubrication. 3rd Int. Symp. Detonation Nanodiamonds Technol. Prop. Appl., St. Petersburg, Russia: Ioffe Physico-Technical Institute; 2008, p. 21–8.
- [13] Chou C-C, Lee S-H. Tribological behavior of nanodiamond-dispersed lubricants on carbon steels and aluminum alloy. *Wear* 2010;269:757–62.

- [14] Praver S, Nugent K., Jamieson D., Orwa J., Bursill L., Peng J. The Raman spectrum of nanocrystalline diamond. *Chem Phys Lett* 2000;332:93–7.
- [15] Berger SB, Soares LES, Martin AA, Ambrosano GMB, Tabchoury CPM, Giannini M. Effects of various hydrogen peroxide bleaching concentrations and number of applications on enamel. *Brazilian J Oral Sci* 2014;13:22–7.
- [16] O'Donnell MD, Candarlioglu PL, Miller C a., Gentleman E, Stevens MM. Materials characterisation and cytotoxic assessment of strontium-substituted bioactive glasses for bone regeneration. *J Mater Chem* 2010;20:8934–41.
- [17] Ma J, Du Y. Synthesis of nanocrystalline hexagonal tungsten carbide via co-reduction of tungsten hexachloride and sodium carbonate with metallic magnesium. *J Alloys Compd* 2008;448:215–8.
- [18] Puzyr AP, Burov AE, Selyutin GE, Voroshilov V a., Bondar VS. Modified Nanodiamonds as Antiwear Additives to Commercial Oils. *Tribol Trans* 2012;55:149–54.

Chapter 4

Single Layered Graphene Oxide as an Additive in Water Lubrication

Abstract

In this chapter, we studied the tribological properties of graphene oxide (GO) monolayer sheets as additives in water lubricant. The study was divided into several sections. The sections were discussed about the dependence of GO dispersion to different parameters in order to understand the friction reduction and wear governance mechanism offered by GO dispersion. The first parameter investigated was the effect of GO dispersion on different mating materials. The material of the ball were set as variable with tungsten carbide (WC), carbon steel (SUJ2) and stainless steel (SUS304) against SUS304 flat plate. The study shows that GO dispersions able to reduce friction coefficient of each mating materials. Then it was found GO adsorption occurred on the lubricated surfaces of both the ball and flat plate, suggesting GO sheets may behave as protective coatings. Other than that, the effects of different concentrations of GO dispersions were also studied. Differ to DNP dispersions; the distinctions in the GO dispersion's concentrations were noticeable. Lastly, the applied load, sliding speed and sliding distance were investigated for WC ball against SUS304 flat plate. The focus of several parameters on WC ball and SUS304 flat plate was due to the best friction coefficient obtained in the test.

4.1 Introduction

Graphene is a single atom thick, with a two-dimensional structure derived from a single layered sheet of graphite, and has recently attracted much attention for its unique properties, including lubricating potential [1–4]. GO has been used as a precursor for large-scale production of graphene. Therefore, there are still a lot of abilities of GO need to be discovered. In conjunction with the necessity to improve tribological properties by water lubrication especially to steel materials, the application of GO as an

additive is interesting to be studied.

Other type of carbon nanomaterials have been studied as water lubricating additives, and have shown good tribological performance [5]. In this case, hydrophilic treatments are vital for the application in water lubricating additives, because materials without any surface treatment are innately hydrophobic [6]. However, hydrophilic treatments to carbon nanomaterials will increase the cost of the additives. On the other hand, GO has many carbon oxygen functional groups, which allow for dissolution in water. This means that no hydrophilic treatments are needed. There was also a report that GO sheets area actually amphiphilic. Amphiphilic is the condition where both hydrophilic and hydrophobic occurred. In latest study, it was revealed that GO sheets

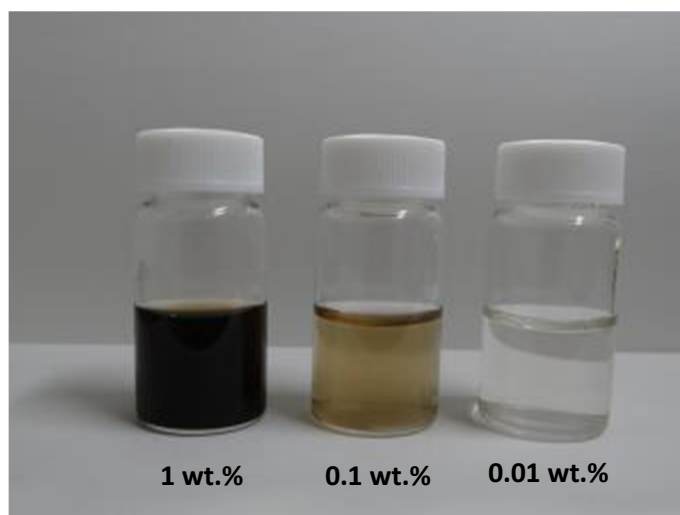


Fig.4.1 Graphene Oxide dispersions with different concentrations

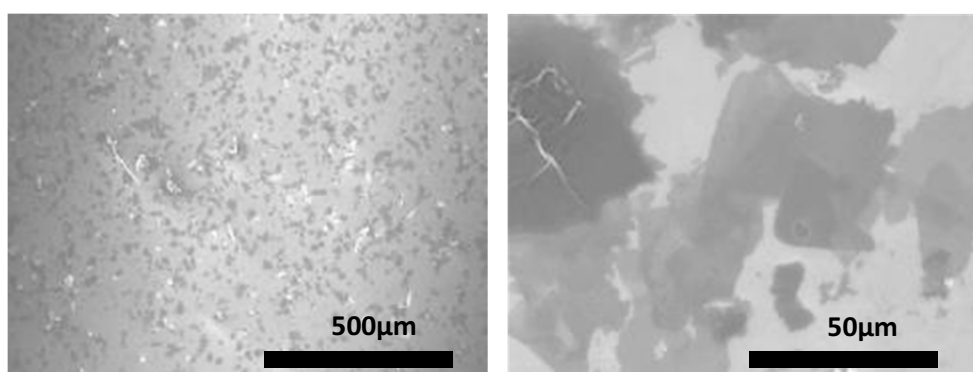


Fig.4.2 Scanning Microscope Images show the Graphene Oxide flakes after dried up on the substrates

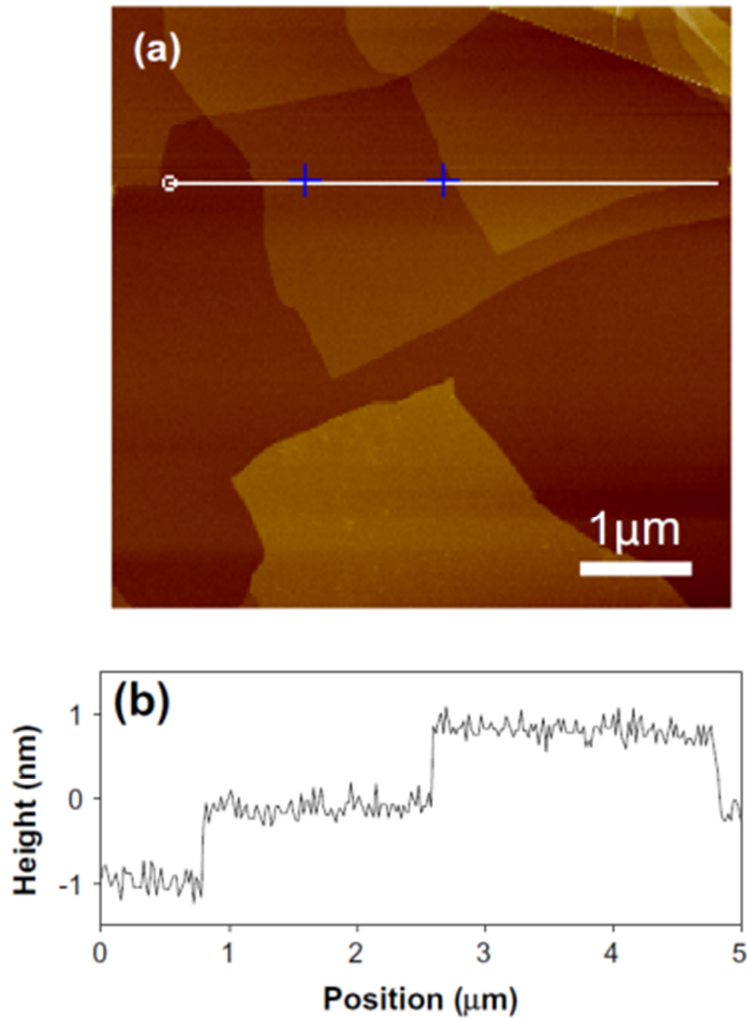


Fig.4.3 Atomic force microscope image shows the thickness of the Graphene Oxide flakes

was actually possess edge-to-center distribution of hydrophilic and hydrophobic domains [7].

In this study, the tribological properties of single layer GO dispersions between pin (ball) and flat plate substrate were investigated. GO used in this study was synthesized by modified Hummers' method. To induce oxidation, microwave irradiation was used during the oxidation process. GO dispersions were show in Fig.4.1 with different concentrations. The highest concentration of GO prepared was 1 wt.% , followed by 0.1 wt.% and 0.01 wt.%. We can barely know the GO appearance by the smallest amount of GO in water as the dispersions seem so clear. Fig. 4.2 shows the GO flakes after dried up on the Si substrate. The SEM observation revealed that the size of

GO flakes in water were from 10 to 50 μm . In addition, most of the flakes size are big and skew to the size of 50 μm as shown in Fig.4.2.

Fig.4.3 shows an atomic force microscopy (AFM) image and height profile of the GO sheets. The sample was prepared by dropping a 0.01 wt.% GO dispersion onto a freshly cleaved mica substrate followed by natural drying. The height of the GO sample was measured at around 1 nm. The distance between the grapheme sheets in graphite is around 0.335 nm. As the surface of GO is composed of a large number of oxygen functional groups, the heights of GO measured by AFM are likely to be more than 0.335 nm (typically around 1 nm) [8]. Therefore it was concluded that the GO flakes used in this study had a single monolayer structure.

4.2 Experiments

The experiment carried out in this chapter is purposely to investigate tribological properties of GO dispersions in different conditions and parameters. The results and discussion have been divided into 4 main sections which based on the dependable of the dispersions in diverse factors. The experiment is mainly conducted with the tribometer as described in chapter 2. Furthermore, the setup and parameter for the experiment in this particular chapter is independent to other chapter.

In this particular chapter, the first experiment was carried out to study the ability of GO dispersions in reducing the friction coefficient in different material combinations. The entire test was conducted by the same flat plate substrate, which was lapped stainless steel, SUS304 (JIS-SUS304). The surface roughness of this plate was approximately 33nm. The differences were only on the counter materials. The counter materials used was 2mm balls which were WC, SUJ2 and SUS304. The second section was the concentrations dependence. In this section, similar materials as first section have been used with the test in 0.01, 0.1 and 1 wt.% of GO dispersions. The prepared dispersions were shown in Fig. 4.1.

Other two sections were dependent on the parameters of the tribological test, which were involved applied load, sliding speed and sliding distance. The applied loads were configured for 1.00N, 1.88N and 3.00N. With the main applied load of 1.88N,

other loads were for investigate the effect of load reduction and increment. The default sliding speed was 300 rpm and the sliding distance was 2 mm. Similar to the applied loads, speed also regulated to lower the speed as 150 rpm and increase it to 450 rpm and 600 rpm. The sliding distance was also shortened to 1 mm and increased to 6 mm and 8 mm in order to investigate the dependence of GO dispersions to the friction coefficient.

Prior to the test, all of the materials were cleaned by ultrasonication in acetone, ethanol, and finally in water for 5 min each. The volume of lubricant fluids used for the friction experiment was approximately 2 ml which was similar to the DNP dispersions. To prevent evaporations for lubricant fluids, the ball and flat plate were covered with an acrylic box. In this study, lubricating fluids did not be added during frictional experiments. The lubricated surfaces of the ball and plate were investigated by optical microscope and scanning electron microscopy (SEM).

4.3 Results and Discussion

The results and discussions were divided into 4 parts. The first part was discussed about the dependence of the GO dispersions as a lubricant on the mating materials. In this chapter also, the mechanism of friction reduction will be explained. Other 3 sections will be discussed regarding the change in the parameter of the lubricant and the test condition. The parameter of the lubricant was the concentration of GO dispersions. Meanwhile the test conditions were applied load, sliding speed and seliding distance.

4.3.1 Material Dependence

The dependence of friction coefficient reduction of different mating materials is summarized in Fig.4.4. The result is obviously shown the ability of 1 wt.% of GO dispersions in reducing the friction coefficient of distilled water regardless of the combination of WC ball, SUJ2 ball and SUS304 ball against SUS304 flat plate. The

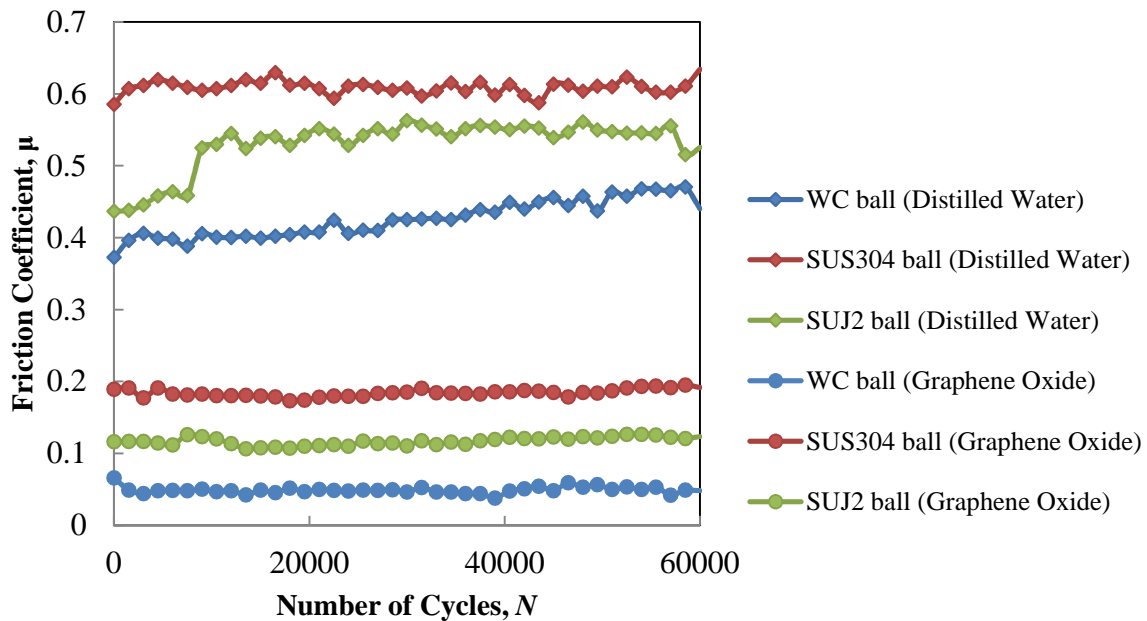


Fig.4.4 The relation of friction coefficient with the ball materials used against SUS304 substrates under distilled water with and without the addition of 1 wt.% of Graphene Oxides

trend of friction reduction is noticeable for all the materials as the similar percentage of friction reduction obtained respectively without any overlapping in the data.

Firstly we can see the different in friction coefficient of each mating materials for the friction test in distilled water. The highest friction coefficient obtained was for the same combination of mating materials, SUS304 ball on SUS304 flat plate. The friction coefficient is as high as 0.6. This result is followed by the friction coefficient of around 0.5 by the combination of SUJ2 ball and SUS304 flat plate. The lowest friction coefficient for the test in distilled water was the around 0.4 for the WC ball on the SUS304 flat plate. From the results, it is clear that the friction ability on two contact surface is dependable on type of materials used. This result also indicates the lubrication regime was boundary lubrication where the roughness of contact surface and the hardness of materials are highly reflected on the friction coefficient.

Also In Fig.4.4, the reduction of friction force in different ball materials are noticeable by the addition of 1 wt.% GO in distilled water. The entire friction coefficients obtained shown a stable results which were in steady-state condition. The

correlation of the reduced frictions from the friction in solely distilled water were also clear where the lowest friction coefficient was as low as 0.05 for WC ball against SUS304 flat plate. It is followed by SUJ2 ball which was 0.1 and SUS304 around 0.2. The friction coefficients by GO dispersions were also stable without any obvious variation of the data. This is supported by the comparison to the data obtained for distilled water. In distilled water, especially for SUJ2, the value of friction coefficient was jumped from 0.45 to 0.5 at 10000 cycles and remains higher until the end of the test. The friction coefficient of WC against SUS304 for distilled water was also not vertical. The value is slightly increasing up to 0.45 at 60000 cycles. This is shown the ability of GO to provide good and stable lubricity to the system. However, with diverse values shown for GO dispersions, the dependent on the mating materials for the system is still occurred.

The mechanism of the friction reduction can be verified by microscope images of the worn area in the wear tracks. The contacted surfaces were washed by ultrasonic

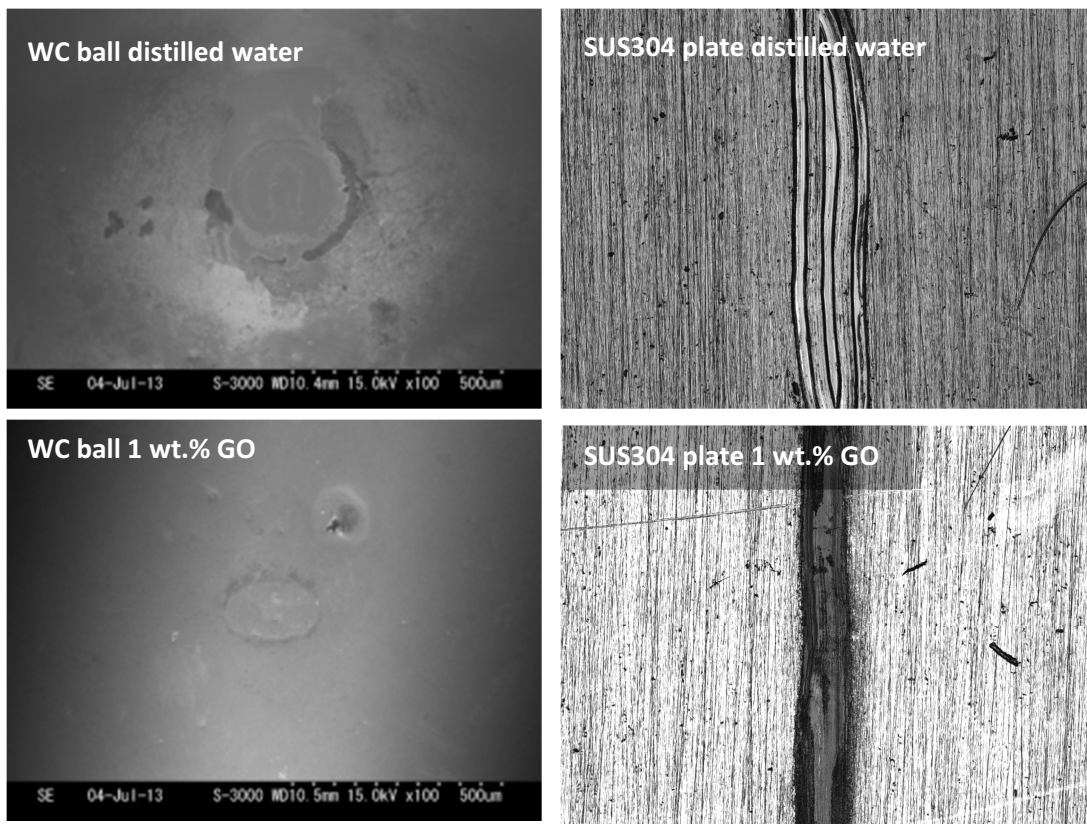


Fig.4.5 The scanning electron microscope images of WC balls and laser microscope images of SUS304 substrates

cleaning in ethanol after the friction tests prior to the microscopic observations. Fig.4.5 shows the SEM images of the worn area on the WC ball surfaces after the test on the left side. On the right side are the images of the worn area on the SUS 304's wear track by the observation via laser microscope. The upper images is the worn from distilled water, meanwhile the lower images is the result from the addition of GO in distilled water. The size of the worn area on the ball surface is larger and seems to be experienced severe damage with the dislocation of the materials particles around the worn area. On the other hand, the worn area of the test in GO dispersions was smaller and oval in shape. The wear on the ball is not increasing such as in the distilled water.

Meanwhile, the observation on the wear track is clearly shows a significant different. The wear track of the test under distilled water was wider than the one in 1 wt.% GO. The severe grooves on the wear track were also observable. The condition of the wear track is clearly shows that the reciprocating movement of the ball was resisted

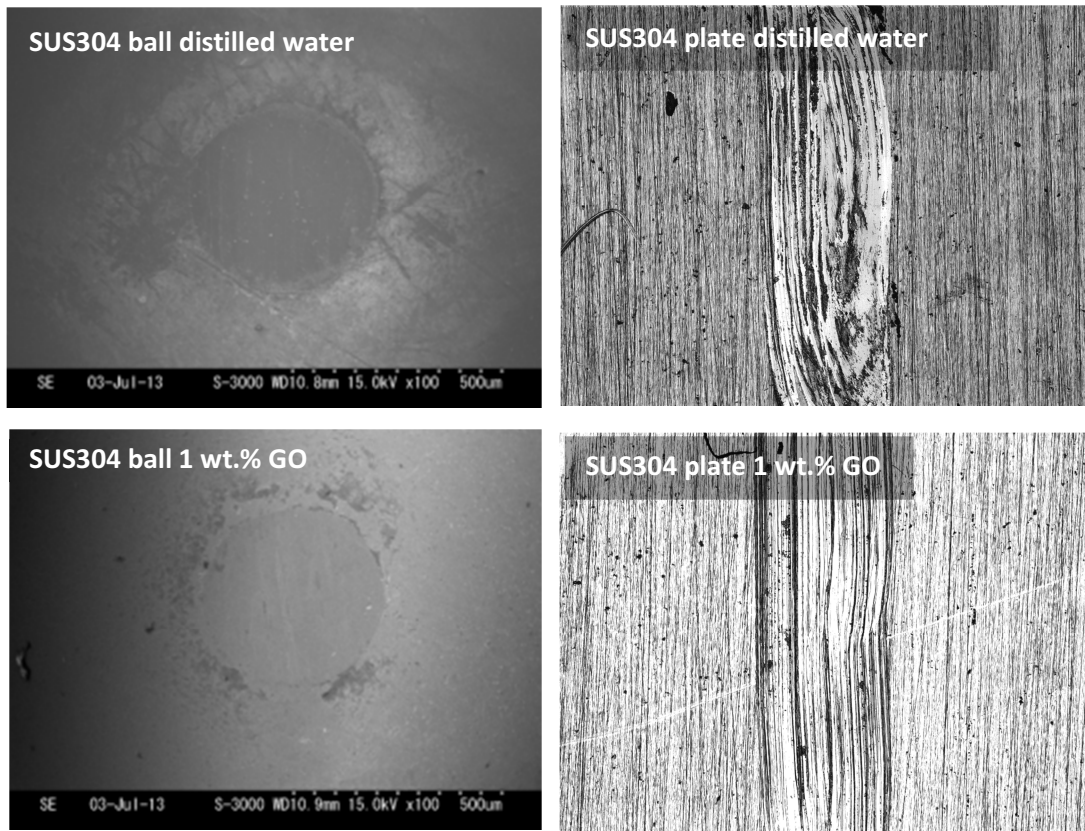


Fig.4.6 The scanning electron microscope images of SUS304 balls and laser microscope images of SUS304 substrates

at both end of wear track. This condition is led to the unparallel groove on the wear. This condition is due to the inability of water to provide lubricating film on the contact surfaces. The continuous movement then resulted to the higher wear on the ball. On the other hand, there was noticeable slightly black substance along the wear track of SUS304. This is probably tribofilm which was formed from GO dispersions during the sliding process of two contact surfaces. From the result comparison in Fig.4.4, we can determine that the formation of tribofilm by GO was able to reduce the friction coefficient down to 0.05. The contact surfaces covered by this tribofilm also respond to the wear occurred on the ball, which was significantly smaller than distilled water.

The Fig.4.6 indicates the wear condition on the SUS304 ball and plate after the sliding friction test. Based on the result of Fig.4.5, it is cleared that the friction coefficient for the combination of these mating materials was reduced by GO dispersions. However the friction coefficient for both in distilled water and 1 wt.% GO dispersions were higher compared to WC ball and SUJ2 against SUS304 flat plate substrate. The worn area on SUS304 ball in both lubricity conditions were almost the same in the size and formation. The structure of the worn area is differing to WC ball because of the ball's original structure. In the SUS304 ball, the surfaces of the worn area are resulted from the removal of the metallic materials. The same size and structure of the wear is due to the same material, SUS304 rubbing on each other surfaces.

Further observation on the wear track shows interesting result. First of all, severe worn can be seen on both wear track for the test in distilled water and also GO dispersions. Similar to worn on the balls, both wear track width were also similar in the size. However, the scratch on the SUS304 plate for the test in GO dispersions shows parallel and straight grooves. The result by distilled water is similar to the images in fig.4.5 where the reason of scratch formation is the same. As previously described, the friction coefficient of the result by SUS304 ball and plate combination is the higher compared to others. It is confirmed by the images itself, where no tribofilm as in fig.4.5 and 4.7 were observed.

Fig.4.7 is the images observed for the test by SUJ2 ball against SUS304 flat plate. The observation on the worn area on the ball shows similar type of wear which is flat circle. However in the size of the worn area is different. In the test under distilled water, the size of worn area is almost the same with the one in Fig.4.6. The surface

features around the worn area were also similar. On the other hand, the size of the worn area was significantly smaller in the test under GO dispersions. This result is highly related to the friction coefficient obtained, which was around 0.1, which is still as low as the friction ability of water based oil lubricant []. In the comparison of all of the different type of balls used, the sizes of worn developed were also differ. The size of the worn area is seemed to be correlated either to the hardness of the ball surface or the mating materials combination. As we know, the largest wear is from the same mating materials, SUS304 ball against SUS304 flat plate.

Lastly is the laser microscopic observation on the worn area in the wear track of SUS304 flat plate by the rubbing with SUJ2 ball. Similar to other two previous tests under distilled water, the wear track width in Fig.4.7 was also wide. However the severe scars are not observable as there was deformation of the wear track with similar movement formation to the result obtained for distilled water as in Fig.4.6. Meanwhile,

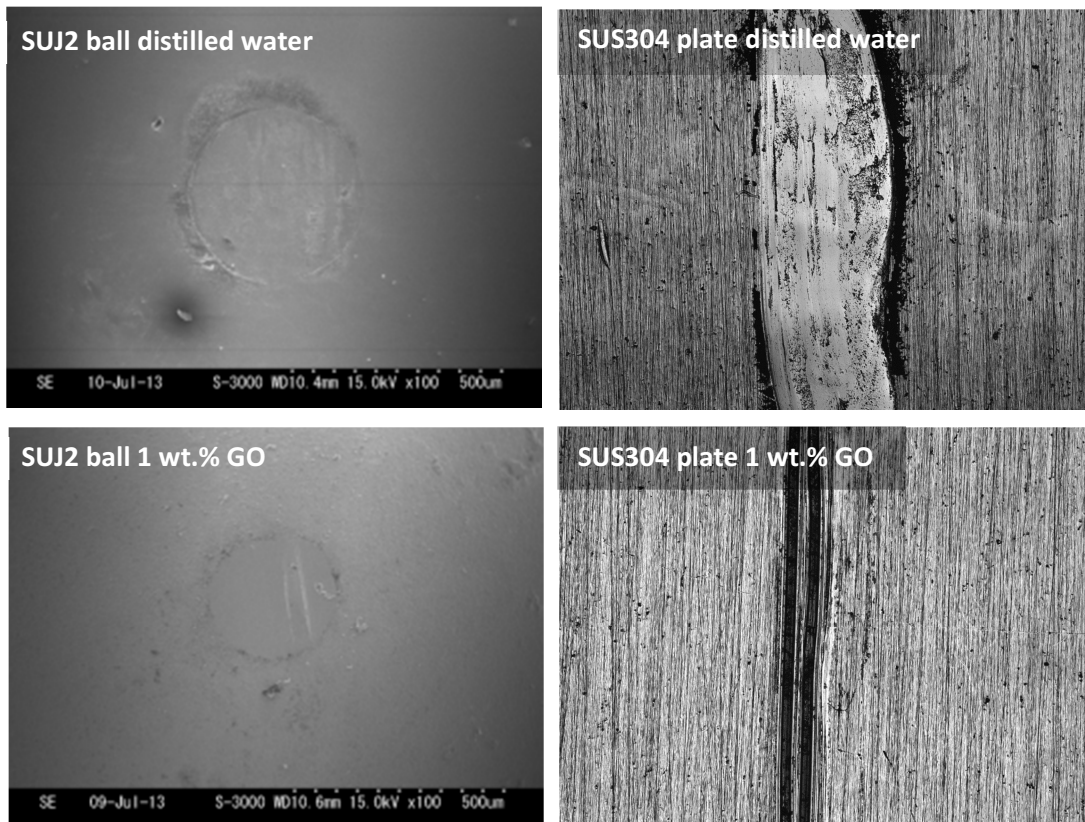


Fig.4.7 The scanning electron microscope images of SUJ2 balls and laser microscope images of SUS304 substrates

the width of the wear track on SUS304 flat plate under GO dispersions is very small. In fact, the size is might be smaller than the on by WC ball against SUS304 plate. However, slightly dark areas is clearly observed indicates the formation of similar tribofilm as previously described. The formation of this tribofilm is might be from the reaction of the GO to the debris form the wear. As the wear in both SUJ2 and WC balls are not embedded on the ball surface as they were different materials. It is different with SUS304, where the debris was tend to be embedded to the ball surface rather than reacted to the GO and form the film.

Further observation by SEM has been carried out as in Fig.4.8 and Fig4.9. Fig. 4.8 shows SEM images of the WC ball surfaces lubricated in distilled water and the GO dispersion. The observation on these specimens particularly by the best tribological result compared to other mating materials. These specimens were also from a different test under the same condition as the result in Fig.4.8. The wear on the WC ball surface

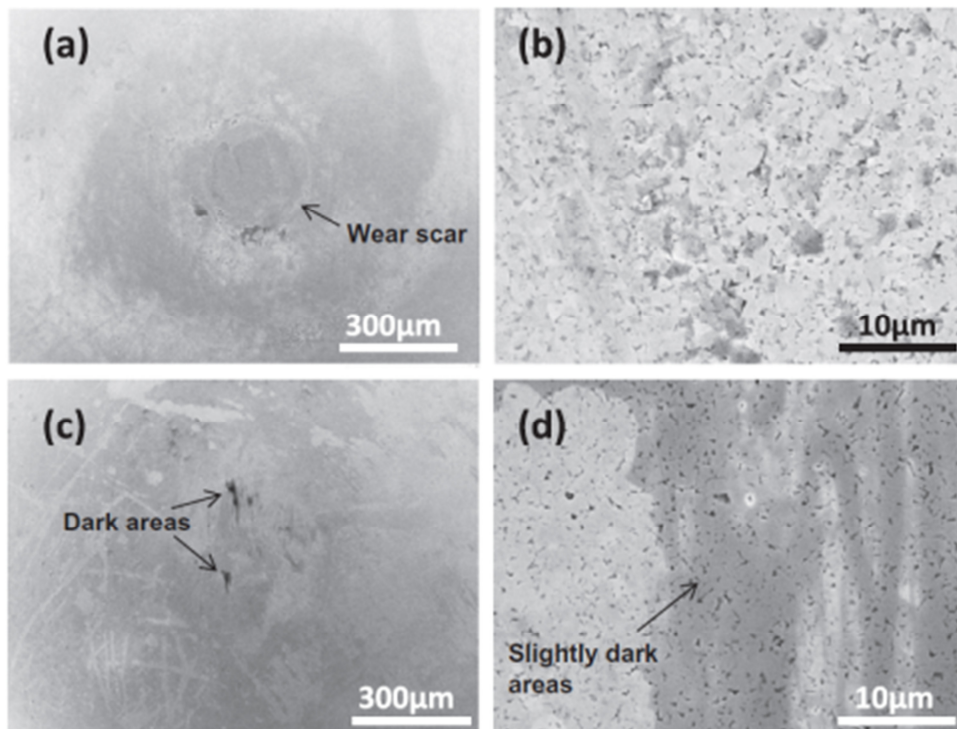


Fig.4.8 SEM images of the WC ball surfaces after a friction test of 60,000 cycles. (a) The surface lubricated with distilled water and (b) a high magnification image. (c) A surface with the GO dispersion and (d) a high magnification image.

lubricated with purified water could be clearly seen in Fig. 4.8(a). The wear observed as formation of a circular wear scar of diameter 300 μm . The wear depth of the WC ball was estimated to be approximately 6 μm based on the scarring area. A high magnification image of the wear surface is shown in Fig. 4.8(b) indicating a loss of particles from the sintered WC surface and an increase in the surface roughness. The surface lubricated with the GO dispersion is shown in Fig. 4.8(c) and did not show any obvious signs of wear. However dark areas were observed on the surface (a high magnification image and carbon elemental mapping of the dark area are shown in Fig. 4.9(a) and (c), respectively). A high magnification image shown in Fig. 4.8(d) indicates that no WC particles were displaced from the surface lubricated with the GO dispersion. It was also noted that some areas of the surface in the high magnification images Fig. 3(d) appeared slightly darker with no apparent morphological changes.

Fig. 4.9(a) and (c) were the SEM images of the ball and flat plate surfaces, respectively, lubricated in the GO dispersion after a friction test of 60,000 cycles. Fig. 4.9(b) and (d) show carbon element mappings measured by EDS on the areas in Fig. 4(a) and (c), respectively. The SEM image of the WC ball surface lubricated with the GO dispersion shown in Fig. 4.9(a) showed slightly dark areas without any morphological changes, and also some much darker areas that corresponded with the adherence of thicker tribofilm. Although the SEM images of the ball and flat surface lubricated with the GO dispersion did not show any wears, the wear ratios should be confirmed by long-duration frictional experiments and/or morphological measurements using atomic force microscopy. The carbon element mappings in Fig. 4.9(b) and (d) showed that the darker areas in the SEM images had higher concentrations of carbon, suggesting that tribofilm from GO sheet may be adsorbed in these dark areas of the ball and flat plate. A few GO sheets would adsorb on the slightly dark areas which formed thin tribofilm. Therefore, the improvement of friction observed seemingly originated from the formation of the adsorption of GO sheets on the contact surfaces. However, the delamination or damages of the adsorbed GO film is not known for the test up to 60000 cycles. Considering the very low and stable friction coefficients shown by the test under GO dispersion, it is likely that non-damaged in the GO tribofilm. Thus, it could be presumed that the either there was no damaging in tribofilm.

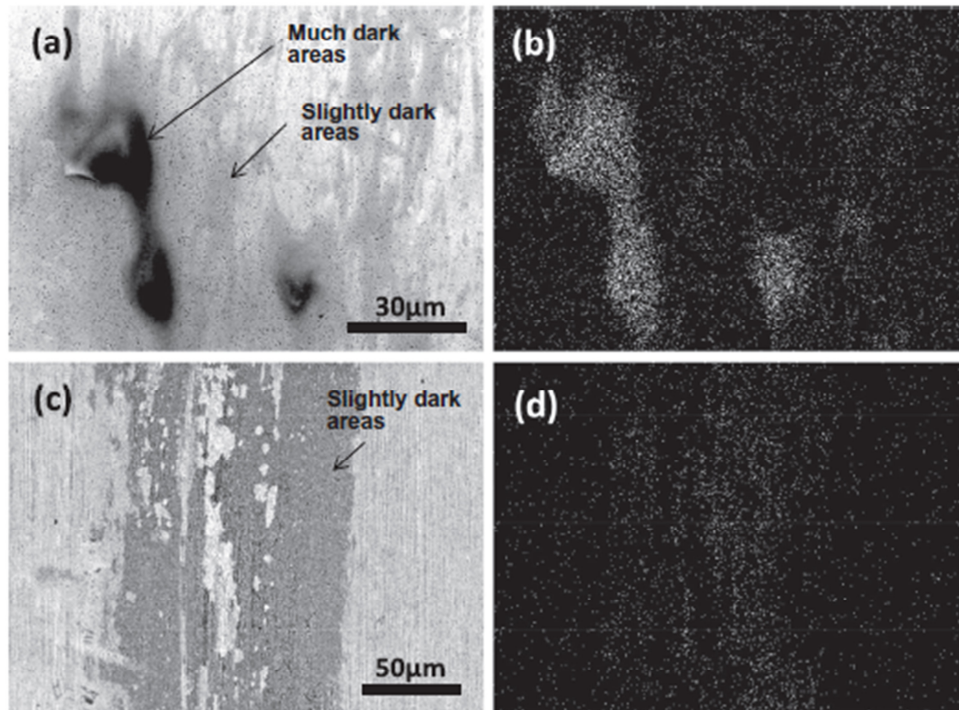


Fig.4.9 SEM images of carbon elemental mappings of the WC ball and stainless steel flat plate lubricated with the GO dispersion after the friction test of 60,000 cycles. (a) SEM image and (b) carbon elemental mapping of the WC ball surfaces. (c) SEM image and (d) carbon elemental mapping of the flat plate.

4.3.2 Concentration Dependence of Graphene Oxide

A diverse results obtained by the combination of different type of materials was direct this study to the concentration controlling of the GO dispersion. This method of experiment was also carried out in previous chapter with the DNP. However, data was analysed for all combination of the materials in this particular chapter. For this purpose, GO dispersion was diluted in distilled water with the concentration of 1, 0.1 and 0.01 wt.% of GO. The data was analysed by divided the results of different materials for better understanding of the friction reduction tendencies. The minimum amount of GO to be used for the optimum friction reduction can be determined of in each specimen.

Fig.4.8 is the result by the best combination of mating materials, WC ball and SUS304 flat plate substrate. As shown in previous section, the friction coefficient of solely distilled water shows as high as 0.6 of friction coefficient. The addition of 1 wt.% of GO to the distilled water as a GO dispersion able to reduce the friction coefficient

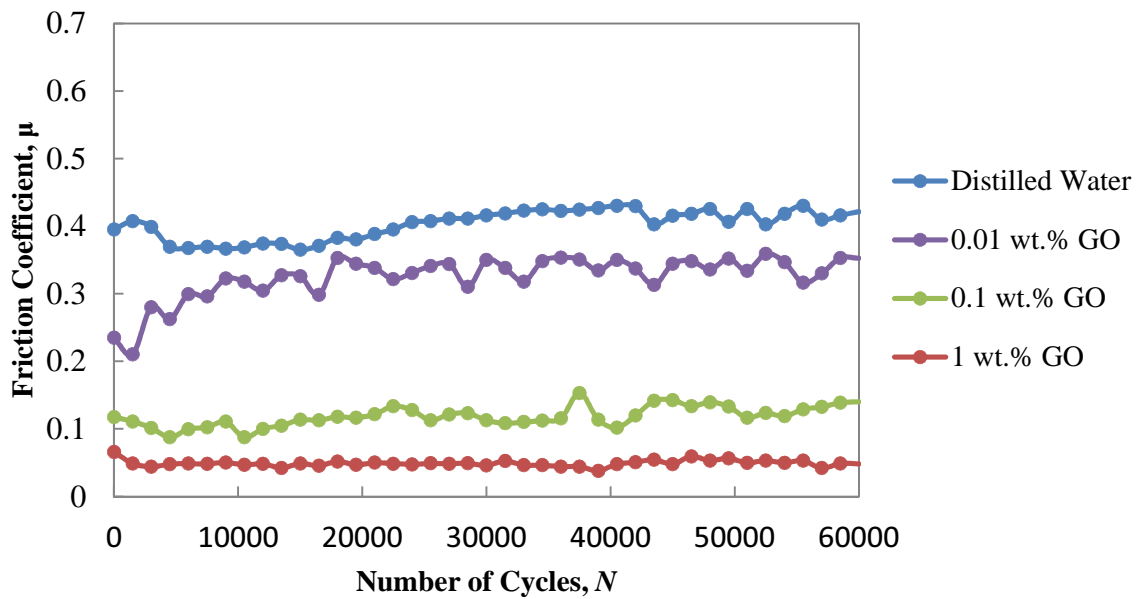


Fig.4.8 The friction coefficient results of WC ball and SUS304 substrate under various concentration dependence of Graphene Oxides compared to distilled water

down to 0.05, which is extremely low. The friction obtained was also stable without any volatile values observed. The dilution of GO dispersion to 0.1 and 0.01 wt.% shown the decreasing of lubricant ability to lubricate the contact surfaces. The friction coefficient by 0.1 wt% GO dispersion was stable at 0.1 with a little volatile. Lastly, 0.01 wt.% of GO addition to distilled water was only able to be reduced down to 0.3.

Despite of giving the highest friction coefficient in comparison to other combination of the materials of ball and flat plate, the friction test of SUS304 ball and SUS304 flat plate shows significant friction reduction. This can be clearly seen from Fig.4.9 by the reduction of an extremely high friction coefficient from 0.6 in distilled water with the addition of different concentration of GO. The friction coefficient for the test under 0.1 wt.% shows lower value compared to 1 wt.% of GO dispersion. However it was gradually increased and shows the same amount as the one in 1 wt.% of GO. The lower friction at the initial state might due to the adherence of GO sheets to the contacting surfaces. The gradual increment might be due to the incomplete formation of GO tribofilm or the sheets are started to damage. Yet, further study is needed to confirm this matter.

On the other hand, the friction coefficient obtained from the lubrication with the lowest concentration of GO shows the similar tendency as Fig.4.8. It can be concluded

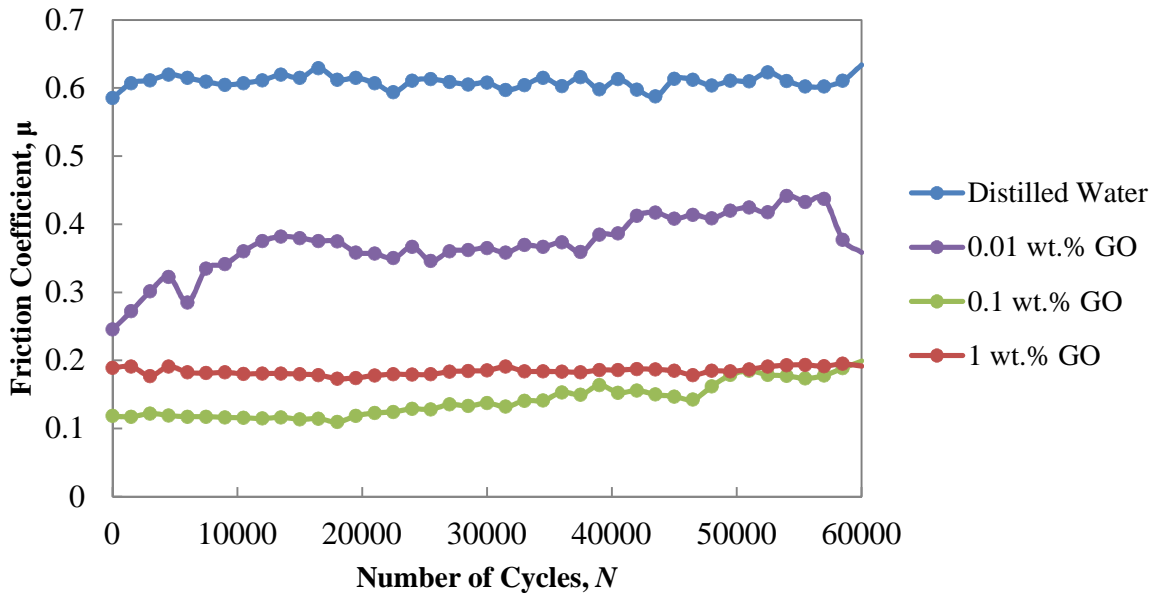


Fig.4.9 The friction coefficient results of SUS304 ball and SUS304 substrate under various concentration dependence of Graphene Oxides compared to distilled water

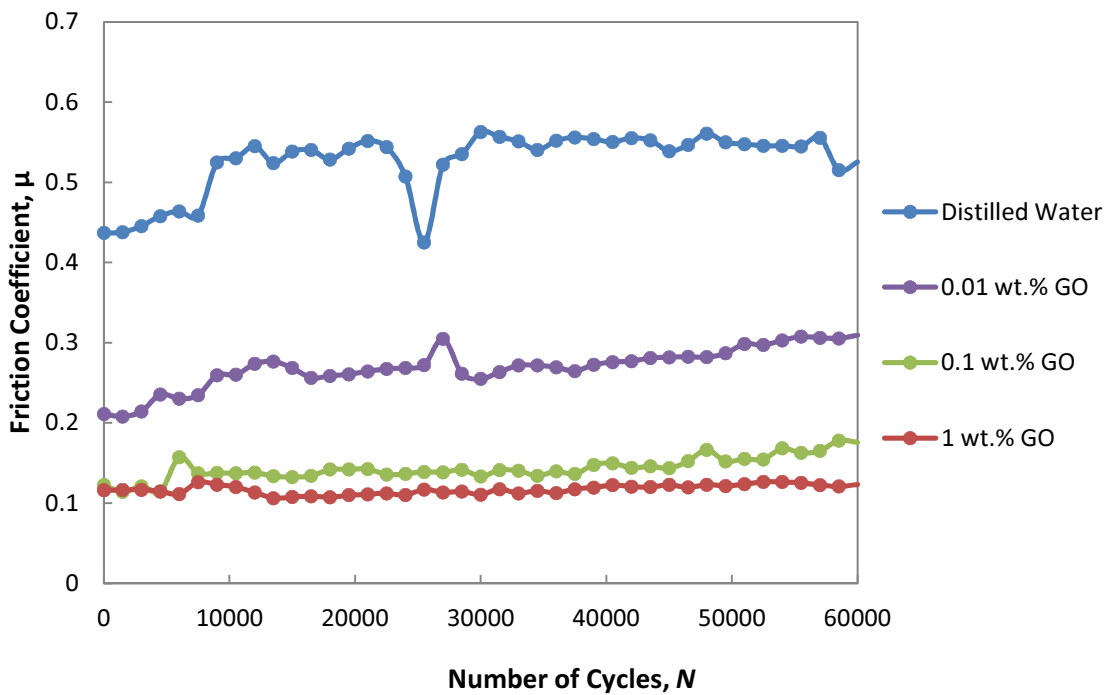


Fig.4.10 The friction coefficient results of SUJ304 ball and SUS304 substrate under various concentration dependence of Graphene Oxides compared to distilled water

that the concentration of 0.01wt.% also reduce the friction coefficient. However, with the small amount of GO sheets dispersed in distilled water, the ability to develop high performance tribofilm might be low. The similar tendency of friction reductions were also observed in Fig.4.10, which we believed that the performance of 0.01 wt.% in friction reduction is almost the same for all materials' combination. The mechanism of the friction coefficient for 0.01 wt.% of GO dispersion is likely not dependent to the materials studied.

The last data in this section is shown in Fig.4.10. The data is from the friction test of SUJ2 ball against SUS304 flat plate. As for other combination of mating materials, the friction coefficient was able to be reduced in all concentration of GO dispersions. The difference in friction reduction of 1 wt.% and 0.1 wt.% were not significant at first when both values obtained are stable at around 0.1. However, at the end of the test at 60000 cycles the friction coefficient lubricated by 0.1 wt.% of GO is slightly higher at 1.5. As described for the results in Fig.4.8, the ability of GO tribofilm to maintain their optimum performance might be decreased. This is due to the low amount of GO sheets in the dispersions.

The formation of the tribofilm from GO sheets of the dispersions is likely to depend on the concentration of GO. This is reflected for the WC, SUS304 and SUJ2 balls against SUS304 flat plate. However, the condition on forming high quality tribofilm cannot be justified solely from this particular experiment.

4.3.3 Load dependence with different speed

Fig.4.11 is the summarization of the friction coefficient for two parameters, the load and the sliding speed. The concentration of GO dispersions used in obtaining the data is 1 wt.% since it gave the best friction reduction result for our study. The materials used were WC ball and SUS304 flat plate, as the best results obtained in material dependent in previous section. From4.11, the result was able to verify the variation of the obtained data with various loads and sliding speed. This result also indicates the condition of parameter where GO dispersions ability in providing good lubrication to

the system. The stable result can be seen when low variation of the data is obtained.

The summarized result shows that the sliding test with an applied load of 1N shows varies result. It can be seen in the sliding speed of 150 rpm where the highest friction coefficient was 0.13 which is far from the mean, 0.05. The similar result also noticeable for 600 rpm, where the highest friction coefficient was 0.35 compared to the 0.1 of their mean. In addition, both of the results for 300 rpm and 450 rpm show higher mean which were 0.1. The variation of the data is also as high as 0.03 to 0.05 in differences. The applied load of 1.8N shows a little variation with less than 0.03 for the

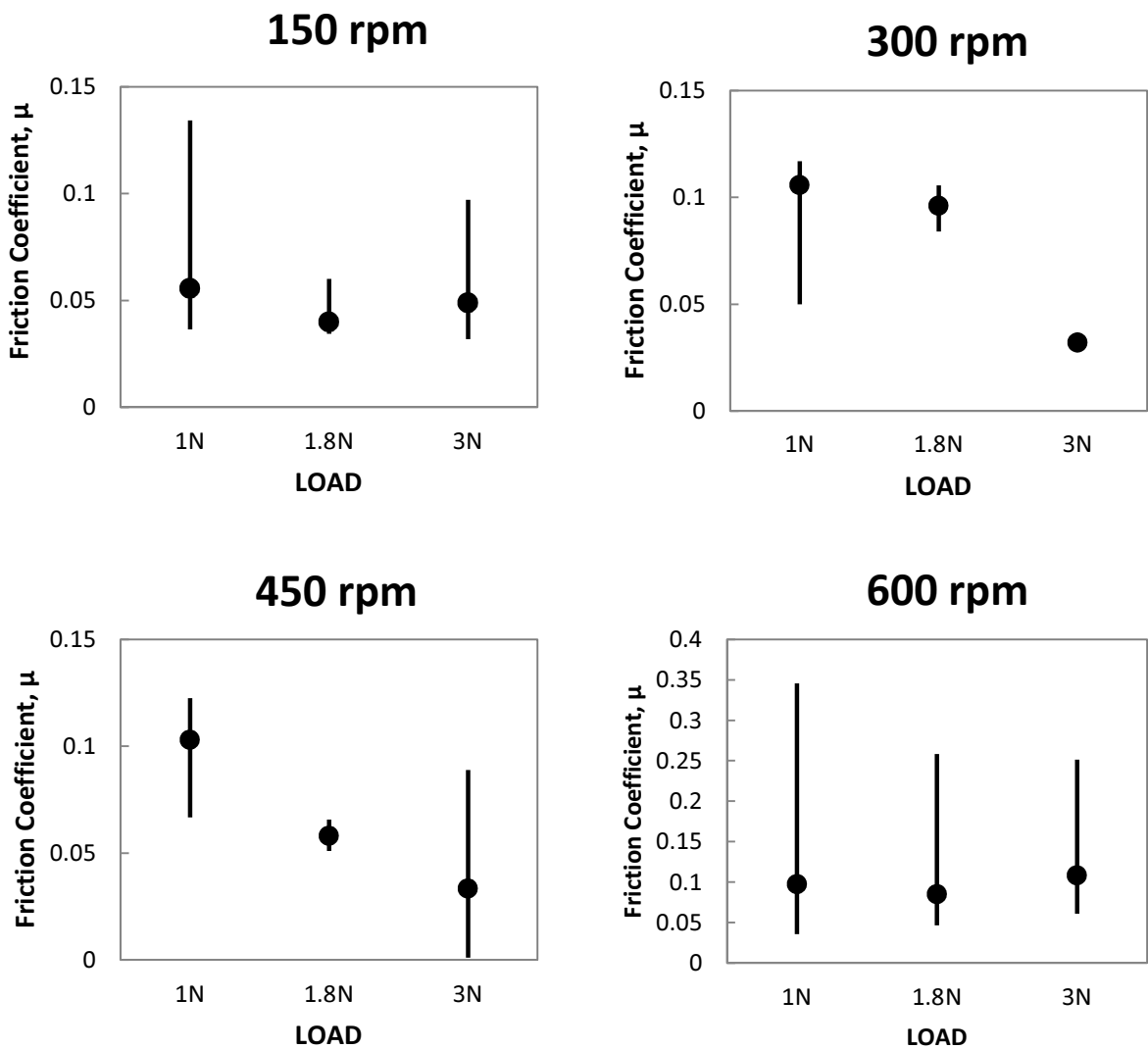


Fig.4.11 The distribution of friction coefficient of WC ball and SUS304 substrate under 1 wt.% of GO dispersion for different loads and sliding speeds

sliding speed of 150 rpm, 300 rpm and 450 rpm and very high for 600 rpm. Sliding speed of 600 rpm for the applied load of 3N also gave the similar result as the applied load of 1.8N. High variation for the result obtained for 600 rpm of speed is due to the ability of GO sheets to gradually form a tribofilm in that speed.

Studying the overall data in Fig.4.11, it is noticeable that the mean for the entire friction coefficient were less than 0.1. The lowest friction coefficient was 0.05, can be seen in the lowest speed, 150 rpm for all applied load. The friction coefficient of 0.05 also can be observed for 300 rpm and 450 rpm. However, the most stable friction coefficient without any variation in the data was shown in the data of 300 rpm with the applied load of 3N. Therefore we were decided to continue our study in the sliding speed of 300 rpm for further understanding about the formation mechanism of the tribofilm.

Fig.4.12 is one of the friction coefficient data obtained for 300 rpm. The data was taken for 20000 cycles with different applied load. The data is corresponding to the

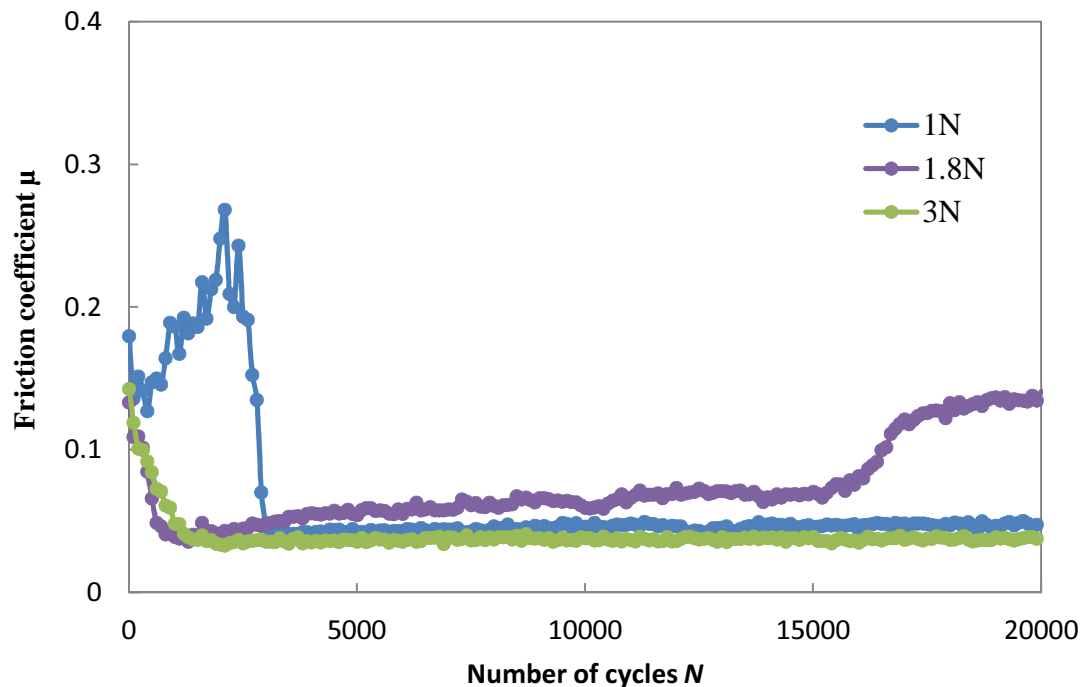


Fig.4.12 The friction coefficient of WC ball and SUS304 substrate in 1 wt.% of GO dispersion for 300 rpm sliding speed and loads of 1.00N, 1.88N and 3.00N

micrograph images in Fig.4.13. Firstly, Fig.4.12 was described that GO dispersion ability in reducing the friction coefficient for all of the condition from high friction with only water. In the steady state, the entire friction coefficient is below 0.1 and amount of friction coefficient were about the same. In the lowest applied load, the friction coefficient was high during the running in period, where the friction was not promptly reduced after the sliding test started. It was started to enter steady state at 2500 cycles. It was due to the applied load which was not enough to produce wear debris for GO to react and form a tribofilm. This similar condition was also happened in other sliding speed for 1N as described in the summarized data by Fig.4.11.

On the other hand, friction coefficient for 1.8N and 3N were promptly reduced after the sliding cycles was 1000. The friction coefficient for both applied load were the same, approximately 0.05. However the friction coefficient of 1.8N of applied load was gradually increased and jumped after 15000 cycles to around 0.1. Although the increment of the friction coefficient was significant in this figure, 0.1 is still far smaller in comparison to the distilled water. Therefore, the tribofilm was not undergoes any delamination or break apart. The increment is might be due to the decreasing quality of the tribofilm. The thickness of tribofilm was also decreased after certain cycles. However, the tribofilm was still remained on the wear track and govern the surfaces from further wear. Meanwhile, the friction coefficient by the applied load of 3N shows a good value until 20000 cycles. This result is the best among others. 3N applied load apparently produced enough wear debris to be react with GO sheets and formed the thick tribofilm.

The comparison of the tribofilm formed in each wear track can be seen in Fig.4.13. The lowest friction coefficient with the mean of 0.05 with insignificant variation on the collected result samples in Fig.3 shows the thickest black compared to others. The magnified image show the noticeable image of GO sheets which form as tribofilm. Similar formation of thick sheet can also be observed in the images of the test under 1.88N. On the other hand, the observation on the weartrack of applied load of 1.88N shows light area of tribofilm. The light area can also be distinguished in other wear track i.e. behind the thick tribofilm. Therefore it is verified that initially, the GO sheets adsorbed to the asperities of the material surfaces. Further rubbing and sliding of contact surfaces will produce wear debris. Enough amount of wear debris then reacts to

GO dispersion. This process is believed to form thicker tribofilm which able to reduce the friction coefficient down to 0.05. However, we were unable to determine the enough amount of wear debris to initiate the formation of thick tribofilm.

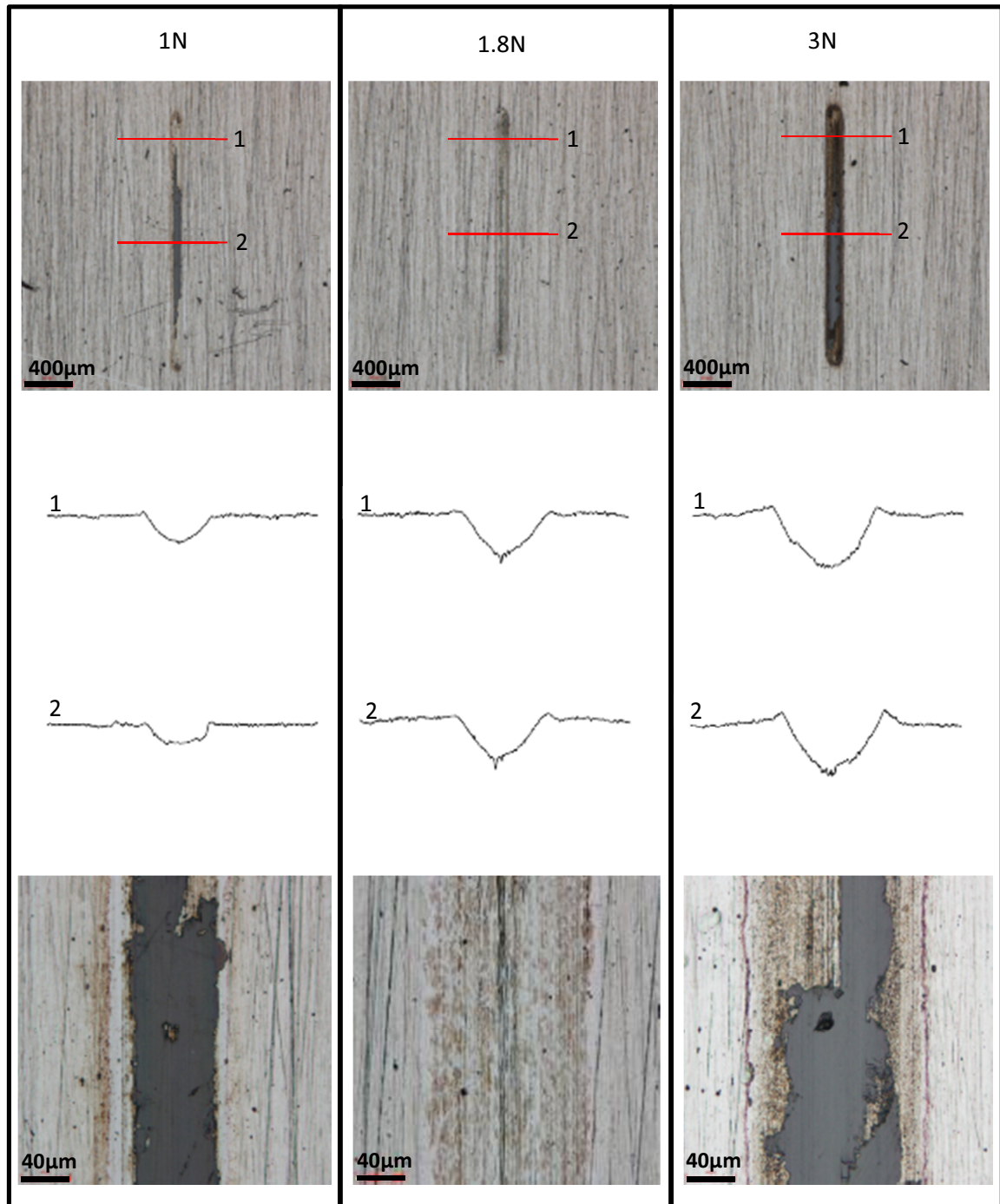


Fig.4.13 The micrographs images and wear profile of SUS304 substrate in 1 wt.% of GO dispersion for 300 rpm sliding speed and loads of 1.00N, 1.8N and 3.00N

Furthermore, the wear profiles analysed from the wear track on two different areas show that the formation of thick tribofilm was occurred. The thickness is noticeable from the smaller depth at the area which the formation of tribofilm is observed.

4.3.4 Speed dependence of varies wear length

The figure 4.13 shows a summarization for different sliding distance. The sliding distance was named as wear length for this section as it indicates the length of the wear developed. The study on the different wear lengths were decided based on the default length used in our study for the entire thesis, which is 2 mm. This 2 mm wear length was compared to the shorter wear length was 1 mm and the longer wear length were 6 mm and 8 mm. the comparison of the wear length was carried out for the different sliding speed. The sliding speed is 150 rpm, 300 rpm, 450 rpm and 600 rpm. Similar to the previous section, the entire data were summarized from friction coefficient vs number of cycles' graph. However, the example of the graph is not included in this particular section. This is because our objective in this section is to distinguish the effect of the distinction in sliding distance by the reciprocating tribological test.

Overall results imply that the friction coefficient obtained was very stable without any fluctuation by the variation of data for the wear length of 1mm, 2mm and 6mm. But, the data was not stable for the wear length of 6 mm by the sliding speed of 600 rpm. Furthermore, the friction coefficient is extremely low for the short wear length. In 1mm and 2mm of the wear length, the friction coefficients were approximately around 0.05 or little bit higher. On the other hand, instead of varies in the data from the mean, the friction coefficient of 6 mm and 8 mm also approximately higher than 0.05 but lower than 0.1.

The results suggest that the sliding speed and wear length setup for this tribological test is highly affect the stable friction coefficient. So, the formation of tribofilm was also highly dependent to the sliding speed and distance. In the longersliding distance and higher sliding speed, GO not able to produce proper lubrication to the contact surface. It is probably the perfect formation of the thick

tribofilm cannot be performed. However, with the mean friction coefficient still under 0.1, it is possible that the thin tribofilm as describe in previous section has been formed. The result also made us continue our other related experiments in regards to GO dispersion for 300 rpm of speed and 2 mm of sliding distance.

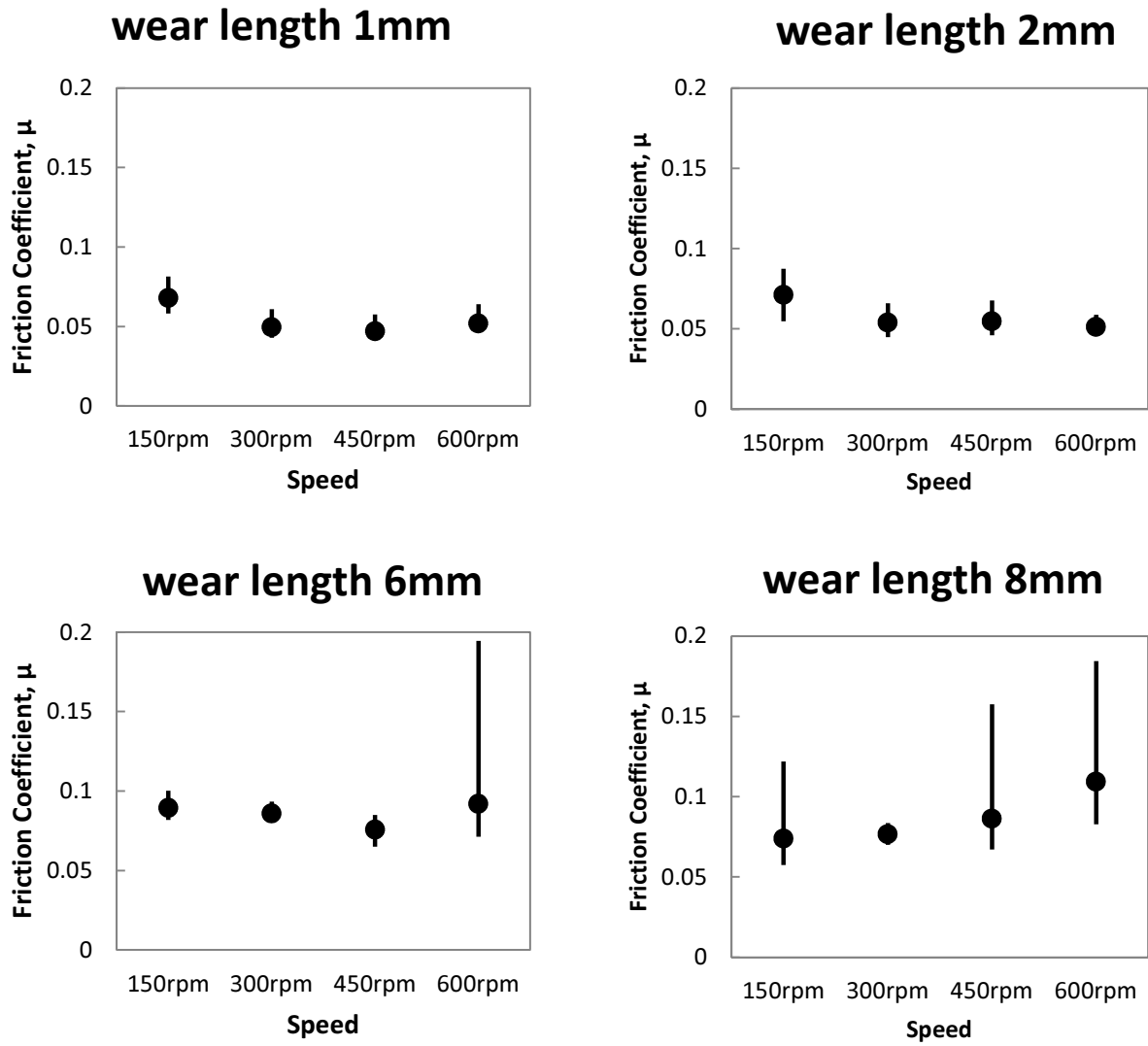


Fig.4.14 The friction coefficient of WC ball and SUS304 substrate in 1 wt.% of GO dispersion for various speeds and sliding distances

4.4 Summary

The study of GO as an additive in water lubrication is important. As a carbon nanomaterials, GO is able to provide high functioning ability in improving tribological properties by water for lubrication. Therefore, in this chapter, the study was highly focus on the mechanism of the friction reduction by GO, and also the investigation on several parameters for the application. The experimental results are summarized as follows;

- 1) GO flakes were well dispersed in water and can be easily diluted in order to produce some different concentrations of GO dispersions. The dispersions were able to be achieved by the presence of carbon oxygen functional group.
- 2) GO dispersions were able to reduce the friction coefficient on several types of materials such as WC, SUJ2 and SUS304 balls on the same flat plate, SUS304 in comparison to the friction test in solely distilled water.
- 3) The observation on the contact surfaces showed no obvious wear after 60,000 friction cycles and the friction coefficient was able to be reduced down to 0.05 for WC ball against SUS340 substrate. The GO flakes are believed to be adsorbed onto the lubricated ball and flat plate surfaces, hence act as protective coatings.
- 4) The concentrations of GO dispersions are important in providing best friction performance of the lubricant. From the results, 1 wt.% of GO offered lowest friction coefficient for each mating materials. When the amounts of GO flakes were reduce, the friction coefficient of the dispersions will be increased.
- 5) The dependence of friction reduction is highly dependent on the condition of GO flakes in the distilled water. It was noticeable from the load and sliding speed dependence that the formation of GO occurred in all condition. However, in order to obtain stable tribofilms, the finest parameters need to be considered. Further investigation on this matter need to be performed.

Overall results obtained suggest good potential for the application of GO sheets as water lubricating additive to reduce friction and surface wear on the steel materials. The tribological performances were due to the GO flakes adsorbed and adhered to the contact surface, which led to the formation of GO tribofilms.

References

- [1] D. Berman, A. Erdemir, A. V Sumant, Few layer graphene to reduce wear and friction on sliding steel surfaces, *Carbon N. Y.* 54 (2012) 454–459. doi:10.1016/j.carbon.2012.11.061.
- [2] J. Lin, L. Wang, G. Chen, Modification of Graphene Platelets and their Tribological Properties as a Lubricant Additive, *Tribol. Lett.* 41 (2010) 209–215. doi:10.1007/s11249-010-9702-5.
- [3] H. Kinoshita, N. Yuta, A.A. Alias, M. Fujii, Properties of monolayer graphene oxide sheets as water-based lubricant additives, *Carbon N. Y.* 66 (2013) 720–723. doi:10.1016/j.carbon.2013.08.045.
- [4] A. Senatore, V.D. Agostino, V. Petrone, P. Ciambelli, M. Sarno, Graphene Oxide Nanosheets as Effective Friction Modifier for Oil Lubricant: Materials , Methods , and Tribological Results, *ISRN Tribol. 2013* (2013) 1–9.
- [5] H. Lei, W. Guan, J. Luo, Tribological behavior of fullerene–styrene sulfonic acid copolymer as water-based lubricant additive, *Wear.* 252 (2002) 345–350. doi:10.1016/S0043-1648(01)00888-2.
- [6] M. Tokoro, Y. Aiyama, M. Masuko, A. Suzuki, H. Ito, K. Yamamoto, Improvement of tribological characteristics under water lubrication of DLC-coatings by surface polishing, *Wear.* 267 (2009) 2167–2172. doi:10.1016/j.wear.2009.04.009.
- [7] L.J. Cote, J. Kim, V.C. Tung, J. Luo, F. Kim, J. Huang, Graphene oxide as surfactant sheets *, *Pure Appl. Chem.* 83 (2010) 95–110. doi:10.1351/PAC-CON-10-10-25.
- [8] X.-Y. Peng, X.-X. Liu, D. Diamond, K.T. Lau, Synthesis of electrochemically-reduced graphene oxide film with controllable size and thickness and its use in supercapacitor, *Carbon N. Y.* 49 (2011) 3488–3496. doi:10.1016/j.carbon.2011.04.047.

Chapter 5

Tribological Effect by the Modification of Graphene Oxide in Water Lubrication

Abstract

In this chapter, an extended study on single-layered Graphene Oxides (GO) has been carried out. The continuity of the study was due to an extremely good friction coefficient and wear results obtained in Chapter 4, which discussed the ability of GO to be used as an additive in water lubrication. The study in this chapter is focusing on the tribological effect by the modification of GO dispersions in their size and pH levels. GO was divided into 3 categories; GO1, GO2 and GO3. GO1 was the original GO as investigated in chapter 4. It has the largest flakes followed by GO3 and the smallest, GO2. All of the dispersions' samples then regulated to pH5, pH7, pH9 and pH10, from their original pH3. The results obtained shows clear distinction where the GO1 not able to maintain their lubricant ability as the friction coefficient increased and the severe wear occurred on the contact surfaces after the pH value exceed pH7. On the other hand, GO2 and GO3 were able to retain their tribological ability except for pH10. The properties deteriorated might be from the increasing of ion content in the dispersion. Therefore, the experiment to reduce ion content in pH10 was carried out for the last section of this chapter. It was able to reduce the friction coefficient even though not able to reach the lowest friction coefficient by pH3.

5.1 Introduction

As described in previous chapter, GO received a lot of attention because of their unique properties especially with lubricating potential [1–4]. GO has many carbon oxygen functional groups, which allow for dissolution in water. However, dynamic features of GO offered by their carbon oxygen functional groups is also important to be

considered. It stems from the fact that the size of basal plane of GO itself will affect the dispersion level of GO in the water [5,6]. GO has many carbon oxygen functional groups, which allow for dissolution in water. A size of GO will also affect a dispersion level in the water [5]. In addition, a pH level of GO dispersion in water will affect the dissolution in water. A pH level of GO dispersions synthesized by the exfoliating process becomes acidity [7]. High acidity is not desirable for the application in metal parts because of corrosion of metal surfaces. Therefore the main focus on this chapter is to study the controllable attributes of GO dispersions as shown in Fig.5.1.

In this study, several modifications on the attributes of GO has been carried out prior to the tribology sliding test. The modification in our study was focusing on the physical and chemical reaction of the GO. The modification effect has been evaluated by the investigation on the distinction in friction coefficient and the wear of each modification. Therefore, the improvement of each modified GO were able to be determined and the ability of GO as an additive in water based lubricant is clearer. In this particular study, tribological properties of 0.1 wt.% different size of GO dispersions in water were investigated using steel plates (SUS304) and tungsten carbide (WC) balls which are widely used in metal working. Both of the materials were also used in the related studies for this thesis. The modification of the GO flakes sizes and pH level

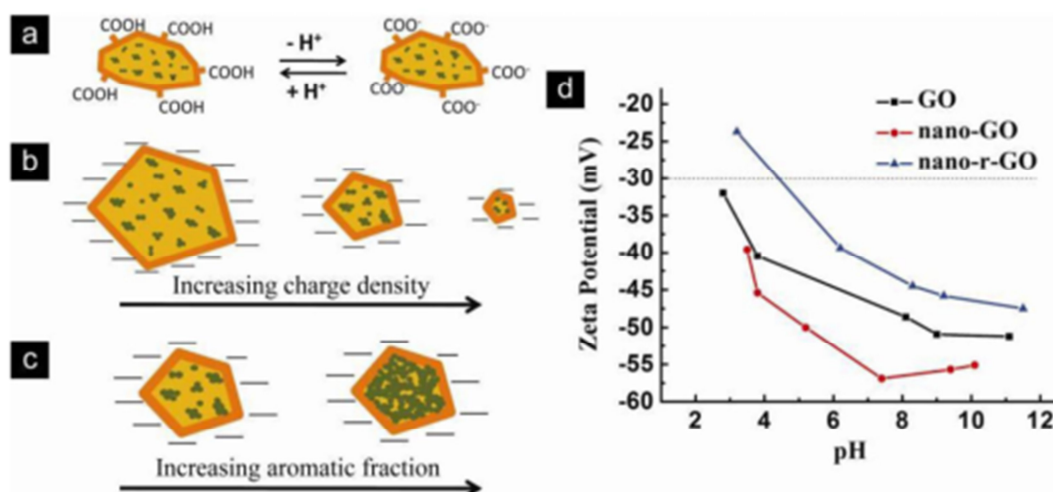


Fig.5.1 The effect of several parameters in GO which directly affect the ability of dispersions as an lubricant additive [5]

were explained in the experimental procedure. Firstly, the influence of the pH level regulation and GO flakes size of the dispersion to the friction coefficient and wear were discussed. Then the contact surfaces especially the worn areas were observed and analysed by optical microscopy and SEM. In the last part, the effect of centrifugation on the GO dispersion on the friction coefficient was shown.

5.2 Experimental

The experiments conducted in this chapter were similar to the previous chapter. The same tribometer and methodology in conducting the experiment and data analysis were carried out. Friction tests were performed with a sliding displacement of approximately 2 mm, a sliding frequency of 300 rpm, and duration of 20,000 cycles, under an applied normal load of 3 N. It was reflected to the best friction coefficient and wear condition obtained based on the study of GO in the chapter 4. Prior to the test, both the SUS304 flat plates and WC balls were cleaned in ethanol, and then water for 5 min each using an ultrasonicator. The cleaned samples were placed in an acrylic box positioned on the sliding track of the tribometer. A sufficient amount of lubricant to cover the sliding area was added (approximately 2 ml). The acrylic box was covered and no water condensation observed inside the box's wall during the experiment indicating no significant evaporation of the water. Lubricated surfaces of the plates and balls were investigated by optical microscopy. All of the plates and balls were carefully washed by ultrasonicing in ethanol before the observation. Widths of plate wear tracks were determined by 3 times measurement average on each two different points. Widths of ball wear scars did by 3 times measurement average on one point.

The lubricant used in this study was a dispersion of Graphene Oxide (GO) which has been prepared in different sizes. For this particular test, the acidity of lubricant dispersions was regulated by adding strong alkaline solution, potassium carbonate K_2CO_3 to the original pH3 of GO dispersions. The addition was delicately conducted and measured for pH5, pH7, pH9 and pH10. In addition, the test materials used in this study were lapped stainless steel (JIS-SUS304) plates and sintered tungsten carbide (WC) balls with a diameter of 2 mm.

5.2.1 Size Modification

One of the reason of friction reduction by GO was the monolayer sheet structure of the GO flakes. There was a study revealed that GO sheets area actually amphiphilic with edge-to-center distribution of hydrophilic and hydrophobic domains [5]. Therefore, the lateral size of GO definitely give a significant effect in friction reduction where GO can adhere to interfaces and lower interfacial energy such as surfactant. The modification of molecules and size adjustment were out of our capability due to the facilities and the main study in our laboratories. Therefore, all of the modified size of GO were supplied by Research Core for Interdisciplinary Sciences, Okayama University. However, the processes of dispersion concentration and acidity regulation

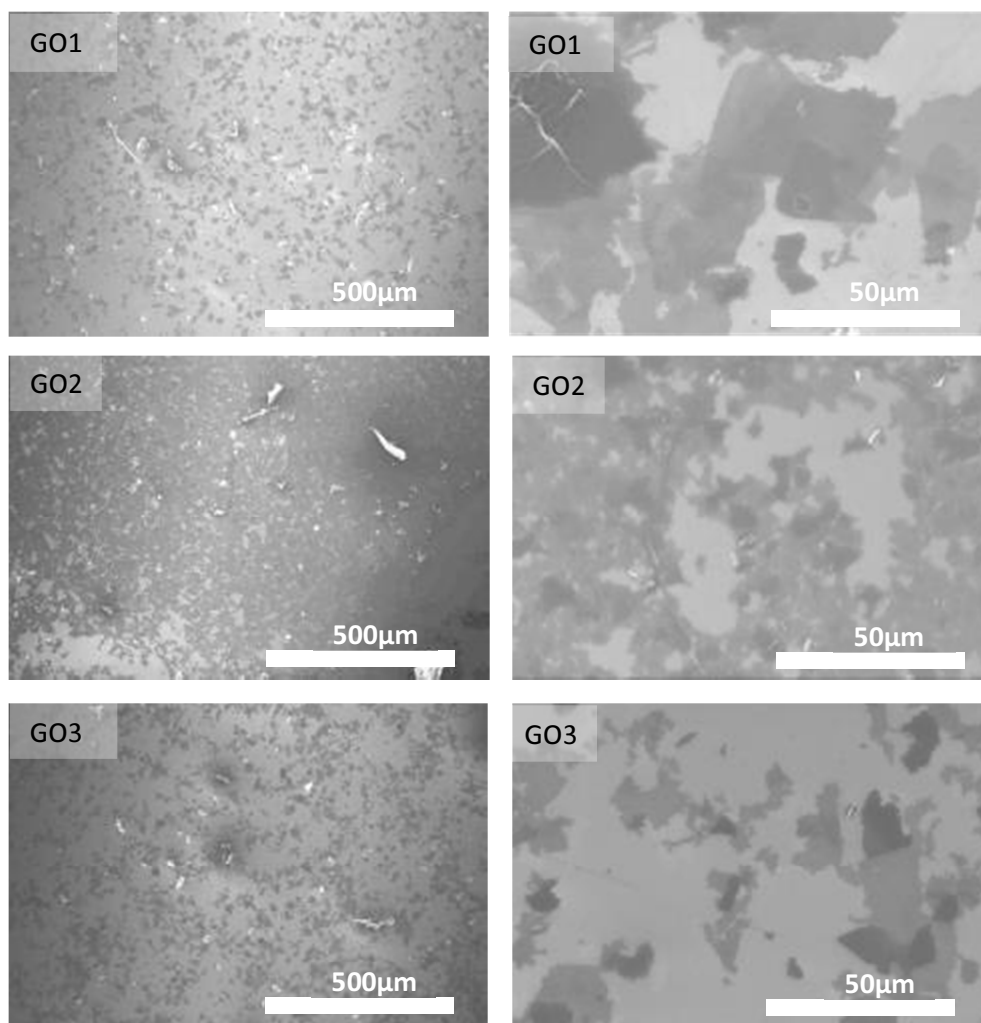


Fig.5.2 The SEM images shows the different in flakes size of GO

have been performed in our laboratory. The size of graphene oxide sheet and acidity study were influenced by the ability of GO to be well dispersed in distilled water. A well dispersed lubricant is believed to increase and stabilize the tribological ability of the lubricant.

Fig.5.2 shows the SEM observation of the prepared GO dispersions. As mentioned, it was divided into 3 main sizes and named as GO1, GO2 and GO3. The distinction in the size of GO can be determined by the size of their flakes as showed in Fig.5.2. The largest flakes size observed was from original GO1 with the sizes were from 10µm up to 50 µm in one direction. It was followed by GO3 which possess smaller size of flakes compared to GO1. The main size in GO3 was 5µm, and the largest flakes up to 20 µm can also be observed although it was significantly low in the amount. The smallest size is provided by GO with the largest size was around 5 to 10µm. The observation on the largest scale (out zoomed) was clearly shown the distinction in GO dispersions. The smallest size of GO flakes, GO2 seems to be well distributed to the entire substrate surface.

5.2.2 pH level Regulation

The pH regulation was carried out in order to reduce the acidity level of GO dispersions. This is because the original GO dispersions is possessing high level of acid due to their producing process. Higher acid will give a bad effect such as corrosion to the metallic materials which is generally used in mechanical systems. The chemical reaction by acid on the metallic materials will also wear them away. The pH adjustments were done by the addition of Pottasium Carbonate (K_2CO_3), which is a strong alkaline solution to GO dispersions. The original pH levels of GO dispersions were around pH3, which is acidic.

The acidity of GO dispersions was delicately regulated into pH5, pH7, pH9 and pH10 from their original state, pH3. The acidity level of the dispersions was measured 3 different days to investigate the stability of the dispersions prepared. The original acidity level of the dispersions did not showed any noticeable difference for the entire

Table 5.1 The Acidity level of Graphene Oxides after several days

GO1	Date	2014.09.17	2014.09.26	2014.09.30
	pH3	2.7	2.7	2.7
	pH5	5.3	4.8	4.7
	pH7	7.0	7.0	7.0
	pH9	9.1	7.5	7.6
	pH10	10.0	9.5	9.4
GO2	Date	2014.09.12	2014.09.16	2014.09.18
	pH3	2.8	2.6	2.7
	pH5	5.3	4.8	4.8
	pH7	7.2	6.7	6.8
	pH9	9.0	7.7	7.7
	pH10	9.9	9.4	9.2
GO3	Date	2014.09.19	2014.09.22	2014.09.29
	pH3	3.2	3.1	3.1
	pH5	5.2	4.8	4.8
	pH7	7.4	7.0	7.0
	pH9	8.9	7.5	7.5
	pH10	10.1	9.6	9.3

sizes of GO used for this study after leaved for several days. It was due to the concentration of H ions which were extremely high for lower level of pH. On the other hand, the pH values seem to be decreased for the earlier day of monitoring for the higher level of pH. The decreasing tendencies were noticeable for the dispersions regulated to pH9. This is because ion activity is easily detected on the higher value of pH which was depending on the decimal logarithm. The complete measured pH values were shown in the Table 5.1. The effect in the increasing of pH for each sizes of GO were investigated by the observation of SEM images as in Fig.5.3, Fig.5.4 and Fig.5.5.

Fig.5.3, Fig.5.4 and Fig.5.5 show the SEM images of GO dispersions before (pH3) and after (pH10) the regulation of pH level was performed. The images on the right side are the magnified images of the left. Observing the comparison of pH3 and pH10 for GO1 as can be seen in Fig.5.3, the size of the GO flakes were remained unchanged after the acidity regulation process. However, the image presented on the left, show a distinction between both types of GO dispersions. The conglomerated of GO flakes was observed in GO1 pH10. It is believed that in higher pH, the zeta potential will be reduced, and GO flakes will be easier to dispersed in distilled water. However,

the bigger size of GO flakes leads to the agglutinated of the flakes between each other.

Meanwhile in Fig.5.4, it is hard to determine the GO2 flakes after the pH value was increased to pH10. However, GO2 flakes might be agglutinated as in Fig.5.3 with

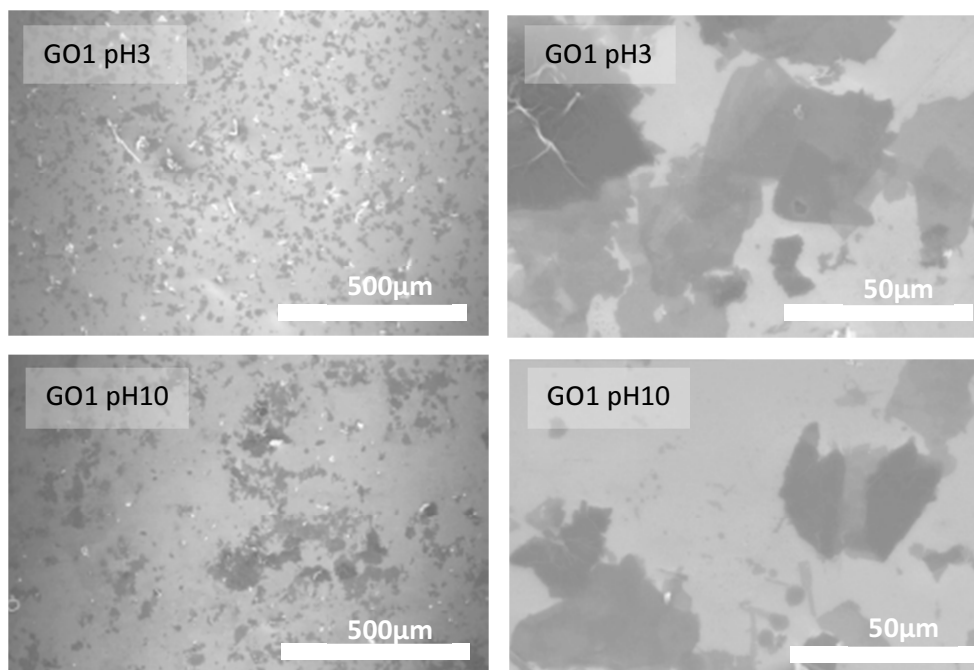


Fig.5.3 The SEM images comparison of pH3 and pH10 for GO1

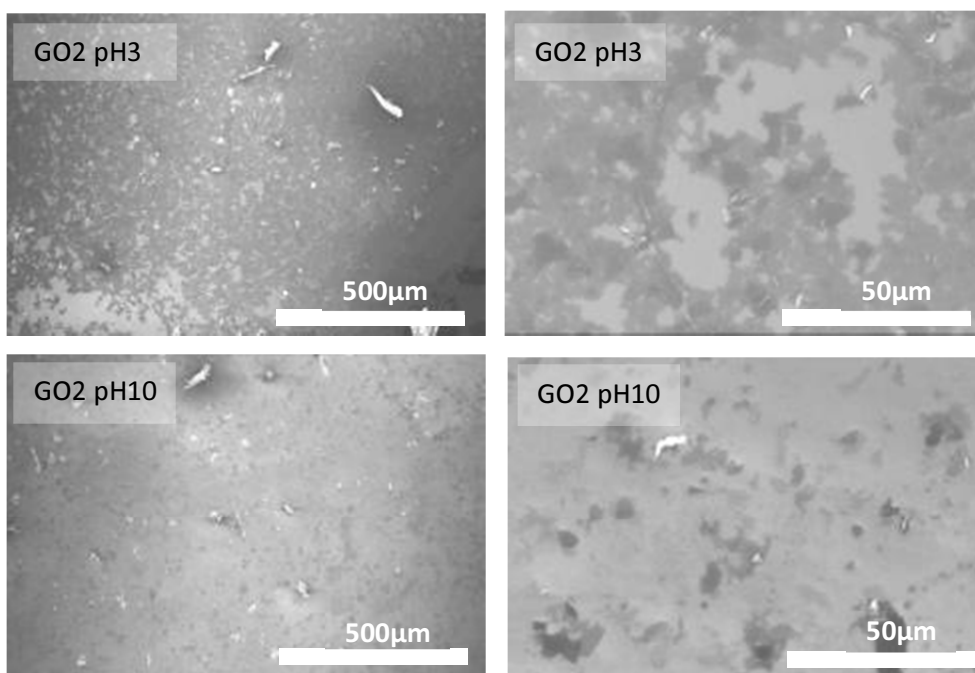


Fig.5.4 The SEM images comparison of pH3 and pH10 for GO2

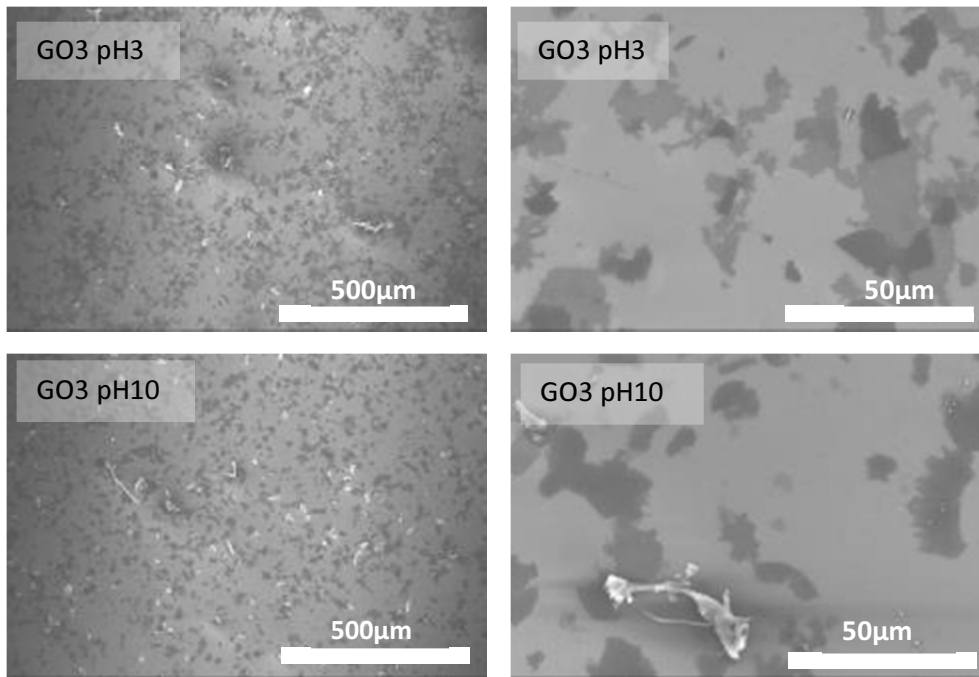


Fig.5.5 The SEM images comparison of pH3 and pH10 for GO3

higher density due to the smaller size of the flakes. Lastly, in Fig.5.5 the size of GO3 flakes was remained unchanged after the increasing of the pH level compared to pH3. However, the distinction in the distribution of the GO3 flakes is can only be determined by the magnified images. The flakes in pH10 seem darker compared to pH3. This is possible that the flakes also accumulated together, but in lower concentration.